REACTIVITIES OF HEAT-TREATED COALS IN STEAM

A. Linares, O. P. Mahajan and P. L. Walker, Jr.

Material Sciences Department, Pennsylvania State University
University Park, Pennsylvania 16802

INTRODUCTION

We have previously reported reactivities of various American coal chars in air (1), CO_2 (2) and H_2 (3). In this paper, we are presenting reactivities of the same set of chars in steam. Reactivities have been measured at 910°C in one atmosphere of N_2-H_2O mixture containing water vapor at a partial pressure of 17.5 torr. The variables chosen for investigation were rank of parent coals, mineral matter content, particle size, reaction temperature and pressure. Effect of addition of H_2 to steam on char reactivity has also been studied.

EXPERIMENTAL

Char Preparation Seventeen U.S. coals (40x100 mesh) varying in rank from anthracite to lignite were used for the preparation of chars. The coals were heated to 1000°C in a N_2 atmosphere at a rate of 10°C/min. Soak time at 1000°C was 2 hr. In order to study the effect of mineral matter removal on char reactivity, selected coals, prior to carbonization, or raw chars, were acid-washed (AW) with 10 volume % HCl or demineralized with a 1:1 HCl-HF mixture.

Procedure A Fisher TGA unit, Model 442, was used for reactivity measurements. About 3 mg of char contained in a platinum pan were heated in N_2 (300 cc/min) up to 1000°C at a rate of 20°C/min. Heating at 1000°C was continued until the char weight became constant. The sample was then cooled to the reaction temperature (910°C) and held at this temperature for 20 min for temperature stabilization. After this, N_2 was replaced by the appropriate reacting mixture. Water vapor pressure was generated by bubbling prepurified N_2 through deaerated distilled water at 20°C. Following introduction of the reacting mixture, the weight of the sample was recorded continuously as a function of time.

Reactivity Measurement Burn-off curves usually had a slow induction period followed by a rate increase. Following the suggestion of Jenkins et al. (1), the reactivity parameter was calculated by the following equation:

$$R = \frac{1}{w_o} \cdot \frac{dw}{dt}$$

where w_o is the starting weight of the char on a dry-ash-free (daf) basis and dw/dt is the maximum rectilinear weight loss rate (mg hr^{-1}).

RESULTS AND DISCUSSION

Reactivity Versus Rank of Parent Coal Reactivity parameters for various chars along with relevant analyses of coals and chars are listed in Table 1. It is seen that char reactivity decreases, in general, with increase in rank of the parent coal. There is a considerable spread in reactivities of chars produced from coals of different rank. The LV bituminous char, PSOC-127, is the least reactive, whereas the lignite char, PSOC-91, is the most reactive, its reactivity being about 250 times that of the PSOC-127 char.

Mineral Matter Removal Removal of mineral matter decreases, in general, subsequent char reactivity. However, in the case of chars derived from higher rank coals mineral matter removal enhances reactivity. Removal of mineral matter from coals prior to their carbonization brings about profound changes in surface area and porosity. The decrease in char reactivity and changes in surface area are much less

pronounced when the chars rather than the coal precursors are acid-washed or demineralized.

Particle Size For a lignite char, PSOC-87, the reactivity parameter is essentially the same for 40x100, 100x150 and 200x325 mesh fractions. However, the reactivity of a LV bituminous char, PSOC-127, increases 4-fold when particle size is reduced from 40x100 to 200x325 mesh, indicating that the reaction is partly diffusion controlled. Upon demineralization, the reactivity parameter for the lignite char decreases for all the three size fractions, whereas the reactivity of the PSOC-127 char increases about 10-fold for each size fraction.

Pressure The dependence of rate on steam partial pressure in the range between 6.5 and 17.5 torr was determined for PSOC-91 char. The reactivity was found to be proportional to steam pressure raised to the 0.60 power.

Temperature Reactivity of a lignite char, PSOC-91, was studied in the temperature range 750-930°C. Below 890°C, the reaction is chemically controlled with an apparent activation energy of 42 kcal/mole. Above 890°C, the reaction is diffusion controlled and has an activation energy of 18 kcal/mole.

Addition of H_2 In order to study the effect of H_2 addition to steam on char reactivity, a mixture of N_2 and H_2 containing 20% H_2 was bubbled through water at 20°C; the partial pressure of water vapor in the mixture was 17.5 torr. Reactivities of a few selected chars in steam, as well as in the steam-H_2 mixture, are given in Table 2. Reactivities of the two lignite chars, PSOC-91 and 87, decrease sharply in the presence of H_2 indicating its strong inhibitive effect. Addition of H_2 has little or no effect on the reactivities of chars derived from PSOC-26, 22 and 24 coals. Reactivity of the LV bituminous char, PSOC-127, increases by 20-fold in the presence of H_2. It is noteworthy that the addition of H_2 to steam increases slightly the reactivity of the raw lignite char, PSOC-138, but has an inhibiting effect on the reactivity of the acid-washed char. These results suggest that in the case of the PSOC-127 and 138 raw chars, H_2 reacts with some catalytically inert inorganic impurity initially present in the char converting it to a catalytically active chemical form and that the inhibitive effect on char reactivity due to H_2 is more than offset by the catalytic effect of the 'regenerated' impurity.

In the steam partial pressure range 6.5 to 17.5 torr, the reactivity of PSOC-91 char in steam-H_2 mixtures is proportional to the steam pressure raised to the 0.93 power.

Reactivity of PSOC-91 char in the steam-H_2 mixture, unlike that in steam, is chemically controlled over the 750-930°C temperature range; the apparent activation energy for the reaction is 84 kcal/mole compared to 42 kcal/mole for the reaction in steam. The higher activation energy in the steam-H_2 mixture is indicative of the strong inhibiting effect of H_2 on the char-steam reaction for PSOC-91.

ACKNOWLEDGEMENTS

This research was supported by ERDA on Contract E(49-18)-2030. Professor William Spackman, Jr. supplied the coals studied.

REFERENCES

1. Jenkins, R. G., Nandi, S. P. and Walker, P. L., Jr., Fuel, 52, 288 (1973).

2. Hippo, E. and Walker, P. L., Jr., Fuel, 54, 245 (1975).

3. Tomita, A., Mahajan, O. P. and Walker, P. L., Jr., Fuel, communicated.

TABLE 1

CHAR REACTIVITY IN STEAM

PSOC Sample No.	Parent Coal ASTM Rank	State	C(daf), %	Char Ash, %	Reactivity, mg hr^{-1} mg^{-1}
91	Lignite	Mon.	70.7	11	2.9
87	Lignite	N.D.	71.2	13	2.8
140	Lignite	Tex.	71.7	12	1.5
138	Lignite	Tex.	74.3	16	1.2
98	Sbb-A	Wyo.	74.3	12	1.0
101	Sbb-C	Wyo.	74.8	8	2.5
26	HVB	Ill.	77.3	20	0.25
22	HVC	Ill.	78.8	23	0.45
24	HVB	Ill.	80.1	14	0.52
67	HVB	Ut.	80.4	5	0.22
171	HVA	W.Va.	82.3	11	0.15
4	HVA	Ky.	83.8	2	0.30
137	MV	Ala.	87.0	19	0.10
114	LV	Pa.	88.2	12	0.07
127	LV	Pa.	89.6	7	0.011
81	Anthracite	Pa.	91.9	6	0.13
177	Anthracite	Pa.	93.5	5	0.11

TABLE 2

EFFECT OF HYDROGEN ADDITION TO STEAM ON CHAR REACTIVITY

PSOC Sample No.	Reactivity, mg hr^{-1} mg^{-1} Steam	Steam-H_2
91	2.9	0.63
91 AW	1.8	0.51
87	2.8	1.0
138	1.2	1.3
138 AW	0.88	0.63
26	0.25	0.24
22	0.45	0.40
24	0.52	0.59
127	0.011	0.20

CATALYSIS OF CHAR GASIFICATION BY MINERALS

A. Tomita, O. P. Mahajan and P. L. Walker, Jr.

Material Sciences Department, Pennsylvania State University
University Park, Pennsylvania 16802

INTRODUCTION

It is well known that most minerals act more or less to catalyze carbon gasification (1,2). In coals, there are two broad classes of inorganic impurities -- the discrete mineral matter, which is usually present in particles greater than about 1 μm in size, and the minor and trace elements, which are more or less associated with the organic phase or mineral phase in a highly dispersed state. Because of current interest in producing low and high BTU gases by coal gasification, it is desirable to know the extent to which inorganic impurities in chars (as a result of being present in the original coals) increases gasification rates. The aim of the present study is to investigate possible catalytic activity of major minerals found in coals for char gasification in air, CO_2 and H_2. Since coals and, hence, chars are invariably associated with many inorganic impurities, a high purity polymer char having a structure similar to coal-derived chars has been used in the present study.

EXPERIMENTAL

Char Preparation The high purity char was obtained by carbonizing Saran (a co-polymer of PVDC and PVC in a ratio of about 9:1) at 900°C in the manner described previously (3). The char was ground and the 200x325 mesh fraction (44x74 μm particle size) heated in N_2 in a fluidized bed reactor up to 1000°C at a rate of 10°C/min. Soak time at 1000°C was 2 hr. The N_2 (77°K) and CO_2 (298°K) surface areas of the char were 900 and 1110 m^2/g.

Minerals The following minerals were used: kaolinite, illite, calcite, dolomite, gypsum, quartz, rutile, pyrite and siderite. The minerals were obtained from Wards Natural Science Establishment, Inc., New York.

Preparation of Char-Mineral Mixtures Various char-mineral mixtures containing 5%, by weight, minerals were prepared by mixing the 200x325 mesh fraction of the minerals with the same size fraction of Saran char. The mixtures were blended for 4 hr in an electric rotating device.

Procedure Reactivities of various char-mineral mixtures were determined in air (1 atm) at 550°C, CO_2 (1 atm) at 960°C and H_2 (20.4 atm) at 940°C. In each case, an electrobalance was used to monitor weight changes occurring during the gasification reaction. Details of the experimental procedure have been described previously (4,5). Briefly, a small amount of the mixture contained in a platinum pan was heated in an inert (N_2 or He) atmosphere to the reaction temperature at a rate of 20°C/min. The sample was maintained isothermally at the reaction temperature for 15 min to ensure thermal stability. Following this, the inert atmosphere was replaced by the reactant gas. Weight changes occurring during gasification were then determined continuously.

Reactivity Measurement In the present study burn-off vs. time curves had a gradual induction period followed by a region in which burn-off increased with time. At higher levels of carbon burn-off, the rates started to decrease. Instantaneous reactivity (R_t) at different reaction times was calculated from the following equation:

$$R_t = \frac{1}{w_t} \cdot \frac{dw}{dt}$$

where w_t and dw/dt are the weight of the unreacted char on a dry-ash-free (daf)

basis and slope of the burn-off vs. time plot at time t, respectively. For reactions in CO_2 and H_2, the reactivity parameter R_c, which represents the constant rate in the region where the kinetics follow a first order rate expression with respect to amount of unreacted char, has been reported. For reaction in air, R_c increased monotonically with conversion so that R_c values cannot be given. Therefore, the reactivity parameter for the reaction in air has been calculated from the following equation:

$$R_o = \frac{1}{w_o} \cdot \frac{dw}{dt}$$

where w_o is the starting weight of char on a daf basis and dw/dt is the maximum rectilinear rate of weight loss.

RESULTS AND DISCUSSION

Reactivity parameters for various char-mineral mixtures in air, CO_2 and H_2 are listed in Table 1. Reactivities could be duplicated within ±2% in all cases.

TABLE 1

REACTIVITY RESULTS

	Reactivity, mg hr^{-1} mg^{-1}		
	R_o in	R_c in	
Mineral	Air	CO_2	H_2
none	1.1	1.9	2.3
siderite	1.0	1.8	5.6
pyrite	1.1	1.3	3.9
dolomite	1.0	2.0	2.0
illite	1.0	1.8	1.4
quartz	-	2.0	2.1
gypsum	1.0	1.5	1.6
rutile	1.1	2.0	1.6
kaolinite	1.2	1.6	1.2
calcite	1.0	1.7	0.6

Reactivity in Air Values of R_o for various samples vary between 1.0 and 1.2. Furthermore, instantaneous rates at a given conversion for different mixtures were found to be essentially the same as for the Saran char itself. These results thus indicate that there is little or no catalytic effect of the minerals studied on char reactivity in air.

Most of the minerals investigated are known to undergo chemical and/or structural changes upon heating to higher temperatures. In order to see if such changes modify activity of the various minerals towards char gasification in air, a few char-mineral mixtures prior to making reactivity measurements at 550°C were heated to 900°C in an inert atmosphere. The reactivities following heat treatment at 900°C were found to be essentially the same as when the heat treatment temperature was 550°C. Thus, the chemical or structural forms of the minerals investigated have no detectable catalytic effect on char gasification in air.

Reactivity in CO_2 It is seen (Table 1) that pyrite, gypsum, kaolinite and calcite inhibit the reaction in CO_2; the effect is most pronounced for pyrite. It is noteworthy that although both C-CO_2 and C-O_2 gasification reactions involve an intermediate oxygen transfer step (1,2), the aforementioned minerals inhibit the reaction in CO_2 whereas they have no such effect in O_2. This shows high catalytic specificity of these minerals for gasification reactions in different oxidizing atmospheres.

The observed inhibitive effect of pyrite may be due to the following. Carbon monoxide is produced during the C-CO_2 reaction. Before CO is desorbed into the gaseous phase, it has a two-dimensional mobility on the surface. During this mobility, CO may collide with pyrite particles producing COS which in turn may dissociate at the reaction temperature into CO and S. This sulfur may be chemisorbed on the char surface. It is known that sulfur and oxygen are chemisorbed essentially at the same active carbon sites (6). Since the first step in the overall gasification process is the dissociative chemisorption of the reactant gas at the active carbon sites, it is obvious that following chemisorption of sulfur the extent of oxygen chemisorption and, hence, gasification rate will be retarded.

Reactivity in H_2 Most of the minerals have an effect, either catalytic or inhibitive, on the hydrogasification reaction. Siderite and pyrite show large catalytic activity. Both these minerals contain iron as a major component. X-ray diffraction studies revealed that during the hydrogasification reaction both these minerals are reduced to elemental iron. It is well known that metallic iron catalyzes the C-H_2 reaction. Illite, gypsum, rutile, kaolinite and calcite have an inhibitive effect on the hydrogasification reaction. The inhibitive effect is most pronounced for calcite. Although it is difficult to explain unequivocally the inhibitive effect of various minerals, we suggest the following reason for the observed behavior. Most inorganic impurities catalyze carbon gasification by providing active sites at which dissociation of reactant molecules can readily occur (2). The dissociated species then diffuse across the substrate surface and react with the active carbon atoms. It is suggested that in the case of the minerals which have an inhibiting effect on char reactivity the reverse of molecular hydrogen dissociation is predominant. That is, H_2 is dissociated at active sites on the char surface producing hydrogen atoms. Some hydrogen atom recombination on the surface of the minerals results in a reduction in the rate of char hydrogasification.

ACKNOWLEDGEMENTS

This research was supported by ERDA on Contract E(49-18)-2030.

REFERENCES

1. Walker, P. L., Jr., Rusinko, F. J. and Austin, L. G., in "Advances in Catalysis", Vol. 11, p. 133, Academic Press, New York, 1959.

2. Walker, P. L., Jr., Shelef, M. and Anderson, R. A., in "Chemistry and Physics of Carbon" (P. L. Walker, Jr., Ed.), Vol. 4, p. 287, Marcel Dekker, New York, 1965.

3. Cariaso, O. C. and Walker, P. L., Jr., Carbon, 13, 233 (1975).

4. Jenkins, R. G., Nandi, S. P. and Walker, P. L., Jr., Fuel, 52, 288 (1973).

5. Tomita, A., Mahajan, O. P. and Walker, P. L., Jr., Fuel, Communicated.

6. Puri, B. R., in "Chemistry and Physics of Carbon" (P. L. Walker, Jr., Ed.), Vol. 6, p. 191, Marcel Dekker, New York, 1970.

UNIFICATION OF COAL CHAR GASIFICATION REACTIONS

P. L. Walker, Jr., O. P. Mahajan and Richard Yarzab

Material Sciences Department, Pennsylvania State University
University Park, Pennsylvania 16802

INTRODUCTION

In the conversion of coal chars to gaseous fuels, the four important gasification reactions are:

$$C + O_2 \rightarrow CO \text{ and } CO_2$$

$$C + CO_2 \rightarrow 2\ CO$$

$$C + H_2O \rightarrow CO + H_2$$

$$C + 2H_2 \rightarrow CH_4$$

We have studied extensively in this laboratory these reactions on coal chars produced from a complete spectrum of American coals from anthracite to lignite (1-4). For each reaction we have found a major increase in char reactivity with decreasing rank of the coal from which the char is produced. Such increase has been explained to be consistent with the three important parameters which control gasification rates of microporous chars. That is, as chars are produced from coals of decreasing rank under fixed conditions of charring, the concentration of carbon sites active to gasification increases, the accessibility of reactant gases to these active sites increases, and the specific activity of inorganic impurities towards catalysis of gasification increases.

In calculating reactivities in the past we have used the simple expression

$$R = \frac{1}{w} \cdot \frac{dw}{dt}$$

where either w is the starting weight of dry, ash-free char and dw/dt is the maximum value found as burn-off proceeds or w represents char weights remaining at various values of time t and dw/dt represents slopes at corresponding times such that R is found to be constant over some burn-off range. It was noted that even though there were major differences in char reactivity (R) as the rank of the parent coal from which chars were produced was changed, the shape of the burn-off versus reaction time plots appeared to be quite similar. If this is so, all reactivity plots should be able to be normalized using an adjustable time parameter, τ, which can conveniently be used as a measure of differences in reactivity for a wide spectrum of chars. This paper concerns itself with examining the feasibility of such a normalizing procedure.

EXPERIMENTAL

Char Preparation U. S. coals varying in rank from anthracite to lignite of 40x100 mesh size were used for the preparation of chars. Information on the coals is given in Table 1. The coals were heated in a N_2 atmosphere at a rate of 10°C/min to 1000°C and held for 2 hr.

Reactivity Measurements Burn-off versus time plots were determined for various chars in air (1 atm) at 405°C, CO_2 (1 atm) at 900°C, steam (.022 atm) at 910°C, and H_2 (27.2 atm) at 980°C. Under these conditions, mass transport resistance to diffusion of reactants down through the shallow bed of char particles (about 3mg)

had a negligible effect on gasification rates; gasification rates could be conveniently measured by weight loss using TGA.

RESULTS AND DISCUSSION

The principle of normalizing reactivity plots is shown in Figures 1 and 2. Figure 1 shows burn-off versus time plots for the lignite char, PSOC-91, reacted in various partial pressures of O_2 at a total O_2-N_2 pressure of 1 atm. As expected, the gasification rate decreases sharply with decreasing O_2 pressure. Figure 2 shows that these individual reactivity plots can be well normalized using a dimensionless time scale such that $t/\tau_{0.5}$ equals one at a fractional burn-off of 0.5. Values of $\tau_{0.5}$, or the times to reach a fractional burn-off of 0.5, decrease from 61.0 min to 14.8 min as the percentage O_2 in the reactant mixture is increased from 2 to 21%.

Figure 2 is more or less typical of the shape of burn-off versus $t/\tau_{0.5}$ plots found for all chars reacted in all gases. That is, at low values of $t/\tau_{0.5}$ there is an increase in slope of the plot, as $t/\tau_{0.5}$ increases. The plot then goes through a maximum in slope, followed by a lengthy region of slowly decreasing slope as fractional burn-off approaches one. Qualitatively, at this time, plots of this shape can be explained on the basis of what is known about the development of porosity and surface area in microporous chars as they undergo gasification. Before gasification, these chars contain closed porosity, that is porosity inaccessible even to helium. With the onset of gasification, two important phenomena occur: i) enlargement of pores that were open in the unreacted char and ii) opening up of closed pores. Since the total number of pores is increased as well as their average radius, specific pore volume and specific surface area increase with increasing carbon burn-off. The specific surface area increases sufficiently rapidly as $t/\tau_{0.5}$ increases that the product of specific area and char weight remaining, that is total area remaining, increases. The result is an increasing slope of the burn-off versus $t/\tau_{0.5}$ plot. At some point, depending upon the pore structure of the individual char, walls between existing pores are gasified away; and the total number of open pores commences to decrease. This leads to specific pore volume and specific surface area ultimately going through maxima as burn-off proceeds. It leads then to the slope of the burn-off versus $t/\tau_{0.5}$ plot going through a maximum value as burn-off proceeds.

This qualitative picture ignores the effect which catalysis by inorganic impurities can have on the shape of the burn-off curve. For example, if a catalyst is initially very active but as burn-off proceeds becomes less active because of sintering or change in chemical state, the $t/\tau_{0.5}$ region over which the gasification rate is increasing can be shortened or indeed removed completely. That is, the maximum rate can be observed immediately as gasification commences. In this case, the catalytic effect on gasification is obviously overshadowing the effect of increase in specific pore volume and specific surface area.

With these points in mind, it is of interest to see the extent to which one equation, with $\tau_{0.5}$ being the only adjustable parameter, can unify all the char reactivity data obtained in this paper.

Computer correlation of data for each gasification medium was conducted, as well as computer correlation of data for all gasification media. Burn-off versus time data for a fractional burn-off up to 0.7 were used in all cases. The suitability of the following equations to correlate the data was tested: a linear equation between burn-off and $t/\tau_{0.5}$, an equation involving first and second power terms in $t/\tau_{0.5}$, an equation involving first and third power terms in $t/\tau_{0.5}$, and an equation involving first, second, and third power terms in $t/\tau_{0.5}$. The latter equation gave the best correlation of the data.

Tables 2 and 3 summarize the results. For the char produced from coal PSOC-140, ten reactivity runs were made with steam. For the ten determinations, a 95% confidence interval on the mean value of $\tau_{0.5}$ is ±0.8. Table 2 shows the wide variation of $\tau_{0.5}$ values found for the chars in each reaction medium as the rank of coal from which the chars were produced changes. Generally, $\tau_{0.5}$ values for each reactant gas fall in the same order, but there are exceptions, as expected, which reflect the uniqueness of each reaction. For example, values of specific catalytic activity of impurities for each reaction are not expected to fall in the same order.

Table 3 presents the best values for coefficients in the cubic equations between fractional burn-off and $t/\tau_{0.5}$ for each reactant, as well as for all reactants. R^2 values give how much of the sum of variance, assuming no correlation between burn-off and $t/\tau_{0.5}$, can be removed by the particular cubic equation. It is obvious that for each individual reactant and also for all reactants the equations given result in a high correlation of results for burn-off versus $t/\tau_{0.5}$.

As discussed earlier, each char-reactant gas mixture shows some region of $t/\tau_{0.5}$ over which the reaction rate is first order in amount of char remaining. Thus computer correlations were also made with the first order model, $\ell n[1/(1 - BO)] = k(t/\tau)$, where BO is fractional burn-off. These results are also summarized in Table 3. If the data perfectly obeyed the first order model, k must equal 0.69 since $t/\tau_{0.5} = 1.0$ at BO = 0.5. Different reactions are seen to be more or less closely described, over a fractional burn-off range up to 0.7, by a first order equation. A reasonably good correlation is found for the C-air reaction, and a low correlation is found for the C-CO_2 reaction.

The success of the cubic equation to further correlate reactivity data was studied for other reaction conditions. It was successful in correlating data for the char-steam reaction as the partial pressure of steam and reaction temperature were varied.

From these studies, it is concluded that a good parameter to use to correlate char reactivity data is the time required to reach a fractional burn-off of 0.5. When this parameter is used, it is also shown that all of our char gasification data can be successfully normalized into burn-off versus $t/\tau_{0.5}$ plots of almost similar shape. Since char reactivity runs also exhibit a $t/\tau_{0.5}$ region where rate is first order in weight of char remaining, it probably is desirable to give first order rate constants for each run over the particular $t/\tau_{0.5}$ region in order to adhere to the more conventional treatment of kinetic data.

ACKNOWLEDGEMENT

This research was supported by ERDA on Contract E(49-18)-2030. Professor W. Spackman, Jr. supplied the coals studied.

REFERENCES

1. Jenkins, R. G., Nandi, S. P., and Walker, P. L., Jr., Fuel, 52, 288 (1973).

2. Hippo, E. and Walker, P. L., Jr., Fuel, 54, 245 (1975).

3. Tomita, A., Mahajan, O. P., and Walker, P. L., Jr., "Reactivity of Heat-Treated Coals in Hydrogen", Fuel, communicated.

4. Linares, A., Mahajan, O. P., and Walker, P. L., Jr., "Reactivities of Heat-Treated Coals in Steam", ACS Fuel Chemistry Division Preprints, New Orleans, March, 1977.

TABLE 1 - COALS USED TO PRODUCE CHARS

PSOC Sample No.	ASTM Rank	State	Ash, % (dry)	C	H	N	Org S
89	Lignite	N.D.	11.6	63.3	4.7	0.48	0.98
91	Lignite	Mon.	7.7	70.7	4.9	0.80	0.30
87	Lignite	N.D.	8.2	71.2	5.3	0.56	0.46
140	Lignite	Tex.	9.4	71.7	5.2	1.30	0.72
138	Lignite	Tex.	10.3	74.3	5.0	0.37	0.51
98	Sbb. A	Wyo.	8.4	74.3	5.8	1.20	1.1
101	Sbb. C	Wyo.	6.1	74.8	5.1	0.89	0.30
26	HVB	Ill.	10.8	77.3	5.6	1.10	2.3
22	HVC	Ill.	10.1	78.8	5.8	1.60	1.8
24	HVB	Ill.	11.8	80.1	5.5	1.10	2.3
67	HVB	Ut.	4.8	80.4	6.1	1.30	0.38
171	HVA	W.Va.	7.6	82.3	5.7	1.40	1.8
4	HVA	Ky.	2.1	83.8	5.8	1.60	0.66
114	LV	Pa.	9.8	88.2	4.8	1.20	0.62
81	Anthracite	Pa.	7.8	91.9	2.6	0.78	0.54
177	Anthracite	Pa.	4.3	93.5	2.7	0.24	0.64

TABLE 2 - $\tau_{0.5}$ VALUES FOR GASIFICATION RUNS

PSOC Sample No.	$\tau_{0.5}$ for Different Reacting Gases, min			
	Air	Steam	CO_2	H_2
89	-	-	5.5	43.5
91	14.8	10.6	5.0	36.5
87	30.0	11.4	-	24.0
140	29.6	19.6	10.3	34.0
138	69.5	28.0	17.0	32.0
98	66.4	-	26.0	50.0
101	21.6	13.6	7.0	37.5
26	121	138	200	59.0
22	99.0	64.0	54.0	33.5
24	78.5	51.0	30.0	32.0
67	134	152	220	34.5
171	-	260	-	96.0
4	-	114	-	49.0
114	-	-	-	126
81	-	255	270	51.5
177	-	330	-	110

TABLE 3 - UNIFICATION OF COAL CHAR GASIFICATION REACTIONS

Reactant	No. of Chars	Cubic Model				First Order	
		a	b	c	R^2	Slope	R^2,%
Air	10	0.317	0.367	-0.182	96.0	0.756	94.1
CO_2	11	0.436	0.189	-0.122	99.2	0.728	78.4
H_2O	13	0.375	0.276	-0.148	99.1	0.761	87.4
H_2	16	0.349	0.283	-0.144	96.6	0.693	88.6
All	50	0.368	0.277	-0.147	98.2	0.727	87.5

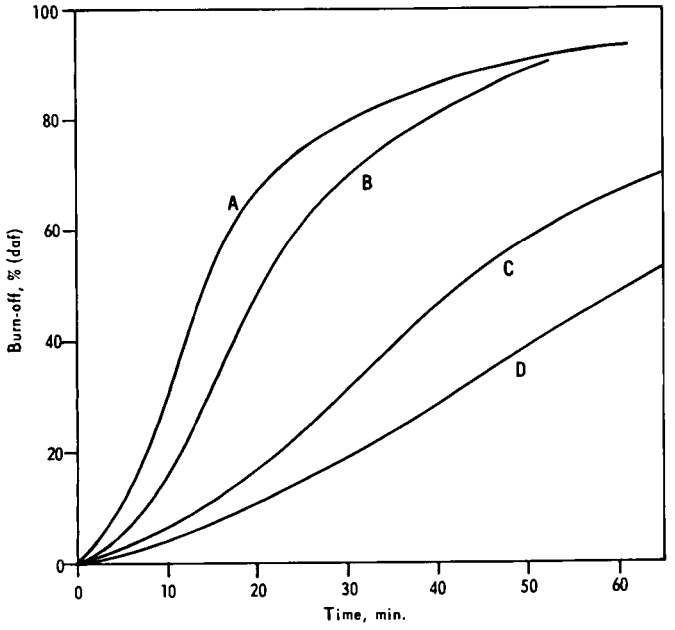

Figure 1. Influence of oxygen concentration on reactivity of PSOC-91 char at 405°C. A, 21% O_2; B, 10% O_2; C, 4% O_2; D, 2% O_2.

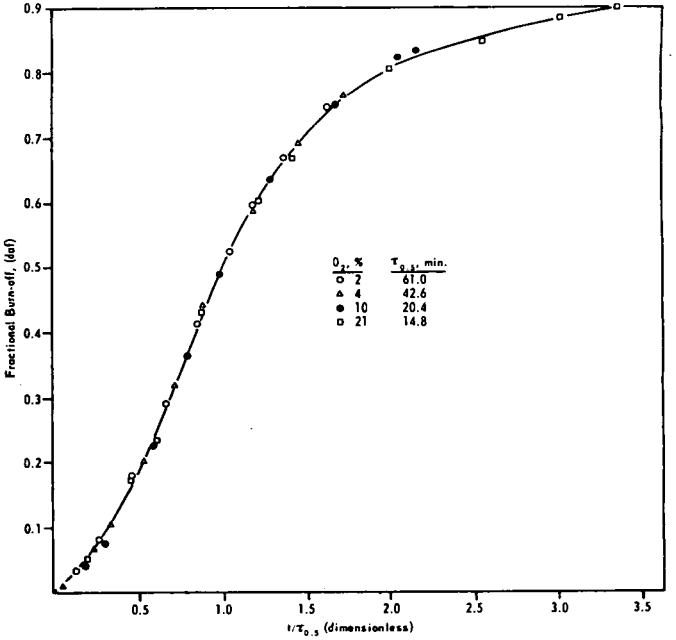

Figure 2. Normalized plot for reaction of PSOC-91 char at 405°C in different concentrations of O_2.

THE REACTIVITY OF COAL CHARS WITH CO_2 AT 1100-1600°C

Ralph T. Yang and Meyer Steinberg
Department of Applied Science
Brookhaven National Laboratory
Upton, New York 11973

INTRODUCTION

Knowledge of the coal char reactivity in the temperature range 1100-1600°C is of fundamental importance in understanding many coal gasification and direct combustion processes. However, due to the intricate interplay of the diffusional steps and the chemical or surface step in this temperature range,(1) studies in this area have been relatively rare compared to studies in the lower temperature range. Recently, a diffusion cell technique has been developed at Brookhaven for measuring the chemical rates in the diffusion/chemical reaction combined-controlled region and the technique has been applied to studies of the kinetics of the reactions between CO_2 and a nuclear graphite in the temperature range of 1200-1600°C.(2) In this paper, we wish to report the initial results of the kinetics of the same reaction at a total pressure of 1 atm using coal chars of varying rank.

EXPERIMENTAL

Apparatus

The apparatus and the gas flow system are essentially the same as described previously,(2) except that the flow system was built on a Cahn-R100 null-type balance instead of a Mettler TA-1 balance. This reactor system is capable of 1700°C and 15 atm or higher pressures and is described elsewhere.(3) It would suffice in this report to note that the alumina diffusion cell had a dimension of 16 x 24 (diameter and length) and the gas flow was downward and at the same flow rate as in the previous work.(2)

Sample Materials and Preparation

The coal samples used were:

Pennsylvania Anthracite,
Illinois No. 6 Bituminous ,and
Montana (Rosebud) Lignite,

all kindly supplied by the Pittsburgh Energy Research Center. The samples were carbonized in N_2 at 1000°C for 16 hrs and subsequently ground and sieved to the size range of 590-840 microns which was the size used throughout this work. A demineralized Montana Lignite sample was also prepared by leaching the sample in a combined acid solution (6.2 M HCl and 7.4 MHF) at 50°C for 48 hrs. The leached sample was rinsed thoroughly and dried and was then carbonized and sized.

DATA TREATMENT

The chemical rates were calculated by using the following solution of the binary-diffusion equation for the diffusion cell:

$$R = \frac{cD\ k_1}{cD = k_1 \ell} \log\ (1 + P_{CO_2}) \qquad (1)$$

where R is the overall rate or the mass flux which was measured gravimetrically; C the molar concentration of the diffusion gases; D the approximate binary-diffusion coefficient; ℓ the path length and P_{CO_2} the partial pressure of CO_2 in the bulk stream. k_1 is the rate constant in the Langmuir-Hinshelwood rate expression and is defined by:

$$R = k_1\ P_{CO_2} \text{ at the surface (or } \ell = 0) \qquad (2)$$

Detailed discussion of these equations and the calculation of D in the temperature range being studied can be found in reference (2). The value of k_1 calculated with equation (1)is in general 2-4% higher than that calculated by using the solutions of the exact multi-component diffusion equations.(2) Also, k_1 is based on per unit area of the cross section of the diffusion cell. Discussion of the usage of this unit and the depth of the reaction zone in the particles can also be found in references (2) and (8).

RESULTS AND DISCUSSION

The rate constant k_1 calculated from equation (1) represents the intrinsic chemical reactivity of the carbon surface. To obtain k_1, a series of measurements of R at varying P_{CO2} were first made, a linear plot of R vs log $(1 + P_{CO_2})$ was then obtained and k_1 was calculated from this plot according to equation (1). The value of k_1 varied with the percentage carbon burn-off and in this work, the value of k_1 was taken in the burn-off range of 20-40%.

In Figure 1, the first kinetic data are summarized for the three coal samples and the leached lignite at selected temperatures. The most prominent feature in this figure is the peaking (or plateauing) of the rate constant at varying temperatures. Except for the anthracite, the peak temperatures are too low to be related to the well-known peaking phenomenon of the reactivity of graphite.(2-6) However, an excellent match can be obtained between the peak temperature and the temperature range for melting of the ash. The three coal samples present a wide range of the ash melting temperatures. The ash softening temperatures (supplied by the Pittsburgh Energy Research Center) and the ash content in the chars (average value of at least three samples) are shown in Table 1. The k_1 measured for the leached Montana lignite showed that the peaking (or plateauing) does not

occur around 1200°C. This result indicates that the match between the peak temperature and the ash melting temperature is not coincidental.

Below the peaking temperatures, the reactivity of the char obeyed the general rule; lignite > bituminous > anthracite. This aspect has been discussed by Walker and Hippo. (7) At higher temperatures, this rule can no longer be applied, as shown in Figure 1. For example, the reactivity of the Illinois No. 6 bituminous coal char is about twice as that of the lignite at 1400°C and the reactivity of the anthracite can also exceed that of the lignite at about 1500°C. Peaking of the reactivity of the anthracite char may be attributable to the peaking phenomenon due to carbon alone. (2-6) The slight plateauing of the rate of the leached sample at above 1300°C was probably due to the residual ash in char.

An attempt was also made to elucidate the relationship between the reactivity and the melting of the minerals by measuring the surface areas of the samples heat-treated at above and below the ash melting temperature. The results are shown in Table 1. Unfortunately, the surface area measured is a total surface area of the carbon and the minerals. Thus, the results of the surface area measurements do not contribute to the proposition that the molten minerals could flow in the micro-structure; covering the surface sites as well as blocking the accessible pores. Nevertheless, this phenomenon is being further investigated in our laboratory.

ACKNOWLEDGEMENT

Professor Robert H. Essenhigh of Penn State University made helpful suggestions. Robert Smol is acknowledged for performing the surface area measurements and calculations. This work was performed under the auspices of the Office of Molecular Sciences, Division of Physical Research, U. S. Energy Research and Development Administration, Washington, D. C.

REFERENCES

1. Walker, P. L., Jr., Rusinko, F., Jr., and Austin, L. G., Adv. Catal., 11, 134 (1959).
2. Yang, R. T. and Steinberg, M., Ind. Eng. Chem. Fundam., accepted for publication.
3. Smol, R., Steinberg, M., and Yang, R. T., Thermochimica Acta, in preparation.
4. Nagel, J. and Strickland-Constable, R. F., Proc. Fifth Carbon Conf., 1, 154 (1962). Pergamon Press, Oxford and New York.
5. Rosner, D. E., Ann. Rev. Mater. Sc., 2, 573 (1972).
6. Rosner, F. E., and Strakey, J. P., Jr., Surface Sc., 24, 77 (1971).
7. Walker, P. L., Jr. and Hippo, E. J., ACS Div. Fuel Chem. Preprints, 20(3), 43 (1975).
8. Golovina, E. S., Soloveka, L. S., and Samsonov, V. G., Solid Fuel Chemistry (Engl. Transl. from Russ.) 8, 127 (1974).

Table 1. Ash content and softening temperature

Char	Ash Content, % of Char	Softening Temp., °C
Pa. Anthracite	5	> 1600
Ill. No. 6 Bitum.	17	1350
Montana Lignite	21	1200
Leached Lignite	2.4	--

Table 2. BET N_2 surface area of Montana lignite chars

Treatment	Surface Area, m^2/g
carbonized at 1000°C	11.9
leached and carbonized at 1000°C	20.2
carbonized at 1400°C	38.4
leached and carbonized at 1400°C	28.5

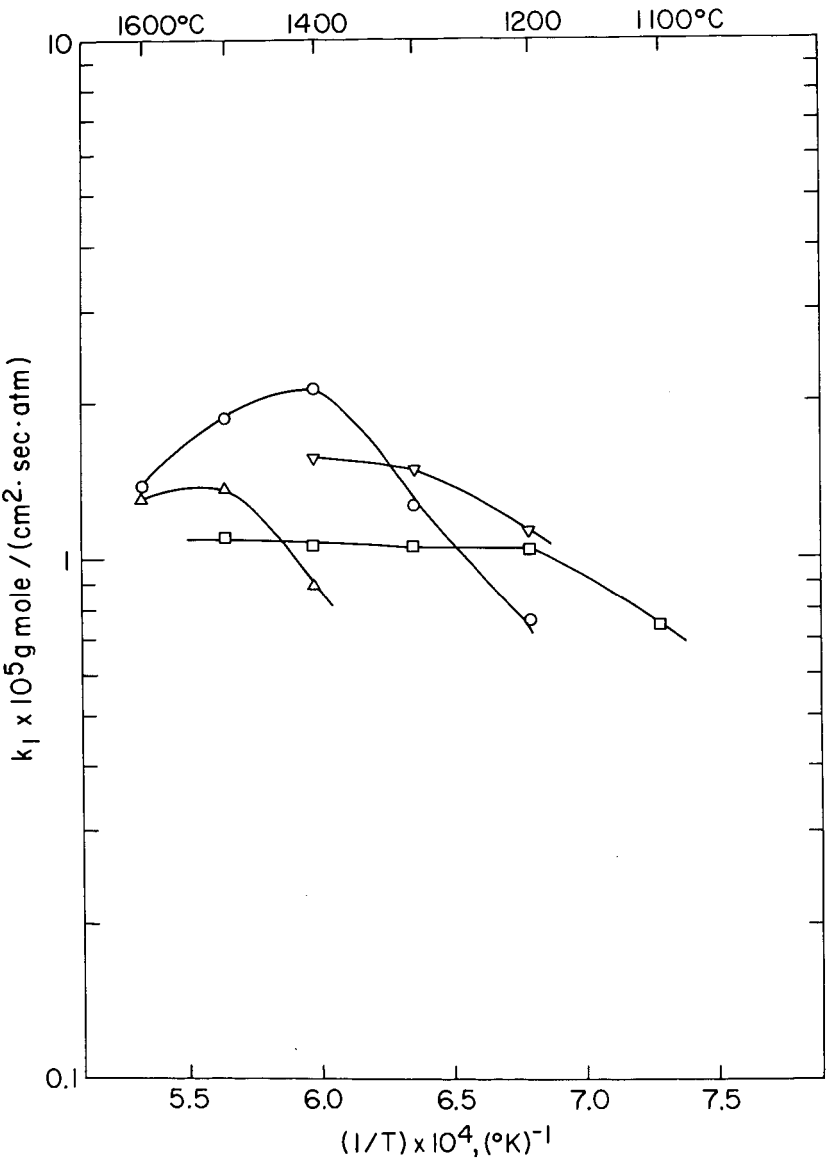

Figure 1. Rate constant vs temperature for the following chars: Pa. Anthracite (Δ), Illinois No. 6 Bituminous (O), Montana Lignite (□), and leached Montana Lignite (▽).

KINETICS OF INITIAL COAL HYDROGASIFICATION STAGES

James L. Johnson

Institute of Gas Technology
3424 South State Street
Chicago, Illinois 60616

INTRODUCTION

For the last 15 years a strong incentive has existed in the United States to develop the technology for commercial gasification of coals to yield high-methane-content gas suitable as a substitute for natural gas. One of the general conclusions derived from the many experimental studies conducted is that the yield of light gaseous hydrocarbons, obtained during initial coal heat-up and for very short periods thereafter, plays an important role in affecting the overall performances and thermal efficiencies of any gasification process. It is during this initial gasification stage that coals undergo devolatilization reactions leading to the formation of carbon oxides, water, oils and tars, and, most importantly, significant quantities of light hydrocarbons — particularly methane — in the presence of hydrogen at elevated pressures. Since, however, the exceptionally high reactivity most coals exhibit for methane formation during initial reaction stages is transient, existing only for a period of seconds at higher temperatures, rational design of commercial systems to optimize methane yields requires as detailed a kinetic characterization of pertinent processes occurring as is possible.

Because of its importance, this reaction has been studied in a variety of experimental investigations using fixed beds (1, 2, 8-12, 17), fluidized beds (3, 4, 12, 17), and dilute solid-phase systems (5-7, 13-16, 19, 20). In spite of the extensive amount of information obtained from these studies, however, primary emphasis in the development of kinetic correlations has been placed on description of the total methane yields obtained after relative deactivation of coal solids has occurred rather than on the more detailed behavior occurring during the transient period of "rapid-rate" methane formation.

An experimental study was therefore initiated at the Institute of Gas Technology (IGT) to supplement existing information, with the objective of quantitatively characterizing intermediate reaction processes occurring prior to completion of the rapid-rate methane-formation reaction. This paper discusses some of the main results obtained thus far in our study of the gasification kinetics of low-rank coals in hydrogen, helium, and hydrogen-helium mixtures. The kinetic models developed to describe light gaseous hydrocarbon formation during initial reaction stages of the coals tested are also described and applied to selected results obtained in other studies directed toward gasification of high-volatile bituminous coals.

EXPERIMENTAL

A schematic diagram of the experimental apparatus used in the study is shown in Figure 1; the details of this system have been described previously (13). The main component of the system is a 1.6-mm internal diameter, 60-m long, helical coiled transport reactor. The reactor tube itself serves as the heating element with electrodes attached along the length of the coil to provide nine independent

heating zones. This unique feature permits the establishment of temperature profiles along the length of the reactor tube that correspond to the desired constant heat-up rates of gas-solids mixtures passing through the tube. The reactor can also be operated isothermally. Coal particles (0.074 to 0.089-mm diameter) are mixed with feed gases at the top of the reactor coil, and the dilute gas-solids mixture (less than 0.1% solids by volume) passes through the reactor coil at temperatures very close to those imposed on the reactor wall. The char produced is collected in a sintered metal filter heated to 300°C for subsequent solids analyses. The gas then passes through a condenser system to collect water and condensable hydrocarbons. The dry gas is analyzed with a mass spectrograph (periodic samples) for major gaseous species and, in some tests, with a flame ionization detector for the concentration of total carbon in hydrocarbon species.

Steady-state conditions are achieved in less than 1 minute after initiation of gas and coal flows, and sufficiently large gas/solid feed ratios are employed to result in less than 5% dilution of the dry exit gas with reaction products. Thus, the partial pressures of feed-gas components remain essentially constant throughout the reactor tube. The main gaseous products measured include carbon monoxide (CO), carbon dioxide (CO_2), hydrogen (H_2), methane (CH_4), and ethane (C_2H_6). Other noncondensable gaseous hydrocarbons, particularly three- and four-carbon aliphatics and possibly some ethylene, were not usually accurately measured with the mass spectrograph due to the low concentrations present. The total carbon in this species group, referred to as C_3+, was determined by difference – that is, by subtracting the carbon in methane and ethane from the total carbon in gaseous hydrocarbon species determined by flame ionization detection. Condensable liquid products were also difficult to quantitatively recover in the laboratory-scale equipment due to the relatively small quantities available. Product water was therefore determined by an oxygen balance and condensable oils and tars by a carbon balance.

TYPICAL RESULTS

The gasification kinetics of three low-rank coals – Montana lignite, Montana subbituminous coal, and North Dakota lignite – were investigated. The compositions of these three coals are given in Table 1, which also includes compositions of several other coals referred to in this paper.

Figure 2 shows some typical product yields obtained for gasification of Montana lignite in hydrogen at 35 atm under conditions of a constant heat-up rate of 30°C/s. With this lignite, devolatilization initiates at some temperature below 500°C. Coal oxygen is evolved primarily as carbon dioxide, carbon monoxide, and water, with a small amount being observed in phenolic oils. Carbon dioxide evolution occurs below 500°C, apparently resulting from decomposition of carboxyl functional groups. Decomposition of other oxygenated functional groups leads to evolution of both carbon dioxide and water, with total available coal oxygen evolution being completed at about 700°C. This is shown more clearly in Figure 3. Although carbon dioxide yields begin decreasing above 650°C, this is due solely to the secondary reaction –

$$CO_2 + H_2 \rightarrow CO + H_2O$$

occurring in the reactor coil, probably catalyzed by the reactor walls.

Table 1. COAL ANALYSES

	Montana Lignite	Montana Subbituminous (This Study)	North Dakota Lignite	Pennsylvania High-Volatile A Bituminous (Ref. 6)	Pennsylvania High-Volatile A Bituminous (Ref. 14)	Pennsylvania High-Volatile A Bituminous (Ref. 11)	Illinois High-Volatile C Bituminous (Ref. 6)	Illinois High-Volatile Bituminous (Ref. 9)	Warwickshire (Eng.) High-Volatile Bituminous (Ref. 16)
Ultimate Analysis, wt% (MAF)									
Carbon	68.61	73.10	70.30	83.93	84.00	82.81	80.26	77.59	80.70
Hydrogen	4.35	4.53	4.47	5.54	5.70	5.69	5.44	5.80	5.86
Oxygen	25.50	19.73	23.60	7.66	7.10	7.70	11.07	10.58	13.44
Nitrogen	0.94	1.16	0.99	1.70	1.70	1.68	1.83	1.25	13.44
Sulfur	0.60	1.48	0.64	1.17	1.50	2.12	1.40	4.78	13.44
Total	100.00	100.00	100.00	100.00	100.00	100.00	100.00	100.00	100.00
Proximate Analysis, wt% (MAF)									
Volatile Matter	45.95	42.45	44.91	39.10	40.90	37.83	39.69	--	38.94
Fixed Carbon	54.05	57.55	55.09	60.90	59.10	62.17	60.31	--	61.06
Total	100.00	100.00	100.00	100.00	100.00	100.00	100.00	--	100.00

B76091862

Oil and tar as well as C_3+ gaseous hydrocarbon evolution occurs below 550°C. C_3+ gaseous hydrocarbon yields decrease, however, above 650°C due to hydrogenation to methane and ethane. Total yields of oil and tar remain relatively constant up to 850°C, although the composition of this fraction changes substantially with increasing temperature, becoming lighter in nature. Conversion of heavier oils to benzene initiates at about 650°C, and, at 850°C, approximately one-half of the total oil/tar fraction consists of benzene.

Methane-plus-ethane yields* increase continuously with increasing temperature, with rates of formation becoming substantial above 600°C. Above 700°C, when primary devolatilization processes are virtually completed, gasification of the intermediate coal structure (semi-char) is the primary reaction that occurs concurrently with the secondary devolatilization of coal hydrogen, leading to the formation of relatively nonreactive coal char. Methane-plus-ethane yields increase significantly with increasing hydrogen pressure, as shown in Figure 4. This contrasts with the kinetics of evolution of primary devolatilization products, which depend for the most part on time-temperature history and not on gas composition or pressure over the ranges of these variables employed.

The main qualitative features exhibited for gasification of Montana lignite in hydrogen at a heat-up rate of 30°C/s were also observed for the other coals tested and for other time-temperature histories. As would be expected, yield-versus-temperature curves such as those shown in Figure 2 are shifted somewhat toward higher temperatures at an increased heating rate of 80°C/s and are shifted toward lower temperatures for isothermal operation with a gas-solids residence time of 7 seconds. Significantly, however, the maximum yields of primary devolatilization products (carbon dioxide, carbon monoxide, water, oils and tars, and C_3+ gaseous hydrocarbons) that can be achieved at sufficiently high temperatures appear to depend solely on coal type rather than on pressure, gas composition, or time-temperature history. This behavior is probably typical only of noncaking low-rank coals. With caking bituminous coals different behavior would be expected, particularly with respect to maximum oil and tar yields, which tend to increase with increased heat-up rate, decreased coal-particle size, and decreased total pressure.

DATA ANALYSIS

A primary objective of this investigation is to quantitatively describe the kinetics of the initial-stage methane-plus-ethane formation for different coals as a function of hydrogen partial pressure and coal time-temperature history. The total methane-plus-ethane yields obtained in the gasification of coals with hydrogen result primarily from three overall reaction processes: direct coal hydrogenation, thermally activated coal-decomposition reactions, and secondary hydrogenation of C_3+ gaseous hydrocarbons. Although some methane and ethane could also be formed by hydrogenation of light oils such as benzene, these reactions should not occur significantly at the conditions employed in this study (18).

---

* Methane and ethane yields are grouped together since it has been previously shown (13) to be likely that, after initial devolatilization, both species are direct products of hydrogen gasification of the coal.

Methane and Ethane From Coal-Decomposition and Secondary Hydrogenation Reactions

In order to isolate the kinetics of direct coal hydrogenation, it is necessary to determine the contributions of coal-decomposition reactions and secondary hydrogenation reactions to total methane-plus-ethane yields. Since a fundamental approach to such evaluations would be extraordinarily complex, if practically possible at all, simplifying approximations and assumptions were made to obtain first-order estimates. Figure 5 shows methane-plus-ethane yields obtained for gasification of Montana lignite in helium at 35 atm for a constant heat-up rate of 30°C/s, and for isothermal operation with a coal-gas residence time of 7 seconds. Based on these data, the methane-plus-ethane obtained from coal decomposition was assumed to occur in two stages: below 600°C a fixed fraction is instantaneously evolved, and, above this temperature, yields increase linearly with increasing temperature up to 780°C when conversion is complete. The assumption that the kinetics of this reaction are independent of coal residence time implies a wide distribution of activation energies for the decomposition steps leading to methane-plus-ethane formation. It was also assumed that the kinetics of this decomposition reaction in a helium atmosphere also apply in a hydrogen atmosphere.

Figure 6 shows yields of C_3+ gaseous hydrocarbons obtained in hydrogen and in helium for gasification of Montana lignite at a coal heat-up rate of 30°C/s. In helium the C_3+ hydrocarbons initially formed do not undergo pyrolysis at higher temperatures up to 810°C, whereas, in hydrogen the yield of this fraction begins to decrease above about 600°C due to hydrogenation to methane and ethane. The overall hydrogenation reactions occurring were assumed to be equivalent to a single first-order reaction:

$$C_3\text{+ gaseous hydrocarbons} \xrightarrow{k_4} \text{methane-plus-ethane}$$

The complete correlation to describe methane-plus-ethane formation from coal thermal decomposition and hydrogenation of C_3+ hydrocarbons has the following form:

$$N = N_0 \left[\alpha' X' + \alpha'' X'' + \alpha''' X'''\right] \qquad 1)$$

where,

X' = conversion fraction of thermal decomposition reactions below 600°C

X'' = conversion fraction of thermal decomposition reactions above 600°C

X''' = conversion fraction of C_3+ hydrogenation reactions

N_0 = total carbon in methane-plus-ethane that can be formed from thermal decomposition and C_3+ hydrogenation reactions, g-atom/g-atom feed carbon in coal

N = carbon in methane-plus-ethane formed from thermal decomposition and C_3+ hydrogenation reactions at any time, g-atom/g-atom feed carbon in coal

$\alpha', \alpha'', \alpha'''$ = coefficients defining the distribution of carbon that can be converted to methane-plus-ethane from the three reactant groups considered.

Based on data obtained with the three low-rank coals used in this study, and on some limited data available in the literature for gasification of a bituminous coal in hydrogen, the following numerical evaluations were made:

$$\alpha' = 0.2$$
$$\alpha'' = 0.3$$
$$\alpha''' = 0.5$$

	N_0, g-atom carbon/g-atom feed carbon in coal
lignite	0.05
subbituminous coal	0.08
bituminous coal	0.10

$$X' = 1.0$$

$$X'' = 0 \text{ at } T < 873°K$$

$$X'' = 0.00555T - 4.845 \text{ for } 873° \leq T \leq 1053°K \qquad 2)$$

$$X'' = 1.0 \text{ for } T > 1053°K$$

and,

$$\frac{dX'''}{d\theta} = k_4(1 - X''')$$

$$k_4 = 1.7(10^4)\exp(-11,830/T),\ s^{-1} \qquad 3)$$

where,

T = temperature; °K in Equations 2 and 3

θ = time, s.

Although the model described above is much oversimplified, it does provide an approximate basis consistent with the data obtained to numerically adjust methane-plus-ethane yields to correspond only to direct coal hydrogenation.

Kinetics of Direct Coal Hydrogenation

In a previous paper (13), a model was proposed to describe the kinetics of the initial stages of direct coal hydrogenation, based only on data obtained with Montana lignite and using a different method to adjust methane-plus-ethane yields than is described above. These data were reevaluated in the context of all the data available at the present time, using the same model assumed previously but with modified and more generally applicable evaluations of kinetic parameters.

A main feature leading to the development of the model is the strong correlation that exists between adjusted methane-plus-ethane yields and coal hydrogen evolution during the secondary devolatilization stage. This behavior is shown in Figure 7 where, at constant hydrogen partial pressure, methane-plus-ethane yields are directly proportional to the secondary coal hydrogen evolved, independent of time-temperature history. Conveniently, the trends exhibited at a specific pressure level cannot be differentiated for the different coals considered. The slopes of the lines drawn in Figure 7 increase with increasing hydrogen pressure, consistent

with qualitative observations made in other investigations of the rapid-rate methane phenomenon.

Variations in coal hydrogen evolution with increasing temperature are described in Figure 8. For a given time-temperature history the amount of coal hydrogen evolved is essentially independent of gaseous hydrogen pressure, and the results obtained with Montana lignite (Figure 8A) show similar behavior in both helium and hydrogen atmospheres.

The results given in Figures 7 and 8 suggest that the formation of active sites, which promote methane-plus-ethane formation through interaction of gaseous hydrogen with the coal, is directly related to the processes in which coal hydrogen is evolved; this latter process involves only thermally activated phenomena occurring independently of gaseous atmosphere and dependent only on time-temperature history. A formal representation of this model is given by the following reactions:

$$CH^0_x \xrightarrow{k_0} CH^*_y \qquad \text{Reaction I)}$$

semi-char — (thermally activated coal hydrogen evolution) — active-intermediate

$$CH^*_y \xrightarrow{k_1} (1-m)CH^0_y \quad \text{(inactive char)}$$

$$CH^*_y \xrightarrow{k_2 \text{ (gaseous hydrogen)}} m\left[zCH_4 + \frac{(1-z)}{2} C_2H_6\right] \qquad \text{Reaction II)}$$

where,

x = atomic ratio of hydrogen to carbon in CH^0_x

y = atomic ratio of hydrogen to carbon in CH^*_y and CH^0_y

z = fraction of carbon gasified as methane in Reaction II

k_0, k_1, k_2 = first-order rate constants, s^{-1}

m = $k_2/(k_1 + k_2)$.

For purposes of quantitative correlation the following definitions are made:

Y = total carbon in adjusted methane-plus-ethane yields, g-atom/g-atom feed carbon

n_H = total coal hydrogen gasified at any time, g-atom/g-atom feed carbon

n^0_H = total coal hydrogen gasified during primary devolatilization, g-atom/g-atom feed carbon

λ = fraction of total feed carbon not evolved as primary devolatilization products (closely related to fixed carbon), g-atom/g-atom feed carbon.

With this model the rate of Reaction I is assumed to be limiting, with the rate of Reaction II being very fast. In addition the ratio k_2/k_1 is assumed to be temperature-independent. From these definitions the conversion fraction, f, of the semi-char CH_x^0 to active-intermediate CH_y^* can be expressed by the relationship:

$$f = Y/m\lambda = (n_H - n_H^0)/(x - y + my)\lambda \qquad 4)$$

From Equation 4 the methane-plus-ethane yield, Y, is related to coal hydrogen evolved by:

$$Y = \frac{m(n_H - n_H^0)}{(x - y + my)} \qquad 5)$$

or,

$$Y = S(n_H - n_H^0) \qquad 6)$$

where,

$$S = \frac{m}{(x - y + my)} \qquad 7)$$

Equation 6 is consistent with the trends given in Figure 7. The slopes, S, of the lines drawn in Figure 7 are tabulated in Table 2, and the value of n_H^0 estimated from Figure 7 is about 0.27, corresponding to the value of coal hydrogen evolved due to primary devolatilization reactions.

The following independent relationship also results from the model assumed:

$$Y(1/S - Z) = \lambda(x - Z) \qquad 8)$$

where,

Z = the atomic hydrogen-to-carbon ratio in the coal at any time during gasification

Table 2. VARIATION IN S WITH HYDROGEN PRESSURE

Hydrogen Pressure, atm	S, g-atom carbon/g-atom hydrogen
18	0.24
35	0.41
52	0.56

Using values of S given in Table 2, at appropriate hydrogen pressures, values of the term $Y(1/S - Z)$ were plotted versus Z for the three coals tested and for the bituminous coal study to yield values of λ and x. A value of $\lambda = 0.80$ was applicable for all the coals considered. A value of $x = 0.65$, obtained for the bituminous coal, was slightly higher than a value of $x = 0.62$, obtained for the two lignites and the subbituminous coal. With these evaluations, values of m were computed as a function of pressure by rearranging Equation 7:

$$m = \frac{S(x - y)}{1 - Sy} \qquad 9)$$

with a value of $y = 0.10$ assumed as a nominal average value based on gasification data obtained with different coals at elevated temperatures for extended times.

Values of m and corresponding values of k_2/k_1 are given in Table 3, and values of k_2/k_1 are plotted versus hydrogen pressure in Figure 9. The linear relationship shown in Figure 9 is represented by the equation:

$$k_2/k_1 = 0.0083P_H \qquad 10)$$

where,

P_H = hydrogen partial pressure, atm.

Table 3. VARIATION OF m AND k_2/k_1 WITH HYDROGEN PRESSURE

Hydrogen Pressure, atm	m	k_2/k_1
18	0.127	0.145
35	0.225	0.290
52	0.307	0.443

From the evaluations made, the adjusted methane-plus-ethane yield is related to the conversion fraction, f, of the semi-char by the relationship:

$$Y = m\lambda f = \frac{0.00664P_H}{1 + 0.0083P_H} \cdot f \qquad 11)$$

In analyzing the kinetics of Reaction I to quantitatively define the functional dependence of f on reaction conditions, the same model described in a previous paper was adopted. The main assumptions of this model are as follows:

- CH_x^0 reacts according to Reaction I by a first-order process, but where there is a distribution of activation energies for the first-order rate constant, k_0.
- The distribution function of activation energies is a constant; i.e., f(E)dE = fraction of total carbon in which the activation energy, E, in the rate constant —

$$k_0 = k_0^0 \exp(-E/RT)$$

is between E and (E + dE).

where,

$f(E) = 0$ for $E < E_0$

$f(E) = C$ (constant) for $E_0 \leq E \leq E_1$

$f(E) = 0$ for $E > E_1$

k_0^0 = pre-exponential factor, s^{-1}

Note that because —

$$\int_{E_0}^{E_1} C\,dE = 1$$

then —

$$C = 1/(E_1 - E_0)$$

From these assumptions, the average conversion fraction of CH_x^0 can be expressed by the following relationship for any time-temperature history:

$$1 - f = \frac{1}{E_1 - E_0} \int_{E_0}^{E_1} \left\{ \exp \left[-k_0^0 \int_0^{\theta} \exp(-E/RT) d\theta \right] \right\} dE \qquad 12)$$

Statistical procedures were used to evaluate the parameters k_0^0, E_0, and E_1 given below, based on best consistency of experimental values of f computed from Equation 4 and calculated values of f computed from Equation 12 for the appropriate time-temperature history:

$k_0^0 = 1.97(10^{-10})$, s^{-1}

$E_0 = 40.8$ kcal/g-mol

$E_1 = 62.9$ kcal/g-mol.

A comparison between experimental and calculated values of f is given in Figure 10. A comparison of experimental total methane-plus-ethane yields and values calculated from the models and numerical evaluations presented in this paper is given in Figure 11.

Although it may be tempting to consider theoretical implications concerning the detailed mechanisms of coal hydrogen evolution during secondary devolatilization, based on the values of k_0, E_0, and E_1 given above, such considerations should be made cautiously. Because of the sensitivity of these evaluations to the statistical numerical procedures employed, and because of the strong covariance between these parameters, significantly different evaluations can be made to reasonably describe data obtained over a wide range of conditions. This point is illustrated in Figure 12, where variations in values of conversion, f, that were calculated using values of the kinetic parameters determined in this study are compared to values of f calculated using a significantly different set that nevertheless describes the same data quite well. This is particularly true for coal residence times ranging from 1 to 10 seconds, which represent the range of conditions most commonly employed in various investigations of initial coal gasification kinetics. The illustration in Figure 12 was constructed to show the magnitude of differences in evaluation of kinetic parameters that could occur in describing data obtained over a wide range of residence times and temperatures for isothermal conditions. Much greater ranges of estimates could result, however, in describing conversions obtained at a single residence time over a wide range of temperatures, or, alternatively, at a single temperature over a wide range of residence times. Thus, although the model proposed does suggest a mechanistic relationship between coal hydrogen evolution and active site formation for coal hydrogenation, the numerical evaluations made to facilitate practical application of the information obtained for reactor design do not provide a substantial basis for a more detailed mechanistic understanding.

Application of Model to Bituminous Coal Gasification

The experimental study described has been limited to use of low-rank coals to minimize plugging of the small-diameter reactor tube employed. It was of interest, however, to make an approximate analysis of some data obtained in other investigations concerned with gasification of high-volatile bituminous coals in

hydrogen-containing gases to obtain an indication of the possible applicability of the model developed to describe behavior with bituminous coals. Figure 13 shows yields of methane-plus-ethane obtained in a variety of studies conducted over a wide range of conditions. Indicated values of coal and gas residence times and hydrogen partial pressures were either reported directly or were deduced from other reported information. The hydrogen partial pressure used for correlation corresponds to the product gas. For systems where significant conversion of the feed gas occurs, which is the case in most of the systems considered, this representation assumes substantial backmixing in the gasification reactor. In all of the studies, either hydrogen or hydrogen-methane mixtures were used as feed gases. The analyses of the feed coals used in the various studies are included in Table 1.

In interpreting the data given in Figure 13, the model developed in this study was assumed. According to this model, experimental values of the function m should vary with hydrogen pressure according to the expression:

$$m = \frac{0.0083P_H}{1 + 0.0083P_H} \qquad 13)$$

Values of m were computed from experimental values of adjusted methane-plus-ethane yield, Y, using the expression:

$$m = Y/\lambda f$$

where $\lambda = 0.80$. Values of Y were computed by subtracting the values of N computed from Equation 1 from the experimental values of total methane-plus-ethane yield. Evaluations of N were made for the appropriate reported gas-solids residence times and reaction temperatures, using a value of $N_0 = 0.10$, estimated for bituminous coal. Values of f were computed using Equation 9 (with values of k_0^0, E_0, and E_1 developed in this study), also at the reported reaction conditions.

In Figure 14, the values of m computed from experimental results obtained with bituminous coals are compared to Equation 13. For hydrogen partial pressures up to about 120 atm, reasonable consistency exists, suggesting that the model developed is applicable for gasification of bituminous coals as well as for gasification of subbituminous coals and lignites.

SUMMARY

The results obtained in this study indicate that the initial gasification of low-rank coals in hydrogen-containing gases at elevated pressures occurs in two stages. The first stage involves thermally activated devolatilization reactions resulting in the evolution of carbon oxides, water, oil and tar, and some light gaseous hydrocarbons, and leading to the formation of an intermediate semi-char. The second stage occurs consecutive to primary devolatilization and involves thermally activated decomposition reactions associated with the secondary devolatilization of remaining coal hydrogen, leading to the formation of a relatively nonreactive char. Significantly, yields of methane-plus-ethane, other than that derived from thermal coal-decomposition reactions or from C_3+ light hydrocarbon hydrogenation reactions, are stoichiometrically related to coal hydrogen evolved during the secondary devolatilization stage. This has suggested a model in which the transitions that occur in conversion of semi-char to char, with associated coal hydrogen evolution, involve the formation of a reactive intermediate carbon

structure that can either rapidly react with gaseous hydrogen to form methane and ethane or can convert to nonreactive char. The ratio of methane-plus-ethane formation to char formation is independent of temperature but is directly proportional to hydrogen partial pressure.

A numerical representation of this model permits detailed prediction of the kinetics of methane-plus-ethane formation for practical application to reactor design for systems using low-rank coals. A strong possibility that this model might also be suitable for application to gasification of high-volatile bituminous coal was also suggested, based on analyses of some available data obtained in other investigations.

ACKNOWLEDGMENT

This paper is based on work conducted at the Institute of Gas Technology with support from the American Gas Association.

LITERATURE CITED

1. Anthony, D. G., "Rapid Devolatilization and Hydrogasification of Pulverized Coal," Sc. D. thesis, Massachusetts Institute of Technology, Cambridge, Mass., 1974.

2. Anthony, D. G. et al., "Rapid Devolatilization and Hydrogasification of Bituminous Coal," Fuel 55, No. 2, 121-28 (1976) April.

3. Birch, T. J., Hall, K. R. and Urie, R. W., "Gasification of Brown Coal With Hydrogen in a Continuous Fluidized Bed Reactor," J. Inst. Fuel 33, 422-35 (1960) September.

4. Blackwood, J. D. and McCarthy, D. J., "The Mechanism of Hydrogenation of Coal to Methane," Aust. J. Chem. 19, 797-813 (1966) May.

5. Feldmann, H. F. et al., "Reaction Model for Bituminous Coal Hydrogenation in a Dilute Phase." Paper presented at the 160th National Meeting of the American Chemical Society, Division of Petroleum Chemistry, Chicago, September 13-18, 1970.

6. Feldmann, H. F., Mima, J. A. and Yavorsky, P. M., "Pressurized Hydrogasification of Raw Coal in a Dilute-Phase Reactor," Coal Gasification, in Adv. Chem. Ser. No. 131 (1974).

7. Glenn, R. A., Donath, E. E. and Grace, R. J., "Gasification of Coal Under Conditions Simulating Stage 2 of the BCR Two-Stage Super-Pressure Gasifier," Fuel Gasification, in Adv. Chem. Ser. No. 69 (1967).

8. Graff, R. A., Dobner, S. and Squires, A. M., "Products of Flash Hydrogenation," in the Proceedings of the 170th National Meeting of the American Chemical Society, Division of Fuel Chemistry, Vol. 20, No. 3, 23-32 (1975).

9. Graff, R. A., Dobner, S. and Squires, A. M., "Flash Hydrogenation of Coal. 1. Experimental Methods and Results. 2. Yield Structure for Illinois No. 6 Coal at 100 Atm.," Fuel 55, No. 2, 109-15 (1976) April.

10. Hiteshue, R. W., Friedman, S. and Madden, R., "Hydrogasification of Bituminous Coals, Lignite, Anthracite, and Char," U.S. Bur. Mines Rep. Invest. No. 6125 (1962).

11. Hiteshue, R. W., Friedman, S. and Madden R., "Hydrogasification of a High-Volatile A Bituminous Coal," U.S. Bur. Mines Rep. Invest. No. 6376 (1964).

12. Johnson, J. L., "Kinetics of Bituminous Coal Char Gasification With Gases Containing Steam and Hydrogen," Coal Gasification, in Adv. Chem. Ser. No. 131 (1974).

13. Johnson, J. L., "Gasification of Montana Lignite in Hydrogen in a Continuous Fluidized Bed Reactor," in the Proceedings of the 170th National Meeting of the American Chemical Society, Division of Fuel Chemistry, Vol. 20, No. 3, 61-87 (1975).

14. Lewis, P. F., Friedman, S. and Hiteshue, R. W., "High Btu Gas by Direct Conversion of Coal," Fuel Gasification, in Adv. Chem. Ser. No. 69 (1967).

15. Mosely, F. and Patterson, D., "The Rapid High-Temperature Hydrogenation of Coal Chars. Part 2: Hydrogen Pressures up to 1000 Atmospheres," J. Inst. Fuel 38, 378-91 (1965) September.

16. Mosely, F. and Patterson, D., "The Rapid High-Temperature High-Pressure Hydrogenation of Bituminous Coal," J. Inst. Fuel 40, 523-30 (1967) November.

17. Pyrcioch, E. J., Feldkirchner, H. L., Tsaros, C. L., Johnson, J. L., Bair, W. G., Lee, B. S., Schora, F. C., Huebler, J. and Linden, H. R., "Production of Pipeline Gas by Hydrogasification of Coal," IGT Res. Bull. No. 39. Chicago, November 1972.

18. Woebcke, H. N., Chambers, L. E. and Virk, P. S., "Thermal Synthesis and Hydrogasification of Aromatic Compounds," Coal Gasification, in Adv. Chem. Ser. No. 131 (1974).

19. Zahradnik, R. L. and Glenn, R. A., "Direct Methanation of Coal," Fuel 50, 77-90 (1971) January.

20. Zahradnik, R. L. and Grace R. J., "Chemistry and Physics of Entrained Coal Gasification," Coal Gasification, in Adv. Chem. Ser. No. 131 (1974).

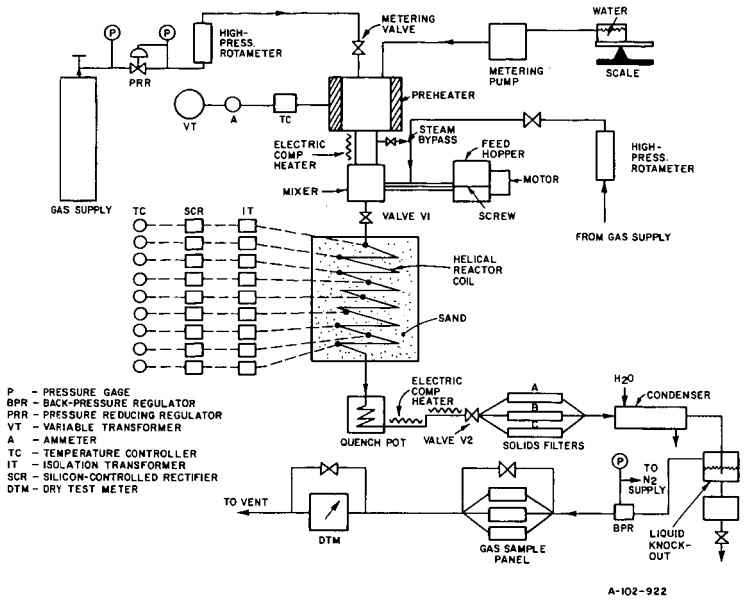

Figure 1. DIAGRAM OF THE EXPERIMENTAL SYSTEM

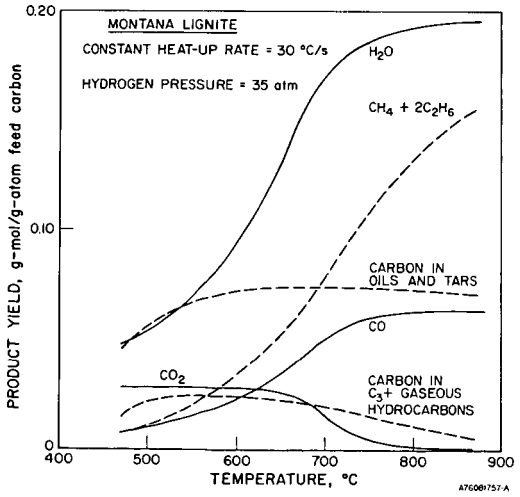

Figure 2. TYPICAL PRODUCT YIELDS FOR GASIFICATION IN HYDROGEN

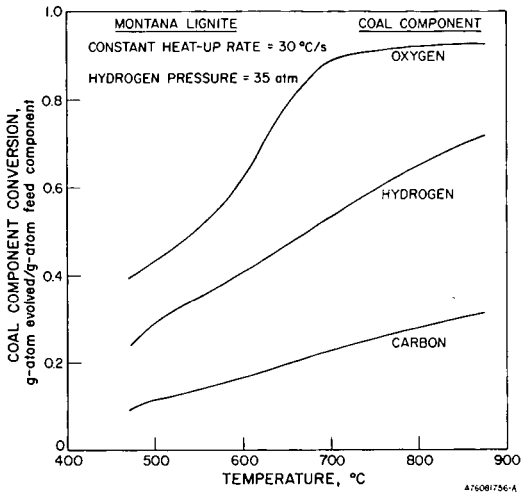

Figure 3. TYPICAL COAL COMPONENT CONVERSION DURING GASIFICATION IN HYDROGEN

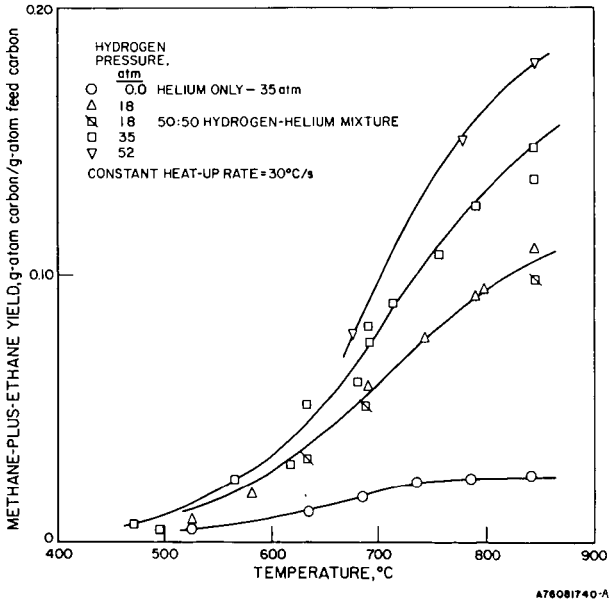

Figure 4. EFFECT OF PRESSURE ON TOTAL METHANE-PLUS-ETHANE YIELDS DURING GASIFICATION OF MONTANA LIGNITE

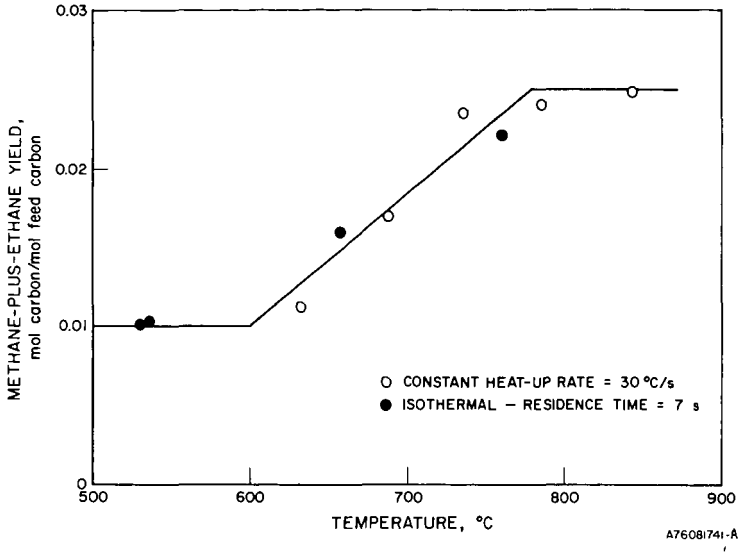

Figure 5. METHANE-PLUS-ETHANE YIELDS FROM PYROLYSIS OF MONTANA LIGNITE IN HELIUM AT 35 atm

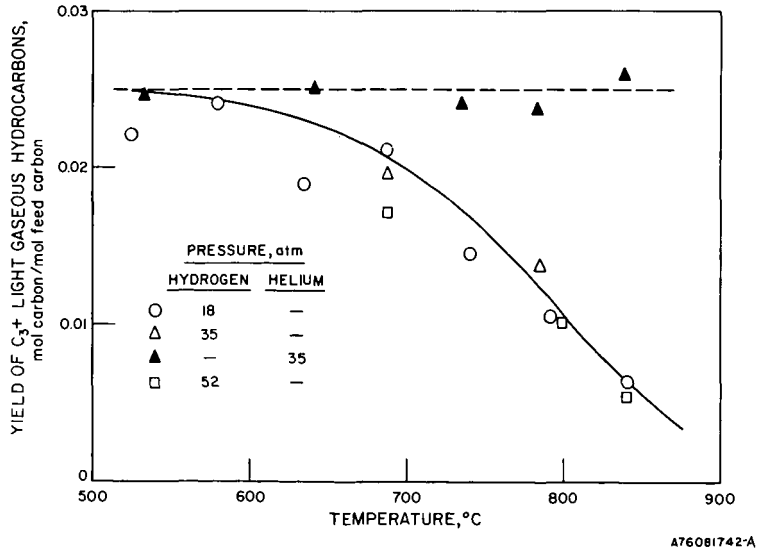

Figure 6. C_3+ LIGHT GASEOUS HYDROCARBON YIELDS FROM GASIFICATION OF MONTANA LIGNITE IN HYDROGEN OR HELIUM (Constant Gas-Coal Heat-Up Rate = 30°C/s)

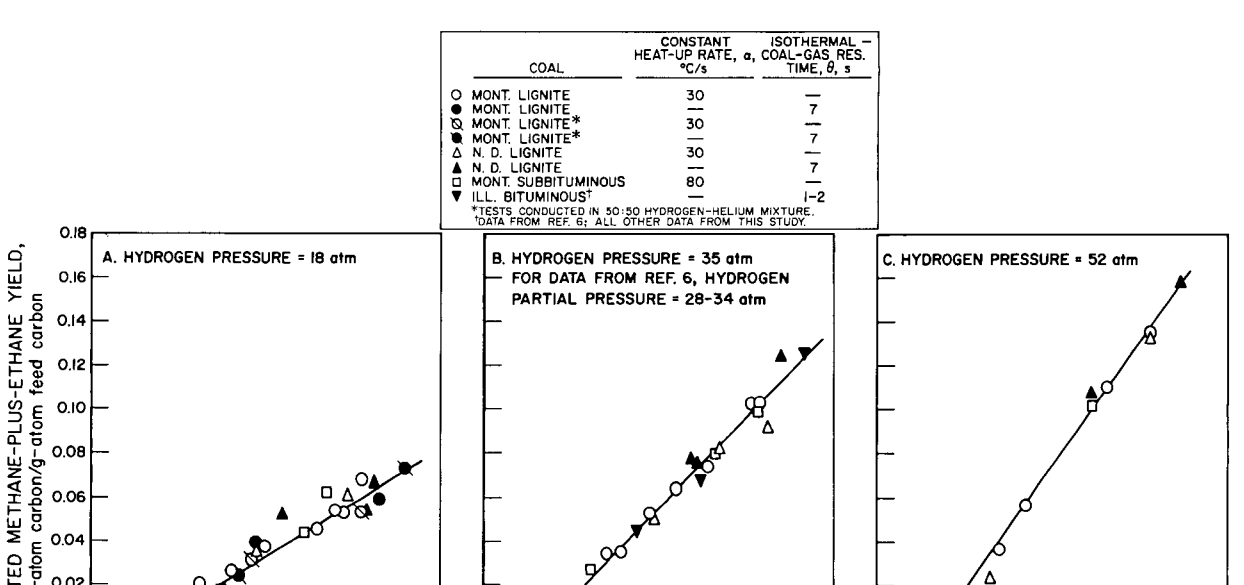

Figure 7. STOICHIOMETRIC RELATIONSHIP BETWEEN ADJUSTED METHANE-PLUS-ETHANE YIELD AND COAL HYDROGEN EVOLUTION

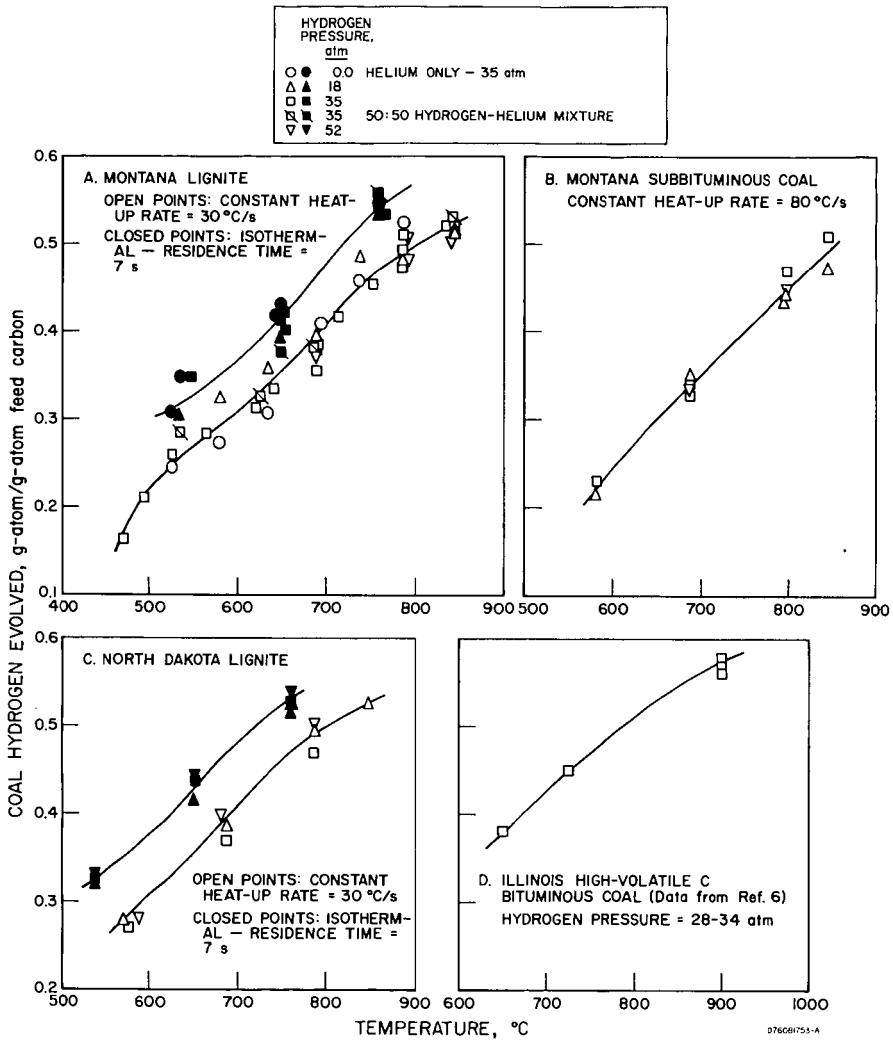

Figure 8. COAL HYDROGEN EVOLUTION DURING GASIFICATION OF DIFFERENT COALS

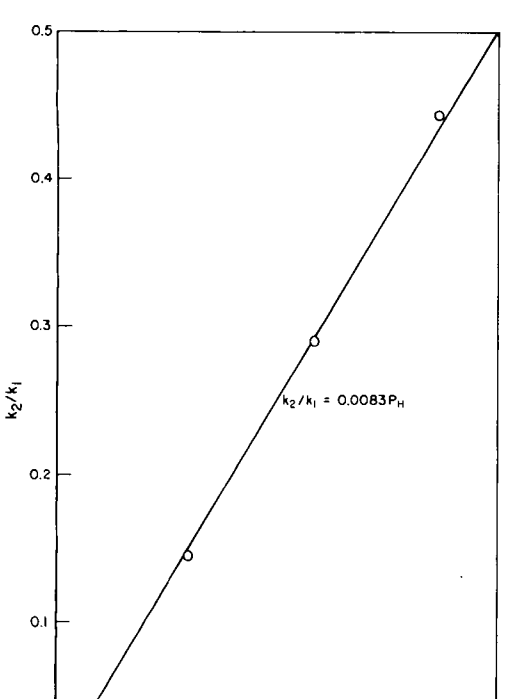

Figure 9. CORRELATION OF RELATIVE RATE RATIO, k_2/k_1, WITH HYDROGEN PRESSURE

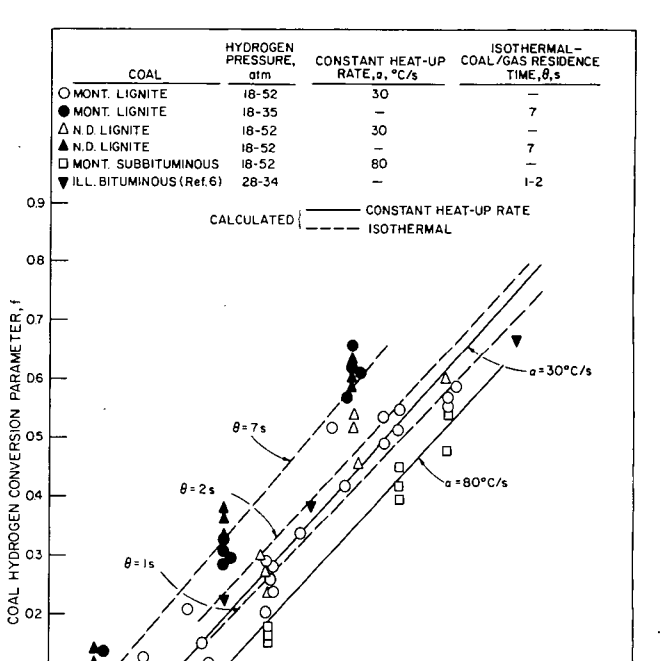

Figure 10. COMPARISON OF CALCULATED AND EXPERIMENTAL COAL HYDROGEN CONVERSION

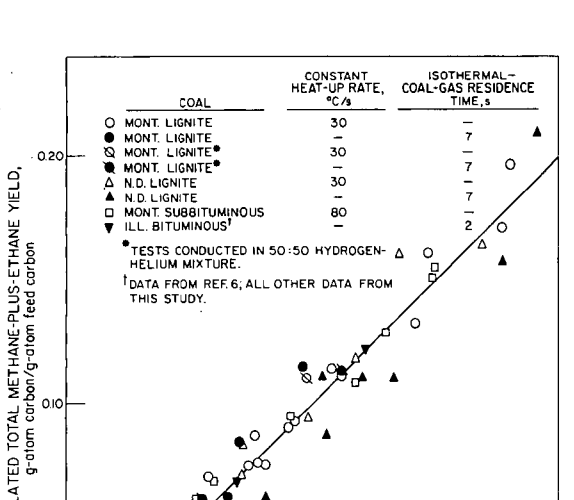

Figure 11. COMPARISON OF CALCULATED AND EXPERIMENTAL TOTAL METHANE-PLUS-ETHANE YIELDS

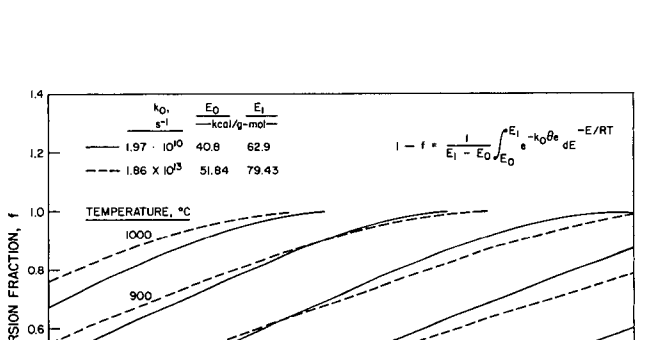

Figure 12. COMPARISON OF MODEL CHARACTERISTICS WITH DIFFERENT SETS OF KINETIC PARAMETERS

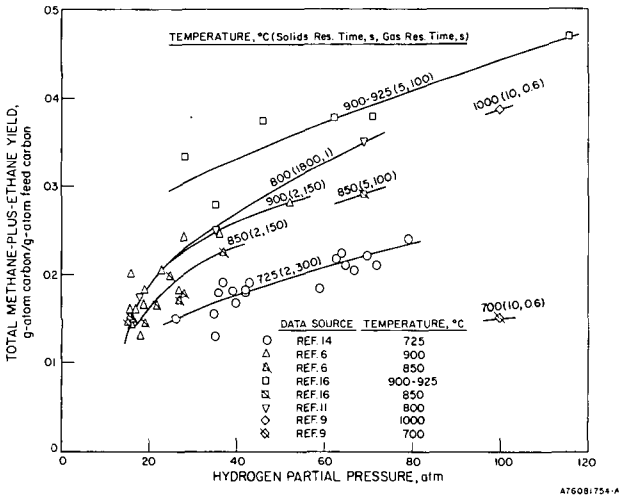

Figure 13. TOTAL METHANE-PLUS-ETHANE YIELDS OBTAINED IN DIFFERENT STUDIES FOR GASIFICATION OF BITUMINOUS COALS WITH HYDROGEN

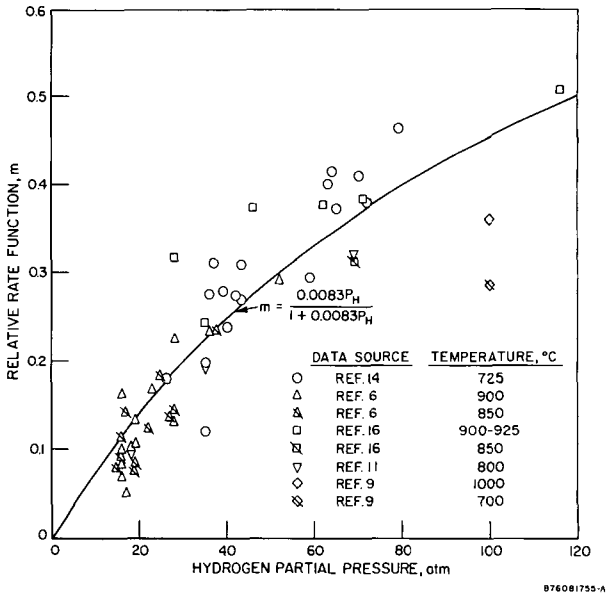

Figure 14. CORRELATION OF METHANE-PLUS-ETHANE YIELDS OBTAINED IN VARIOUS INVESTIGATIONS FOR HIGH-VOLATILE BITUMINOUS COAL GASIFICATION IN HYDROGEN

A NOVEL APPROACH TO GASIFICATION OF COAL USING CHEMICALLY INCORPORATED CATALYSTS

S. P. Chauhan, H. F. Feldmann, E. P. Stambaugh, and J. H. Oxley

Battelle, Columbus Laboratories
505 King Avenue, Columbus, Ohio 43201

K. Woodcock and F. Witmer

Energy Research and Development Administration
Washington, D.C. 20545

INTRODUCTION

Battelle's Columbus Laboratories is developing new approaches to gasification of coal, with ERDA sponsorship, using known gasification catalysts that are chemically incorporated into the coal. The chemical incorporation of a catalyst is achieved by treating the coal with the catalyst and water at elevated temperatures and pressures, usually in the presence of an aqueous alkali solution. The process is a modification of the proprietary Hydrothermal Coal Process for reducing the sulfur content of coal (1).

Earlier work on chemical incorporation of gasification catalysts was done with in-house funds using the "so-called" power-plant grind or 70 percent minus 200 mesh coal since the process was originally intended for producing a low-sulfur fuel suitable for pulverized firing in boilers. In earlier work, coal was treated with CaO (the catalyst) in the presence of a solution of NaOH. The results showed that the Battelle process completely eliminated the agglomeration (caking) tendency of highly-caking, Pittsburgh seam coal and greatly increased the hydrogasification and steam gasification reactivities (2). It was also found that the Battelle-treated coal, abbreviated as BTC, was much more reactive than coal impregnated with CaO by slurrying with CaO and water at room temperature followed by drying as is conventionally done.

Several catalyst systems have been studied so far. This paper is concerned with further development of the catalyst treatment system consisting of CaO, which is a (hydro)gasification* catalyst for coal, and NaOH which facilitates chemical incorporation of calcium species in coal. Specifically, the paper deals with (a) the effect of particle size of raw coal and catalyst treatment time on hydrogasification properties of BTC, (b) determination of product distribution for (hydro)gasification of BTC, (c) correlation between the properties of batch-produced BTC and continuously-produced BTC, and (d) advantages of using BTC over preoxidized coal.

PROCESS DESCRIPTION

In the case of the catalyst treatment system consisting of CaO and NaOH, the BTC for (hydro)gasification is prepared by four major processing steps. First, the coal of desired particle size is slurried with a mixture of CaO, NaOH, and water. Second, the coal-catalyst slurry is heated to an elevated temperature where it is held sufficiently long to allow chemical incorporation of calcium. Third, the catalyst-impregnated coal is separated and washed to remove excess water and sodium species which can be regenerated and reused. Fourth, and finally, the BTC is dried to the desired moisture level.

During the catalyst treatment, up to 3 percent calcium chemically binds to the coal while a controlled quantity of CaO is physically incorporated throughout the

*The term (hydro)gasification refers in this paper to both hydrogasification and steam gasification of coal.

coal particles. The evidence for chemical incorporation of calcium comes from experiments wherein the BTC was treated with a sugar solution to dissolve the physically-incorporated calcium.

The NaOH apparently helps facilitate the effective penetration and reaction of CaO with coal. It is postulated that NaOH first reacts with coal, opening up its structure and thus facilitating the diffusion of calcium into the coal particles, and then calcium displaces the sodium from coal along with reacting with reaction sites not containing sodium. Usually, a fraction of a percent of sodium remains in BTC after treatment either because of incomplete displacement of chemically-bound sodium by calcium or due to incomplete removal of physically-incorporated sodium by washing. More information on this is provided elsewhere (3).

EXPERIMENTAL DETAILS

The impregnation of coal with catalyst was carried out in a batch reactor system as well as a continuous reaction system called "Miniplant". The (hydro)gasification properties of the BTC produced in these reactor systems were determined in a high-pressure thermobalance (TGA) reactor and in a small, batch-solids fluid-bed gasifier. Table 1 shows the compostion of the raw coal, from Montour #4 mine of Pittsburgh #8 seam, used to product BTC.

TABLE 1. COMPOSITION OF RAW COAL

	Weight Percent
Proximate Analysis	
Moisture	0.70
Ash	9.95
Volatile Matter (dry)	37.5
Fixed Carbon (by difference)	51.9
Total	100.0
Ultimate Analysis	
Moisture	0.70
Ash	9.95
Carbon	73.5
Hydrogen	5.25
Nitrogen	1.4
Sulfur	2.6
Oxygen (by difference)	6.6
Total	100.0

Batch Treatment Reactor

The batch experiments on the production of BTC were conducted in a "quick-charge", one-gallon autoclave system shown schematically in Figure 1. In all experiments conducted, the mixture of coal, CaO, and water was heated to the operating temperature and then the NaOH solution was added to the preheated autoclave through the charging bomb. The operating temperature was regained within 3 to 5 minutes after charging NaOH, at which point the zero treatment (retention) time was recorded. Several samples of coal-catalyst slurry were withdrawn and then quickly cooled during an experiment in order to determine the effect of treatment time on properties of BTC.

The catalyst-impregnated (treated) coal was separated from the spent caustic solution and washed under nitrogen with distilled water to remove the excess sodium species and then dried under partial vacuum at 60°C in an inert atmosphere.

Continuous Treatment Reactor (Miniplant)

The experiments on the continuous production of BTC were conducted in the Miniplant system according to the flowsheet shown in Figure 2. The catalyst impregnation took place continuously in a series of stirred-tank reactors, the size and number of which depended on the treatment time and the pumping speed for the coal-catalyst slurry. The nominal pumping speed of the high-pressure pump was 6 gallons per hour. After catalyst impregnation, the product slurry was cooled and then passed through a pressure letdown valve. The BTC was separated from the spent caustic solution (which can be regenerated and reused) in a centrifugal filter, washed with tap water to remove sodium species and then dried in air in a rotary dryer. All processing steps until the first filtration were integrated into continuous operation.

High-Pressure Thermobalance Reactor

The tendency of BTC for agglomeration during hydrogasification and the hydrogasification reactivity relative to raw coal and preoxidized coal were determined in a high-pressure thermobalance reactor (TGA) system described earlier (2). During a thermobalance run, the mass of a coal sample is monitored continuously. From the mass versus time data, the MAF fractional conversion, X, versus time plots are obtained. A convenient way to compare the reactivity of one coal with another is to compare the times, t_x, required for a given fractional conversion, X. An average reactivity of BTC relative to raw coal, R_x, corresponding to a fractional conversion X, may thus be defined as

$$R_x = \frac{(t_x)_{\text{Raw Coal}}}{(t_x)_{\text{BTC}}} \qquad 1)$$

Some BTC and raw coal samples had to be pelletized prior to hydrogasification because they were too fine for the 100-mesh basket used for holding the samples. The rest of the samples, containing only a small amount of -60 mesh size particles, were screened to obtain the +60 mesh fraction for the thermobalance experiments.

Batch-Solids Fluid-Bed Gasifier

The batch-solids fluid-bed gasifier system, shown schematically in Figure 3, was used to determine product yield data for (hydro)gasification of BTC and preoxidized coal from the Synthane Process. The reactor tube was 1-1/2-inch I.D. x 3-inch O.D. x 48 inches long. The distributor plate was made of 100-mesh stainless steel screen and placed at the center of the reactor tube.

In all experiments conducted, a 50 g batch of coal was charged through an electrically-operated ball valve in less than 10 seconds to the heated reactor after establishing the desired feed gas rate. The off-gas was allowed to pass through, in order, a hot trap, a water condenser, a water trap, and a cold trap prior to gas analysis. The total volume of the product gas was determined with a dry gas meter. An infrared analyzer (IR) was used to continuously monitor the methane (CH_4) concentration of the product gas. A small bleed stream was taken from the product gas via an isokinetic probe to collect a sample for analysis by a gas chromatograph (GC) at the end of a run. The char was recovered from the reactor at the end of a run and weighed. Also, the weights of the glass wools placed in the hot trap and low-temperature trap were determined before and after a run to determine the yield of tar plus oil.

A carbon balance was made for each run. The product yield data were adjusted to obtain perfect carbon balances.

EXPERIMENTAL RESULTS

Effect of Particle Size and Treatment Time

Earlier work on (hydro)gasification of BTC was done using 70 percent minus 200 mesh coal. However, because of the problem in using 200 mesh or finer coal for the fluid-bed gasifier, it was desirable to know the effect of catalyst treatment time on the (hydro) gasification characteristics of BTC produced from coarser raw coal. Therefore, experiments were conducted on coals with particle size ranging from 6350 μm (0.25 inch) to 74 μm (200 mesh). The catalyst treatment was carried out at 250°C, in the presence of a solution of NaOH, using a CaO/coal ratio of 0.13. The experiments were conducted on coal ground and screened to the following sizes: 0.25 inch to 0.187 inch (4 mesh); -20+28 mesh; -35+48 mesh; -65+100 mesh; -150+200 mesh; and 70 percent -200 mesh. While nearly all of the calcium remained in the BTC, the sodium content increased from about 0.1 percent of MAF coal for 200 mesh coal to about 0.8 percent for 20 mesh coal due to inefficient washing of larger particles (3).

To illustrate the dependence of hydrogasification reactivity on coal particle size and coal treatment time, the time required to hydrogasify 50 percent of the MAF BTC is shown in Figure 4 as a function of coal treatment time and coal particle size. Figure 4 shows that the reactivity increases with treatment time, leveling off a value that does not seem to depend on the particle size. However, the time required to achieve maximum reactivity increases with particle size. For example, a treatment time of about 10 minutes is sufficiently long to achieve near-maximum reactivity with 70 percent minus 200 mesh coal, while 20 minutes are required to achieve nearly the same reactivity with -20+28 mesh coal. The BTC produced from 0.25-inch to 0.187-inch size raw coal was not hydrogasified since the particles were too large for the thermobalance reactor.

Figure 5 shows the complete thermobalance data for raw coals of different particle sizes as well as for BTC produced from these coals. For the treated coals, the time of treatment was 60 minutes which, according to the data shown in Figure 4, was longer than necessary. The reason for the somewhat higher reactivity for the coarser coal is that it was not pelletized which can lower the reactivity, depending on the compaction pressure used for pelletization. Figure 5 indicates the potential that treatment has for reducing the total reactor volume in a gasification plant. For example, if one assumes a 20-minute coal residence time is required for treatment, Figure 5 indicates the resulting BTC can be hydrogasified to a 65 percent conversion level in less than 3 minutes, while raw coal requires 90 minutes for the same level of conversion. Thus, the total volume required for treatment plus hydrogasification should be considerably less for BTC than for raw coal.

The data in Figure 5 show that the value of the average relative reactivity R_X, defined in Equation 1, increases with X. For example, for BTC from -20+28 mesh raw coal, the values of R_x at X equal to 0.5, 0.6, and 0.7 are 17, 29, and 49, respectively. This is due to the fact that raw coal is deactivated while BTC is not during hydrogasification, as discussed later.

The increase in hydrogasification reactivity due to treatment was found to be accompanied by a reduction in the tendency for agglomeration during hydrogasification and at the treatment time required to achieve maximum reactivity, the agglomerating tendency was completely eliminated. For example, treatment of -20+28 mesh coal for 20 minutes produced a completely nonagglomerating BTC, and treating the same raw coal for 11 minutes produced a BTC that had a slight tendency for agglomeration, while the raw coal had a severe tendency for agglomeration. Furthermore, it was found that coarser particles required a longer treatment time to completely destroy the agglomerating tendency of coal. For example, a treatment time of 10 minutes was sufficient to completely eliminate the agglomeration tendency of 70 percent minus 200 mesh coal, while BTC produced from -20+48 mesh coal after treatment for 11 minutes still had a slight tendency for agglomeration.

The free swelling index (FSI) of BTC treated for 120 minutes and raw coals were also determined in this study. The rationale for doing this was that FSI determination is easy and quick and that a zero value for FSI is a necessary (but not sufficient) condition for completely destroying the agglomeration tendency during hydrogasification. It was found that the FSI of raw coal particles as large as 0.25 inch could be lowered from 8 to 0 by the Battelle treatment. The treatment of 0.25-inch size particles was carried out to determine if the Battelle treatment could be used to produce nonagglomerating feedstock for moving-bed gasification systems such as Lurgi. The material balance data for treatment experiments showed that there was no loss of volatile matter or carbon, within errors of measurement, during catalyst treatment. On the other hand, preoxidation, which is commonly employed for reduction of FSI of coal, results in the loss of 20 percent or more volatile matter.

It should be pointed out that the CaO/coal ratio of 0.13, used in the above experiments, was about two times the ratio necessary to achieve maximum hydrogasification reactivity.

The steam gasification reactivity of BTC was not determined in the thermobalance because maximum steam gasification reactivity is achieved before maximum hydrogasification reactivity. Earlier data with fine coal showed that BTC having maximum steam gasification reactivity can be gasified at 675°C at about the same rate as raw coal at 850°C (2). (The activation energy for steam gasification of BTC was found to be 23 kcal/mole.) Based on earlier data, the times required for a fractional conversion of 0.7 at 850°C and 500 psig for raw coal and BTC (having maximum-possible hydrogasification reactivity) are expected to be about 50 minutes and 5 minutes, respectively.

Fluid-Bed Data for (Hydro)gasification of BTC and Preoxidized Coal

Experiments were conducted in a batch-solids fluid-bed gasifier to determine product distribution for BTC gasified with hydrogen, steam, and hydrogen plus steam. Because of the small size of BTC used (about 50 g) and because of problems with batch operation, only the carbon balance data could be obtained with reasonable accuracies. The results showed that not only the (hydro)gasification reactivity of BTC was as high as indicated by thermobalance data, but also that the yields of ethane (C_2H_6) and ethylene (C_2H_4) were much greater than observed with raw coal or preoxidized coal in commercial or advanced coal gasification processes.

Data were also obtained on the gasification of preoxidized coal from Synthane Process to make a direct comparison between the (hydro)gasification properties of BTC and preoxidized coal.

Hydrogasification Data. The yield data for three typical runs with BTC and one run with preoxidized coal are summarized in Table 2. These data show that under comparable treatment conditions, the total carbon conversion is much greater for BTC than for preoxidized coal because of the higher hydrogasification reactivity of BTC. The relative reactivity of BTC is actually much greater than may be apparent from the total carbon conversion data because most of the carbon gasified in the case of the preoxidized coal is actually the volatile carbon. In fact, it can be shown that the base carbon conversion for BTC in Table 2 is more than about three times that for preoxidized coal. The high hydrogasification reactivity of BTC compared to preoxidized coal is also demonstrated by the thermobalance data plotted in Figure 6. It can be seen from Figure 6 that the time for 70 percent conversion of MAF coal is less for BTC even though preoxidized coal is hydrogasified at 50°C higher in temperature and at 4 times the hydrogen partial pressure (i.e., 1000 psig versus 250 psig).

One of the most interesting observations in this study was that a very significant amount of carbon was converted to C_2H_4 and C_2H_6. For example, the combined conversion of carbon to C_2H_4 and C_2H_6 in Runs Nos. 9, 12, and 13 were 13.1, 22.3, and 14.4 percent, respectively. In fact, in Run No. 12, there was more carbon converted to C_2H_4 plus

C_2H_6 than to CH_4. The conversion of so much carbon to C_2H_4 and C_2H_6 is unusual since in most of the advanced gasification processes, such as Synthane and Hydrane, the fraction of coal carbon converted to these species is only a couple of percent. Indeed, the data in Table 2 for preoxidized coal show that the combined yield of C_2H_4 and C_2H_6 was only 2.3 percent. The rates of production of C_2H_4 and C_2H_6 were found to be negligible after the first one and one-half minutes in all runs. Thus, the C_2 hydrocarbons are formed primarily during hydrogasification of the most reactive carbon. The yields of these hydrocarbons were found to be lower at higher temperatures.

At this stage, the results on the yields of C_2H_4 and C_2H_6 should be interpreted cautiously because of differences expected in the coal heat-up rates and gas-phase residence time between the batch-solids gasifier and a continuous gasifier.

It should be pointed out that isothermal operation could not be achieved during hydrogasification runs because of unsteady state operation and because the hydrogasification reaction is highly exothermic. The methane concentrations in the off-gas during a run was as high as 35 percent by volume which occurred at about one minute after charging coal to the gasifier. The temperature was highest at the point of maximum rate of methane production.

TABLE 2. COMPARISON OF YIELDS FOR HYDROGASIFICATION OF BTC AND PREOXIDIZED COAL

	BTC (-20+28 mesh Raw Coal treated for 20 minutes)			Preoxidized Coal (+65 mesh)
Fluid-Bed Run No.	9	12	13	15
Total Pressure, psia	265	265	290	265
P_{H_2} in Feed Gas, psia	265	265	290	265
Temperature Range, °C	755-1045	750-850	880-1090	850-930
Reaction Time, minutes	13	10	10	12
Carbon Conversion, wt %				
CH_4	36.6	17.5	39.0	21.2
C_2H_4	2.0	10.1	6.0	0.3
C_2H_6	11.1	12.2	8.4	2.0
Tar and Oil	5.2	6.2	4.1	3.0
Oxides	4.3	5.6	4.4	3.5
Total	59.2	51.6	61.9	30.0
Percent Carbon Converted to C_1+C_2 Hydrocarbons	49.7	39.8	53.4	23.5

The temperature dependence for the specific rate of methane production in the post-devolatilization region is shown in Figure 7. These data were generated from one fluid-bed run since temperature was not constant. The straight line for Arrhenius plot suggests that there is no deactivation of BTC during hydrogasification in the carbon conversion range of 40 to 55 percent, verifying results from thermobalance data discussed later. The rates in Figure 7 were corrected for variation of partial pressure of hydrogen during the run using the first-order power law dependence for hydrogen partial pressure found from thermobalance data. The rate expression for specific rate of carbon conversion to methane in the post-devolatilization region is

$$-\left(\frac{1}{1-X_c}\right)\frac{dX_c(CH_4)}{dt} = 88\,(P_{H_2})\,\exp\,(-13{,}800/T) \qquad 2)$$

where, t is the time in minutes, P_{H_2} is in psia, T is the temperature in degrees kelvin, X_c is the total carbon conversion, and $X_c(CH_4)$ is the fraction of carbon converted to CH_4. Equation 2 should be valid up to a value of X_c of about 0.65 to 0.70 at a hydrogen partial pressure of 225 psia and to X_c values greater than 0.7 at higher pressures.

The data in Figure 7 show that the batch fluid-bed data, that have been corrected for the presence of as much as 15-20 percent methane, correlates well with thermobalance data. For the thermobalance data, the specific rate of MAF coal conversion was used, which is nearly the same as the left-hand side of Equation 2 in the post-devolatilization region.

The fractional conversion of carbon to tar plus oil was found to vary between 4 and 7 percent for runs with BTC using hydrogen as a feed gas. The yield of tar plus oil was found to decrease with temperature as found by other investigators (4). It is expected that the yield of tar and oil from BTC will be lower in a continuous fluid-bed gasifier where the coal can be introduced into the fluid bed directly and in which the coal can be heated very rapidly. The composition or the quality of tar and oil formed from BTC could not be determined because of the small amounts of samples available. It is expected though, based on our work on the pyrolysis of BTC, that the organic liquids (tar and oil) from BTC are significantly lower boiling than the organic liquids from untreated raw coal.

There was little or no H_2S detected by GC in off-gas from gasification of BTC. Furthermore, sulfur analysis of BTC and char showed that more than 90 percent sulfur was retained in the char during hydrogasification. It is believed that sulfur in char is present as CaS.

Steam Gasification Data. Table 3 summarizes typical yield data for BTC gasified with steam and steam plus hydrogen along with data for gasification of preoxidized coal (from Synthane Process). The data for Runs Nos. 14 and 16 show that the steam gasification reactivity of BTC is much greater than that of preoxidized coal as expected. Also, the rate of hydrocarbon formation and the ratio of C_2 hydrocarbon yield to CH_4 yield for BTC is greater than for preoxidized coal.

TABLE 3. COMPARISON OF YIELDS FOR GASIFICATION OF BTC AND PREOXIDIZED COAL WITH STEAM AND STEAM PLUS HYDROGEN

	BTC (-20+28 mesh Raw Coal treated for 20 minutes)		Preoxidized Coal (+65 mesh)	
Fluid-Bed Run No.	14	17	16	19
Total Pressure, psia	255	205	215	205
P_{H_2} in Feed Gas, psia	0	111	0	111
P_{H_2O} in Feed Gas, psia	66	94	57	94
P_{He} in Feed Gas, psia	189	0	158	0
Temperature Range, °C	785-795	780-800	800-810	850-890
Reaction Time, minutes	12	12	14.5	17
Carbon Conversion, wt %				
CH_4	10.6	25.9	7.1	15.1
C_2H_4	2.1	2.0	1.0	0.2
C_2H_6	2.1	4.6	0.5	0.8
Tar + Oil[(a)]	4.2	1.9	2.5	0.6
Oxides	79.0	47.2	14.2	11.3
Total	98.0	81.6	25.3	28.0
Percent Carbon Converted to C_1+C_2 Hydrocarbons	14.8	32.5	8.6	16.1

(a) Underestimated because some oil was condensed in the steam condenser.

Runs Nos. 17 and 19 were conducted with steam-hydrogen mixtures in order to simulate more closely the conditions in a continuous, steam-oxygen, fluid-bed gasifier. Again, BTC is found to be more reactive and more selectively gasified to C_2 hydrocarbon than preoxidized coal. Note that the Yield of C_2 hydrocarbons and CH_4 increases with hydrogen partial pressure in the range studied. For example, the yield of C_2 hydrocarbon

in Run No. 14 (in which the partial pressure of H_2 in the off-gas was 15 psia) was 4.2 percent, in Run No. 17 (P_{H_2} = 111 psia) it was 6.6 percent, and in runs with pure hydrogen (P_{H_2} = 265 to 290 psia) it varied from about 13 to 22 percent.

The rates of production of various gases during Run No. 17 (P_{H_2} = 111 psia) are plotted in Figure 8. Integration of these rate data to various levels of carbon conversion showed that all the C_2 hydrocarbons and about 95 percent of the CH_4 were produced during the gasification of the initial 55 percent of carbon. Thus, the combined yield of C_1 and C_2 hydrocarbons, or what may be called "equivalent CH_4", will be 31-32 percent for 60-70 percent total carbon conversion. On the other hand, extrapolation to 60 percent carbon conversion of the rate data for preoxidized coal (Run No. 19) showed that the combined yield of C_1 and C_2 hydrocarbons was 20.5 percent.

The batch fluid-bed data for preoxidized coal were extrapolated to estimate the equivalent CH_4 yield corresponding to the operating conditions employed in the 4-inch I.D. Synthane gasifier operating at 570 psig. The estimated value was 15.8 percent which corresponds well with the 15.2 percent actually observed (5,6). Using a similar estimation procedure for BTC, the equivalent CH_4 yield for a single-stage, fluid-bed, steam-oxygen gasifier operated at 750°C and 300 psig was projected to be in the neighborhood of 26 percent. (The minumum equivalent CH_4 yield for BTC should of course be 14.8 percent, as determined from Run No. 14, corresponding to P_{H_2} equal to 15 psia only.) Thus, the equivalent CH_4 yield for BTC is expected to be significantly higher for BTC than for preoxidized coal for single-stage, steam-oxygen gasification.

The data in Table 3 show that steam gasification of BTC can be carried out at a reasonable rate at a temperature well below 790°C, as also found earlier (2). The data in Table 3 also illustrate the suppressive effect that increasing the hydrogen partial pressure has on steam gasification rate of BTC. This effect has been noted by other investigators (7,8). The simplest physical explanation for the lowering of the steam gasification rate by hydrogen is that the hydrogen adsorbs on reaction sites making them unavailable to steam.

As in the case of hydrogasification, little or no H_2S was detected in the off-gas during steam gasification of BTC, indicating that sulfur was captured by CaO (probably as CaS). The advantage of retaining sulfur in the char as CaS is that the char can be burnt in an environmentally-acceptable manner to provide for the energy requirements of the gasification plant.

Continuous Production of BTC

The objectives behind continuous production tests for production of BTC were to establish that BTC could be produced continuously and to establish the correlation between batch and continuous (Miniplant) tests.

It was found that BTC, having hydro(gasification) properties superior to raw coal, could be produced from coarse as well as fine coal on a continuous basis. The (hydro) gasification properties of Miniplant-produced BTC were found to be the same as for batch-produced BTC. For example, the thermobalance data in Figure 9 show that the hydrogasification reactivity of Miniplant-produced BTC was the same as for batch-produced BTC. Furthermore, data from batch-solids fluid-bed gasifier showed that the distribution of the products from (hydro)gasification was nearly independent of the type of reactor used for production of BTC.

Hydrogasification Rate Analysis

An interesting finding in this study was that there was no deactivation of BTC during hydrogasification, in the post-devolatization regime, up to an MAF fractional conversion of about 0.75. On the other hand, the rate of hydrogasification of raw coal was found to decline more or less exponentially in the post-devolatization regime. This remarkable difference between the hydrogasification properties of BTC and raw

coal is illustrated in Figure 10 where the specific rate of hydrogasification, defined as $(-dX/dt)/(1-X)$, is plotted against X, where X is the fractional conversion of MAF coal. (It is not clear whether the higher initial devolatilization rate for BTC is due to higher reactivity or simply faster heat-up because the BTC particles remained discrete while the raw coal particles expanded into a sponge-like mass.) Figure 10 shows that the reactivity of BTC relative to raw coal increases with X. The decline in specific rate of hydrogasification with increasing conversion for the raw coal is a clear indication of decreasing reactivity brought about by the increasing graphitization that occurs in the untreated coal. That graphitization occurs has become very widely accepted among investigators in this area. Thus, it may be speculated that the chemical incorporation of the catalyst prevents graphitization of BTC during hydrogasification to a fractional conversion of about 0.75. Wood (9) and Gardner (10) have also reported lowering of the tendency for deactivation of coal in the presence of a catalyst. However, their catalysts were much less effective than the catalyst in BTC because their catalysts were only physically and (probably) less-effectively incorporated in coal.

The reason for decline in the specific rate for BTC after X equal to 0.75 is not understood. But this may suggest an alternate hypothesis for the role of the catalyst in BTC. It may, for example, be hypothesized that the role of the catalyst is to simply extend the limit for rapid rate methanation stage for base carbon conversion proposed by Johnson (7) and others (11).

CURRENT STATUS OF PROGRAM

Under current ERDA sponsorship, several catalyst systems are to be evaluated as alternatives to the system comprising of NaOH and CaO. The objective is to minimize the cost of SNG or medium-Btu gas production from high-sulfur caking coals.

Presently, the catalyst system comprising of CaO alone is being evaluated in detail. Since no NaOH is required in this process, there is no need for washing of BTC or regeneration of spent leachant. Furthermore, the high-pressure slurry containing BTC, water and the catalyst may be slurry-fed to a gasifier. The results to date with the CaO system have been very encouraging.

CONCLUSIONS

The data on the Battelle treatment of coal with CaO in the presence of NaOH shows that nonagglomerating BTC having a very high (hydro)gasification reactivity compared to raw coal can be produced from raw coal particles as large as 20 mesh. The maximum-possible hydrogasification reactivity of BTC is independent of raw coal particle size. But, -20+28 mesh coal requires about twice as long a treatment time as 70 percent minus 200 mesh coal to achieve the maximum-possible reactivity. The increase in the reactivity of coal due to treatment is accompanied by a decrease in the tendency for agglomeration during hydrogasification. And, at the treatment time required to achieve maximum reactivity, the agglomeration tendency is completely eliminated. The FSI of coal particles as large as 0.25 inch from Pittsburgh #8 seam is found to be reduced from 8 to 0 due to Battelle treatment.

It has been established that the BTC produced in a continuous treatment plant has the same (hydro)gasification properties as BTC produced in a batch reactor.

Comparison of (hydro)gasification properties of BTC and preoxidized coal from Synthane Process shows that (a) (hydro)gasification reactivity of BTC is much higher, (b) (hydro)gasification of BTC yields substantially greater quantities of C_2H_4 and C_2H_6, and (c) the equivalent CH_4 yield for BTC is significantly higher for steam gasification. The BTC also retains most of the sulfur in char, probably in the form of CaS, during (hydro)gasification. Thus, combustion of char from BTC is not expected to require an SO_2 scrubber.

The hydrogasification rate analysis of the data shows that there is no deactivation of BTC during hydrogasification in the post-devolatization regime up to a fractional conversion of 0.75 while raw coal reactivity declines almost exponentially with X.

The above advantages of BTC over raw coal and preoxidized coal suggest that Battelle catalyst treatment should allow more reliable, environmentally-acceptable and more economic utilization of high-sulfur, Eastern U.S. coals.

ACKNOWLEDGEMENTS

The authors wish to express their appreciation to Mr. Gary Felton for providing help in designing the batch-solids fluid-bed gasifier, to Mr. Sam Tam for carrying out the Miniplant tests, and to Mr. Herm Nack for his continued interest and valuable suggestions. The financial support for this study was provided by ERDA.

REFERENCES

(1) Stambaugh, E. P., Miller, J. F., Tam, S. S., Chauhan, S. P., Feldmann, H. F, Carlton, H. E., Foster, J. F., Nack, H., and Oxley, J. H., "The Battelle Hydrothermal Coal Process", Paper presented at the "Second Annual Symposium on Coal Gasification, Liquefaction, and Utilization", held at University of Pittsburgh (August, 1975).

(2) Chauhan, S. P., Feldmann, H. F., Stambaugh, E. P., and Oxley, J. H., Preprints of Fuel Division, American Chemical Society Meeting, 20 (4), 207 (1975).

(3) A Novel Approach to Coal Gasification Using Chemically Incorporated Catalysts, Phase I Summary Report to ERDA, BMI-1953, August, 1976.

(4) Feldmann, H. F. and Yavorsky, P. M., Proceedings of the Fifth Synthetic Pipeline Gas Symposium, American Gas Association Catalog No. L5 1173, 1974, p. 287.

(5) Johnson, C. A., Proceedings of the Fifth Synthetic Pipeline Gas Symposium, American Gas Association Catalog No. L5 1173, 1974, p. 125.

(6) Dobner, S., Graff, R. A., and Squires, A. M., "Analysis of Trials of Synthane Process", Report prepared for HRI, City College of New York (March, 1974).

(7) Johnson, J. L., Coal Gasification, Advances in Chemistry Series 131, Edited by L. G. Massey, American Chemical Society, Washington, D. C., 1974, p. 145.

(8) Feldkirchner, H. L. and Huebler, J., I&EC Process Design and Development, 4 (2), 134 (1965).

(9) Wood, R. E. and Hill, G. R., Preprints of Fuel Division, American Chemical Society Meeting, 17 (1), 1972.

(10) Gardner, N., Samuels, E., and Wilks, K., Coal Gasification, Advances in Chemistry Series 131, Edited by L. G. Massey, American Chemical Society, Washington, D. C., 1974, p. 217.

(11) Moseley, F. and Paterson, D., J. Inst. of Fuel, 38, 13 (January, 1975).

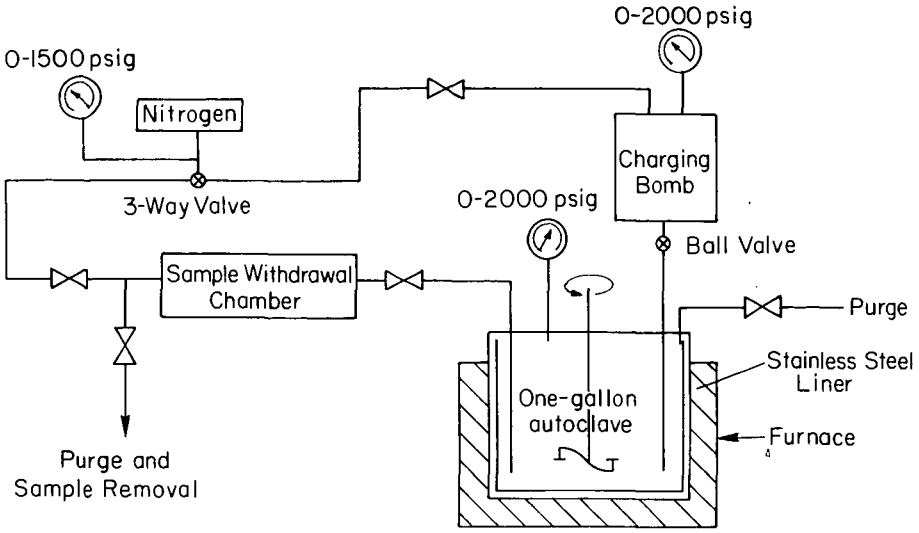

FIGURE 1. SCHEMATIC DIAGRAM OF THE BATCH REACTOR SYSTEM FOR PRODUCTION OF BTC

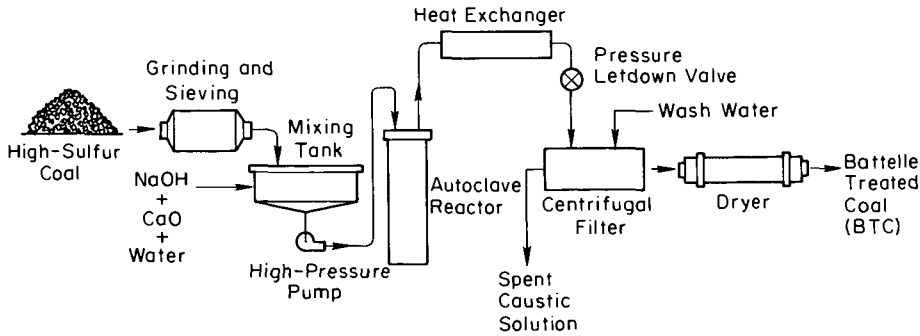

FIGURE 2. FLOWSHEET OF PROCESS FOR PRODUCTION OF BTC IN THE CONTINUOUS REACTOR (MINIPLANT)

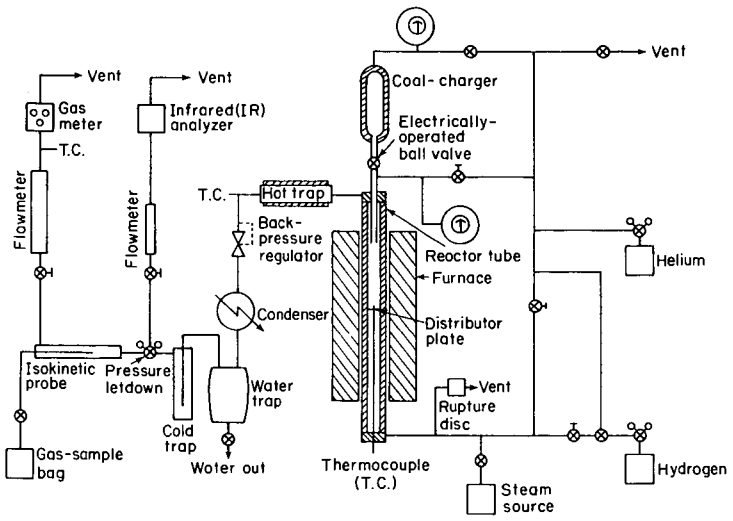

FIGURE 3. SCHEMATIC OF THE BATCH-SOLIDS FLUID-BED GASIFIER

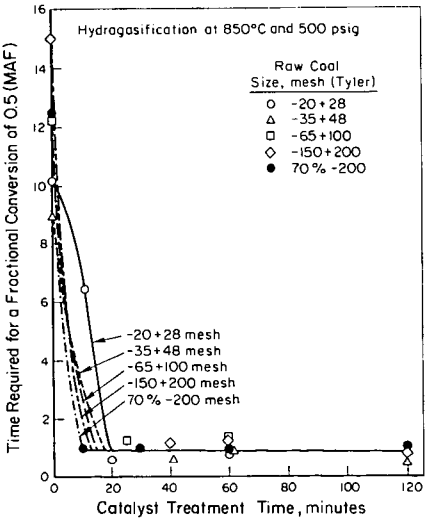

FIGURE 4. DEPENDENCE OF THE TIME REQUIRED FOR A FRACTIONAL CONVERSION OF 0.5 FOR HYDROGASIFICATION OF BTC ON PARTICLE SIZE OF RAW COAL AND CATALYST TREATMENT TIME

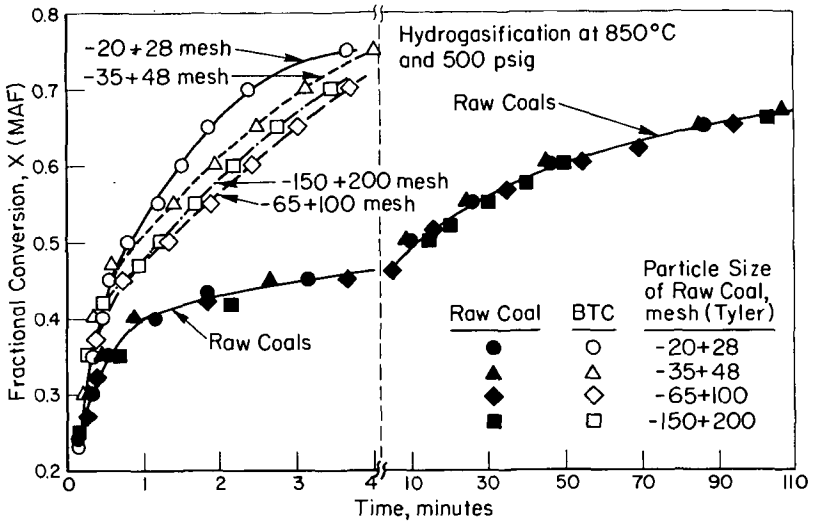

FIGURE 5. EFFECT OF RAW COAL PARTICLE SIZE ON THE HYDROGASIFICATION REACTIVITY OF BTC RELATIVE TO RAW COAL. CATALYST TREATMENT TIME = 60 MINUTES

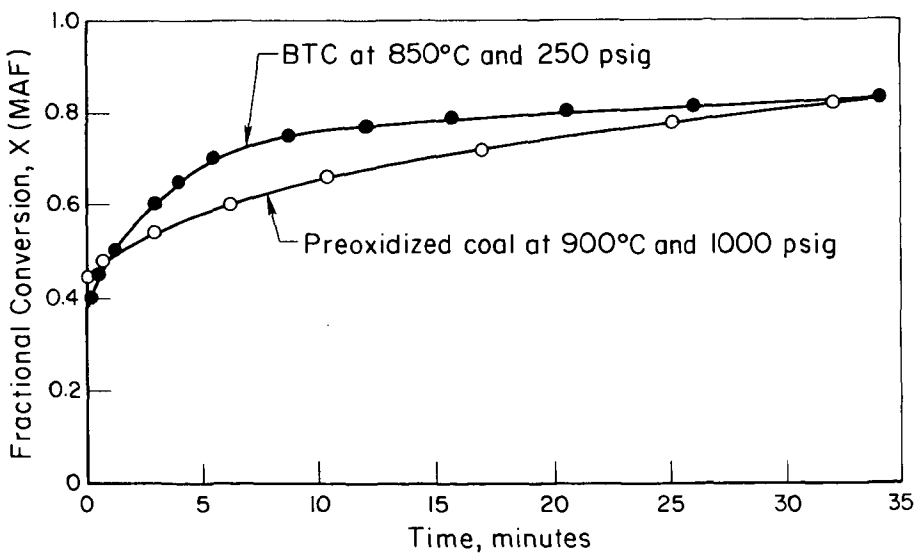

FIGURE 6. COMPARISON OF THE HYDROGASIFICATION REACTIVITY OF BTC (TREATMENT TIME = 20 MINUTES) WITH PREOXIDIZED COAL

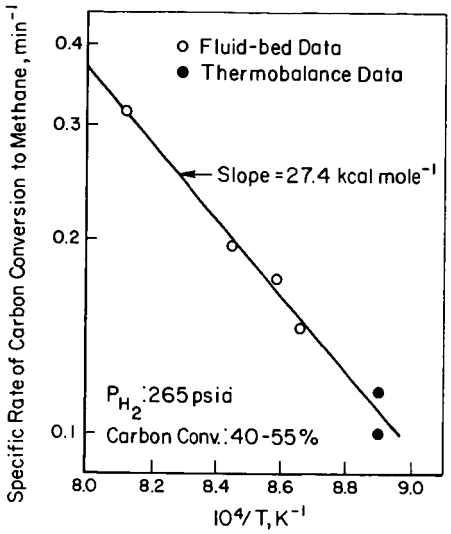

FIGURE 7. ARRHENIUS PLOT FOR SPECIFIC RATE OF CARBON CONVERSION TO METHANE FOR BTC (FLUID-BED RUN NO. 13)

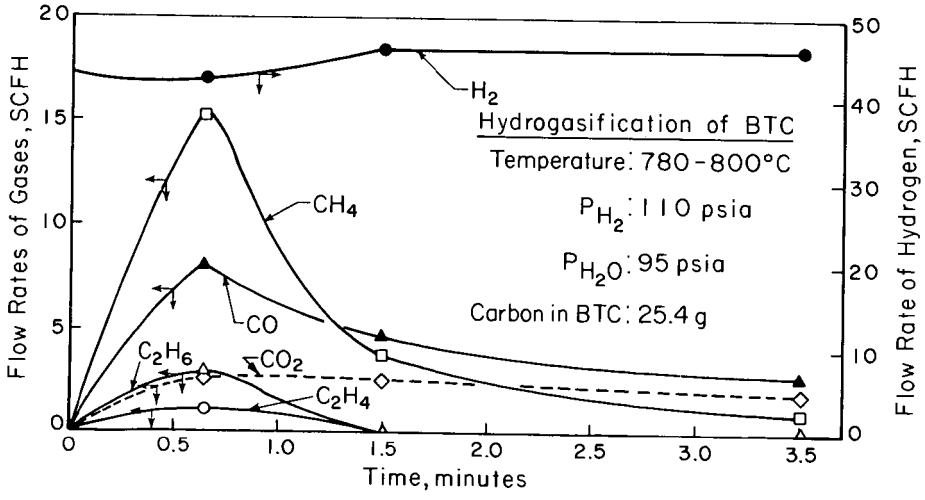

FIGURE 8. FLOW RATES OF VARIOUS GASES EXITING FROM THE FLUID BED DURING GASIFICATION OF BTC WITH STEAM PLUS HYDROGEN (FLUID-BED RUN NO. 17)

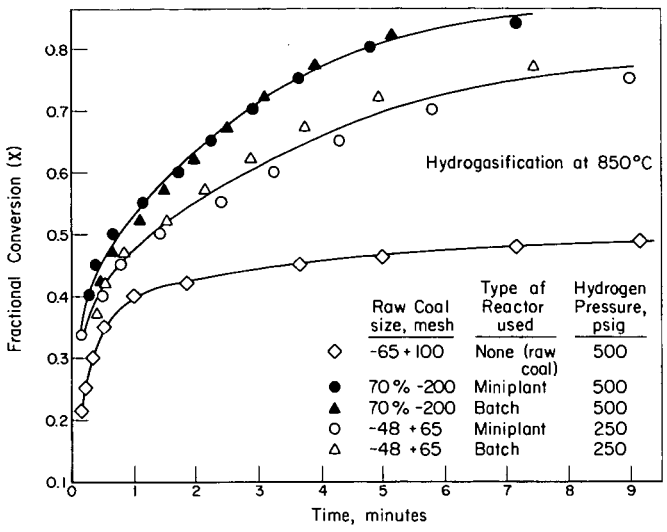

FIGURE 9. COMPARISON OF THE HYDROGASIFICATION REACTIVITY OF BTC PRODUCED IN THE MINIPLANT WITH THE REACTIVITY OF RAW COAL AND BTC PRODUCED IN THE BATCH AUTOCLAVE (CATALYST TREATMENT TIME = 20-35 MINUTES)

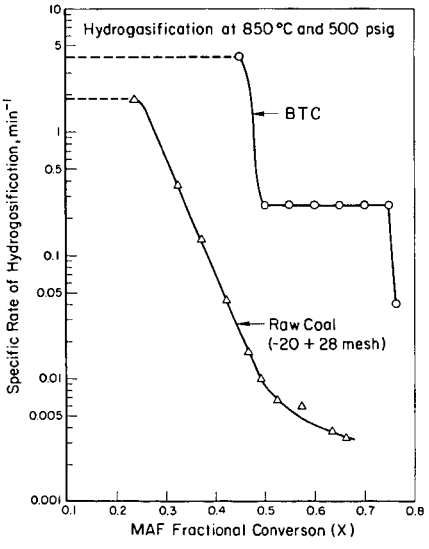

FIGURE 10. PLOTS OF THE SPECIFIC RATE OF HYDROGASIFICATION VERSUS FRACTIONAL CONVERSION FOR RAW COAL AND BTC (TREATMENT TIME = 20 MINUTES)

Gasification of a German Bituminous Coal With H_2O, H_2 and H_2O-H_2 Mixtures

P. P. Feistel, K. H. van Heek and H. Jüntgen

Bergbau-Forschung GmbH
4300 Essen 13
Federal Republic of Germany

A. H. Pulsifer

Department of Chemical Engineering
and
Engineering Research Institute
Iowa State University
Ames, Iowa 50011, USA

Bergbau-Forschung has been developing a coal gasification process for a number of years. In this process heat from a high-temperature, gas-cooled nuclear reactor is used as a source of energy for the endothermic steam-carbon reaction (1). All of the coal is thus converted to gas which is a real advantage in countries where the cost of coal is high such as is the case in the Federal Republic of Germany.

As part of the development work on this process, the reaction of several different coal samples with steam, hydrogen and steam-hydrogen mixtures has been investigated extensively in the laboratory. The objective of this work is to develop information needed to design the gasifier used to carry out steam gasifiction of coal, particularly when hydrogen is present in the system. The results of this investigation with one particular coal, a hard or bituminous coal, is discussed here. During the course of the investigation, samples of this coal were gasified at various steam and hydrogen partial pressures in both pure gases and in steam-hydrogen mixtures. The total system pressure was varied between 1 and 70 atm and runs were conducted over a range of temperatures from 600 to 1100°C.

Apparatus and Procedure

The experimental apparatus has been described previously (2). The coal sample was gasified in a small packed bed reactor that essentially behaved as a differential reactor (Fig. 1). Both isothermal and non-isothermal runs were conducted. During the isothermal runs, the system was heated to the desired temperature using a heating rate of about 200°C/min. The temperature was then held constant. During the non-isothermal runs, the temperature of the system was increased at a constant rate of 10°C/min.

The gasification agent, namely steam, hydrogen or a mixture of both, was fed continuously to the system at a high rate so that the product gas concentration remained small. The products of the reaction were analysed continuously by a mass spectrometer. The apparatus was designed for two different modes of operation, type A for gasification with steam and type B for gasification using steam-gas mixtures.

The coal used was a German bituminous coal, Hagen coal. Analytical data for this coal are shown in Table 1.

Calculational Procedure

The gas analyses from the mass spectrometer were processed directly by a laboratory computer and the carbon conversion was calculated from the amounts of

CH_4, CO and CO_2 in the product gas. Kinetic constants for the gasification rate were determined for each of the gasification agents using the following rate expression:

$$\frac{dX_B}{dt} = k\ (1-X_B) \qquad 1)$$

where X_B = base carbon conversion as defined by Johnson (3)
t = time
k = kinetic constant

Several other rate expressions were evaluated including the one suggested by Johnson (3). Each of these expressions included an additional term to try to account for the decrease of reaction rate with carbon burn-off. However, none of the expressions fit the data any better than equation 1, so only the kinetic constants for this rate expression are reported here.

Results and Discussion

Steam gasification

Only non-isothermal runs were conducted with steam as the gasification agent, with the temperature of the sample being raised from about 200 to 1100°C using a constant heating rate. Five steam gasification runs were made, 3 at 10 atm and 2 at 40 atm. The main components of the product gas were H_2, CO and CO_2 as previously observed (2). Small amounts of methane also were produced, and the gas composition was not greatly affected by the total pressure.

Since the effects of coal devolatilization on the product gas rate and composition were important up to temperatures between 600 and 700°C, only the data above 700°C were analyzed to obtain kinetic constants. This was done by fitting the integrated form of equation 1 to the base carbon conversion-time data assuming that the Arrhenius equation described the effect of temperature on k. Values of the frequency factor, k_o, and activation energy, E, were therefore calculated from this procedure. These describe the total rate of base carbon conversion in the reactor. If it is assumed that the carbon dioxide is produced via the gas-phase water gas shift reaction, then these parameters describe the rate of the carbon-steam reaction. However, there was no evidence to indicate that this was the true reaction sequence.

The fit of equation 1 to the carbon conversion data was excellent, as was true of any of the equations used, and a correlation coefficient greater than 0.99 was obtained for each run. Average values of k_o and E for the two pressures used are shown in Table 2.

Table 2. Kinetic parameters for steam gasification of Hagen coal.

Pressure, atm	k_o, 1/min	E, kcal/mol
10	3.8×10^4	32.0
40	1.3×10^3	23.0

Examination of the kinetic parameters shown in Table 2 indicates that steam pressure affects the gasification rate. The kinetic constant for steam gasification, k_{H_2O}, was related to both steam pressure and temperature by the following equation:

$$k_{H_2O} = \frac{1.88 \times 10^6 \exp(-2.24 \times 10^4/T) P_{H_2O}}{(1 + 1.56 \times 10^5 \exp(-1.65 \times 10^4/T) P_{H_2O})} \quad 2)$$

Several runs were made with Hagen coal at pressures less than 10 atm. Results from these runs were not adequately described by equation 2, with the indication being that the steam pressure had only a small effect on gasification rate at pressures less than 10 atm.

Hydrogasification

There seems to be general agreement that hydrogasification of coal occurs in three stages, devolatilization, rapid-rate methane formation and low-rate gasification. If the coal sample is heated rapidly to temperatures above 800°C, devolatilization and rapid-rate methane formation occur rapidly and together, and are followed by low-rate gasification (3). Below 800°C, rapid-rate methane formation is slower and occurs over an extended period of time and is therefore more difficult to separate from the low-rate gasification period. Results from the gasification of Hagen coal with hydrogen qualitatively fitted this description of hydrogasification. To determine the rate of hydrogasification of Hagen coal, a series of isothermal experiments were conducted at 10 and 70 atm and at temperatures between 600 and 1150°C. Because of the initial heating period, it was difficult to draw conclusions about the period of rapid-rate methane formation. However this period lasted for less than 15 minutes once the sample reached the reaction temperature and therefore data taken after this period were used along with equation 1 to determine kinetic constants for low-rate hydrogasification. The product gas was generally pure methane during this period, indicating that the only reaction taking place in the system was that between C and H_2 to form CH_4. In a few of the runs, particularly at 10 atm and temperatures of 700°C or below, the product gas contained some CO.

The correlation coefficients obtained with equation 1 were again greater than 0.99 for all runs. The gasification rate seemed to decrease slightly with increasing carbon conversion, but equation 1 still represented the data as well as any of the equations tried. Values of k_o and E for the two pressures used were derived from the values of the kinetic constants and are shown in Table 3.

Table 3. Kinetic parameters for hydrogasification of Hagen coal.

Pressure, atm	No. of runs	k_o, 1/min	E, kcal/mol	Correlation coeff.
10	10	1.28	15.6	-0.987
70	14	32.1	17.8	-0.978

The hydrogen pressure strongly affects the hydrogasification rate. The effect of temperature and pressure were correlated using equation 3, which is similar in form to equations suggested by several other investigators (3,4).

$$k_{H_2} = \frac{0.00402 \exp(-5200/T) P_{H_2}^2}{1 + 0.00648 \exp(4100/T) P_{H_2}} \qquad 3)$$

Gasification with Steam -H_2 Mixtures

To determine the effect of hydrogen partial pressure on the rate constant for steam gasification, a series of isothermal runs was carried out over the temperature range from 700 to 1100°C. Total pressures of 10 and 40 atm were used, with hydrogen partial pressures between 1.7 and 32 atm.

Equation 1 was again used to determine kinetic constants from the base carbon conversion-time data. Data taken during the run after the first 15 minutes at temperature were used in the calculations so as to avoid the effect of the rapid-rate methanation period. Correlation coefficients greater than 0.99 were obtained for all runs.

Several investigators have treated the kinetic data from coal gasification with H_2-H_2O mixtures by assuming that three basic reactions were occuring (3,5,6). However, to simplify the calculational procedure, it was assumed that the only reactions occurring with Hagen coal were the two that would occur in either pure steam or hydrogen. The rate of steam gasification in the H_2-H_2O mixture, then, assuming that the rate of hydrogasification is independent of steam partial pressure, was the difference between the measured rate constant and the rate constant for the carbon-hydrogen reaction under the same operating conditions. The latter was calculated from equation 3 and was generally less than 10% of the measured rate constant.

The data taken at various hydrogen and steam partial pressures and at 800 and 900°C were examined and the following equation was derived to describe the effects of temperature and the partial pressure of each gas.

$$k_{H_2\text{-}H_2O} = \frac{1.88 \times 10^6 \exp(-2.24 \times 10^4/T) P_{H_2O}}{(1 + 1.56 \times 10^5 \exp(-1.65 \times 10^4/T) P_{H_2O} + 3620 \exp(-9830/T) P_{H_2})} \qquad 4)$$

Temperature has the largest effect on the gasification rate in steam-hydrogen mixtures. In fact, if the effect of steam and hydrogen partial pressure are ignored, the kinetic constants can be fitted with the Arrhenius equation with a correlation coefficient of -0.904. The resulting activation energy is 33,400 cal/mol and the frequency factor is 2.51×10^4 1/min.

Conclusions

The rate of gasification of a bituminous coal sample in steam, hydrogen and steam-hydrogen mixtures has been measured and the rates correlated by assuming that the base carbon conversion rate was proportional to the amount of base carbon present. Expressions were then found to describe the effects of temperature and steam and hydrogen partial pressures on the rate constants for the steam-carbon and hydrogen-carbon reactions.

Acknowledgement

This paper is based on work done while A. H. Pulsifer was on leave from Iowa State University and located at Bergbau-Forschung GMBH. The support provided by the University and the Alexander von Humboldt Foundation during this time is gratefully acknowledged.

Literature Cited

1. Jüntgen, H. and K. H. van Heek, Nuclear Eng. and Design, 34, 59 (1975).

2. van Heek, K. H., H. Jüntgen and W. Peters, J. Inst. Fuel, 46, 240 (1973).

3. Johnson, J. L., in Advances in Chemistry Series No. 131, "Coal Gasification," 145 (1974).

4. Zielke, C. W. and E. Gorin, Ind. Eng. Chem., 47, 820 (1955).

5. Blackwood, J. D. and F. McGrory, Aust. J. Chem., 11, 16 (1958).

6. Curran, G., and E. Gorin, U.S. Off. Coal Res. R&D Rept. No. 16, Interim Rept. No. 3, Book 2, Government Printing Office, Washington, DC (1970).

Table 1. Coal analyses.

	Hagen
Proximate analysis, wt.%	
Volatile Matter (maf)	39.2
Moisture	3.7
Ash (mf)	6.3
Ultimate analysis, wt.%	
Carbon (maf)	82.0
Hydrogen (maf)	5.0
Oxygen (maf)	8.2
Nitrogen (maf)	1.5
Sulfur (mf)	2.7

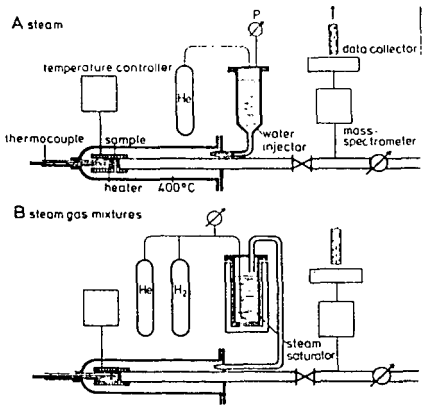

Figure 1. Experimental Apparatus.

Steam gasification of coal in an internally heated fluidized bed

P.P. Feistel, K. H. van Heek, and H. Jüntgen
Bergbau-Forchung GmbH, 4300 Essen 1, Germany

Abstract

A process is being developed for the steam gasification of coal using heat from a high temperature, gas cooled nuclear reactor. To produce the information needed to design such a system, a 10 cm diameter, internally heated fluidized bed was constructed and has been in operation for several years. A variety of coals have been gasified with steam in this device at pressures up to 40 bar and temperatures between 700 and 900 ^{o}C.

Gas compositions, gas yields, heats of reaction and steam decompositions have been determined in the fluidized bed as a function of the operating conditions. Carbon gasification rates have been derived from this data and the variation in gas composition has been correlated using "temperature approach" functions. The effect of the operating conditions on fluidized bed density and heat transfer coefficient also has been investigated.

1. General considerations to an allothermal process

Bergbau-Forschung GmbH Essen develops a process for steam gasification of coal by using process heat from high temperature nuclear reactors. This requires research and development in the field of allothermal gas generators. The envisaged allothermal gas generator is heated by an internally mounted bundle of heat exchanging tubes which are flown through by the gaseous reactor coolant helium . As the helium pressure amounts to 40 bar the steam

gasification is performed at the same pressure. To attain good heat transfer the heat exchanger is located within a fluidized bed of coal and steam [1,2,3]. The coal throughput of such an allothermal gas generator is determined by the heat balance (fig. 1). For a first evaluation of the heat balance assumptions had to be made concerning

- the reaction heat and its dependence on gas analysis,
- the kinetic constants of different feedstocks [4,5,6],
- the heat transfer from the heat exchanger into the fluidized bed, and
- the density of the fluidized bed at high temperatures and pressures.

In the meanwhile experiments have been carried out to measure the above mentioned quantities and their dependence on operating conditions as temperature, pressure, and steam excess.

2. Experimental

Bergbau-Forschung GmbH operates since 1973 a small scale pilot plant in which coal or carbonized coal is gasified in an internally heated fluidized bed at high temperatures and pressures (approx. 1 kg/h). The experimental set up is given in fig. 2. Steam is raised, superheated electrically and fed through a grid into the reaction volume, where a fluidized bed is maintained. . The feedstock is dosed from above by means of a rotating pocket type valve. The crude gas is then passed through a cyclon and a ceramic filter for the separation of particles is then cooled with air, depressurized, dried, volumetrically metered and continously analyzed by mass spectrometer.

- 3 -

The reaction volume of the gas generator is cylindrically shaped (Ø 100 mm, heated height 400 mm). The reaction heat necessary for endothermal steam gasification is generated by an electrically heated metallic spiral. This so called immersion heater is mounted within the fluidized bed in direct neighborhood to the insulation. The diameter of the spiral (80 mm) corresponds to the distance of the heat exchanging tubes in a large scale gasifier.

Fig. 3 illustrates how the heat transfer from the heat exchanger into the fluidized bed is measured. A top view of the reaction volume and the heat exchanger is given, the latter one has a total surface area A and generates an electrical power P. By two thermocouples, one of which has direct contact with the heat exchanger and the other one is mounted on half of the radius, an effective temperature difference can be determined. The experiments already performed have shown, that just the temperature at half the radius can be used as first order approximation for the mean temperature of the fluidized bed . The heat transfer coefficient α is then calculated by the equation given in fig. 3: $P = \alpha \cdot A \cdot (T_1 - T_2)$.

The devices for determination of height and density of the fluidized bed are shown schematically in fig. 4. By means of three pressure measuring tubes, the first of which is mounted directly above the grid , the second 180 mm above and the third in the freeboard two pressure differences are given. As the measured pressure difference Δp_1 belongs to the known height h_1 the actual height h of the fluidized bed can be calculated. Using then the formula for the hydrostatic pressure the density of the fluidized bed follows.

3. Results

3.1. Gas composition and thermodynamic calculations

During a run an on-line process computer calculates for instance [7]:

- the frequency of coal feeding,
- the content of the gas generator,
- the absolute carbon conversion,
- the relative carbon conversion,
- the composition of the dry product gas,
- the steam velocity in the gasifier,
- the molar steam carbon ration in the gaseous phase
- the steam decomposition.

Fig. 5 shows data concerning gas production and gas composition during the first 500 minutes of a run at 40 bar and 750 ^{o}C with carbonized high volatile bituminous coal "Leopold". The particle sizes used were $<$ 0,5 mm. The lower part of the picture shows that after about 200 minutes the gas composition has been essentially constant and the dry product gas consisted of about 50 % H_2, 26 % CO, 16 % CO_2 and 8 % CH_4.

Runs with carbonized Rhenish lignite show more CO_2 and H_2 but less CO and CH_4. The reason for this almost complete conversion of CO to CO_2 which is to be expected forthermodynamic reasons is the relatively high amount of catalytically effectiv substances in the mineral matter of Rhenish lignite which increases the reaction rate on the one hand and shifts the gas composition more toward thermodynamic equilibrium on the other hand.

The thermodynamics of steam gasification of coal in the absence of free oxygen can be described by three linearly independent reactions, as for instance:

$$C + H_2O \Leftrightarrow CO + H_2 \qquad (1)$$
$$CO + H_2O \Leftrightarrow CO_2 + H_2 \qquad (2)$$
$$CO + 3H_2 \Leftrightarrow CH_4 + H_2O \qquad (3)$$

The homogeneous system is determined by two linearly independent reactions as for instance (2) and (3).

Fictitious equilibrium constants can then be calculated from the crude gas as for instance for reaction (3)

$$K_p\ (\vartheta_G) = \frac{P_{CO} \cdot P_{H_2}^3}{P_{CH_4} \cdot P_{H_2O}} \qquad (4)$$

and lead to fictitious equilibrium temperatures {8}. Doing pure thermodynamic calculations the equilibrium temperatures for all reactions used and the reaction temperature coincide. To account for deviations from equilibrium one has to allow different equilibrium temperatures ϑ_G. These temperatures ϑ_G are generally not correlated with each other and do not coincide with the reaction temperature ϑ_R. The difference

$$\Delta\vartheta = \vartheta_G - \vartheta_R \qquad (5)$$

is called approach-value of the individual reaction and does depend implicitly on pressure, steam-carbon-ratio, feedstock and experimental set-up.

The gas composition in a system at thermodynamic equilibrium is given by reaction temperature and pressure. At non-equilibrium the approach-values for each of the linearly independent reactions at operating conditions must be known additionally. This

knowledge is now available for some coals being gasified in our small scale pilot plant and is used not only for the representation of the experimental results, but also for the prediction of operating conditions in large scale gas generators.

Some results of our calculations are given in fig. 6. Fig. 6a shows the CH_4-content in the dry product gas as a function of the steam-carbon-ratio and the reaction temperature. It follows that methane contents of 15 % will be achieved at steam-carbon-ratios of 10 and reaction temperatures of 800 ^{o}C, whereas the methane content decreases to values smaller than 1 % with higher steam-carbon-ratios and higher temperatures. As methane formation is strongly exothermal the overall steam gasification reaction heat decreases with increasing methane content in the product gas. According to fig. 6b the reaction heat at low temperatures and low steam-carbon-ratios is less than 1000 kcal/kg feedstock, whereas at high steam-carbon-ratios and high temperatures it attains about 1500 kcal/kg feedstock. In fig. 6c data for steam decomposition are given. It follows that a steam decomposition of about 10 % and more can be attained in our small scale pilot plant at steam-carbon-ratios of 10 and gasification temperatures of 800 ^{o}C. A conservative extrapolation of these data from the height of the fluidized bed used here (40 cm) to the height of a fluidized bed in a commercial scale gasifier (3 m) shows that degrees of steam decomposition of more than 30 % can be expected.

3.2 Reaction kinetics and mean gasification temperature

The reaction rate constant used here indicates what percentage of carbon in the solid phase is converted into the gaseous phase by heterogeneous reactions as for instance by (1). The reaction rate defined this way and all kinetic constants derived from it depend implicitly on the composition of the gaseous phase due to the coupling between heterogeneous and homogeneous reactions.

Fig. 7 shows data concerning the reaction rate constants at various temperatures using carbonized high volatile coal "Hagen" as feedstock. At temperatures between 750 and 860 °C the reaction rate constants in the fluidized bed vary between 0,5 and 4,2 % C/min. In a laboratory scale fixed bed differential reactor slightly higher values were measured. The following explanation is suggested: In a differential reactor the concentration of product gas components is negligible and therefore no backward reactions take place. In the upper layers of the fluidized bed, however, hydrogen in the range of some percentages is present. Therefore the reaction rate constants from the upper part of the fluidized bed should be compared with corresponding laboratory values using mixtures of steam and hydrogen as gasifying agent. Experiments carried out under this aspect showed that using carbonized high volatile coal the reaction rate decreases when hydrogen is added {9}.

In a laboratory scale differential reactor the gasification temperature can be determined by a single thermocouple. In contrast to this a three-dimensional temperature field exists in the interior of the fluidized bed reactor used here. 12 thermocouples are used to determine this field. Fig. 8 shows the temperature variation 185 mm above the grid. The temperature is the highest in the neighborhood of the electrically heated spiral and decreases towards the center of the fluidized bed. The decrease is especially marked at low steam velocity. Using particle sizes between 0,1 and 0,5 mm a steam velocity of 11 cm/sec is just sufficient for fluidization whereas the fluidized bed collapses at steam velocities of 8 cm/sec. Experiments with even smaller particle sizes showed that using a sieve fraction < 0,1 mm steam velocities of 3 cm/sec are sufficient for fluidization at 40 bar.

Concerning the calculation of a mean temperature of the fluidized bed a first approximation is the integration of the temperature distribution over the reaction volume. Thus a geometric mean value is received which does not take into account that the gasification temperature depends exponentionally on temperature and thus the volume elements in the neighborhood of the heat exchanger add more to the gasification throughput than the colder elements in the center of the fluidized bed. Therefore a logarithmic averaging has to be performed for which the activation energy must be known. The activation energy, however, can only be determined when the logarithmic gasification temperature is known. This problem is solved by iteration.

3.3 Heat transfer

The steam velocity does influence not only the horizontal temperature profiles, but also the heat transfer from the heat exchanger into the fluidized bed. In fig. 9 steam velocity w and heat tranfer coefficient α are given during an experiment at 40 bar and 830 ^{o}C. During this run carbonized high volatile bituminous coal "Leopold" smaller 0,1 mm was gasified. The heat transfer coefficient α was calculated according to fig. 3. Between 70 and 270 minutes and using a steam velocity of about 4 cm/sec the heat transfer coefficient decreased from 1200 to 900 $kcal/m^2h^oC$. This can be attributed to an enrichment of ash within the gas generator. The division of α into a radiative and a convective part shall not be discussed here. In fig. 10 the dependance of the heat transfer coefficient α on steam velocity w is shown for two different particle sizes. The steep increase and the subsequent maximum is known {10, 11}. Our experiments at high temperatures and high pressures, however, do not cover the region at very high steam velocities and the transition between fixed bed and fluidized bed at low steam velocities. Our

experiments show as a peculiarity that αMAX is smaller for smaller particles. This can be by explained by heat exchanger fowling.

3.4 Density of the fluidized bed

Fig. 11 shows the time dependance of the pressure differences Δp and Δp_1 during a run at 40 bar using carbonized high volatile bituminous coal. Both pressure differences increase simultaneously in the beginning till height h_1 is reached, than Δp_1 remains essentially constant, whereas Δp increases further due to feeding. As soon as the desired height of the fluidized bed is attained the feeding is stopped. Then Δp decreases slowly due to gasification and carry-over. The pressure difference Δp is thus direct information concerning the height of the fluidized bed and can be used for controlling the frequency of feeding. The evaluation of the pressure differences according to the equations given in fig. 4 show that the density of the fluidized bed using carbonized high volatile bituminous is in the range of 300 kg/m^3.

4. Conclusion

Experiments performed in a small scale pilot plant are used for the determination of

- heats of reaction,
- kinetic constants,
- heat transfer coefficients,
- densities of the fluidized bed.

Though further experiments have to be performed the data already existing are used as basis for extensive computer studies and sensitivity analyses, which are necessary for the design and optimization of a future large scale gasification plant in combination with a high temperature nuclear reactor. All results received till now prove the feasibility of steam gasification of hard coal using nuclear heat at a temperature level of 950 ^{o}C.

Literature

1. K.H. van Heek, H. Jüntgen, and W. Peters
Erdöl und Kohle, Erdgas, Petrochemie 26, 701 (1973)

2. H. Jüntgen, K.H. van Heek, and J. Klein
Chem.Ing.Techn. 46, 937 (1974)

3. K.H. van Heek, H. Jüntgen, and W. Peters: Paper to the 8th Synthetic Pipeline Gas Symposium Chicago, Oct. 1976

4. H.W. von Gratkowski, Ullmanns Encyclopädie der techn. Chemie 10, 376 (1958)

5. G.G. von Fredersdorff and M.A. Elliot, in H.H. Lowry: Chemistry of coal utilization, London, Wiley & Sons 892 (1963)

6. K.H. van Heek, H. Jüntgen, and W. Peters
J. Inst. Fuel 46, 240 (1973)

7. A. Sulimma, H. Seiler, and P.P. Feistel
Erdöl und Kohle, Erdgas, Petrochemie (in press)

8. F.D. Rossini et al., Selected values of chemical thermodynamic properties Nat'l Bur. Standards Circular 500, U.S. Govt. Print Office, Washington, D.C. (1952)

9. P.P. Feistel, K.H. van Heek, H. Jüntgen: Paper to the First European Symposium on Thermal Analysis, Salford, Sept. 1976

10. A. Mersmann, Chem. Ing. Techn. 38, 1095 (1966)

11. E. Wicke and F. Fetting, Chem. Ing. Techn. 26, 301 (1954)

Acknowledgement

The work described in this paper is performed within the framework of a cooperation between Bergbau-Forschung GmbH Essen, Gesellschaft für Hochtemperaturreaktor-Technik mbH Bensberg, Hochtemperatur-Reaktorbau GmbH Köln, Kernforschungsanlage Jülich GmbH, and Rheinische Braunkohlenwerke AG Köln concerning the project "Prototyp plant Nuclear Process heat" (PNP) sponsored by the Federal Republic of Germany, Bundesministerium für Forschung und Technologie and the Land Nordrhein-Westfalen.

Heat Consumed = Heat Transferred

$$q \cdot k_0 \cdot e^{-E/RT} \cdot \gamma \cdot V = h \cdot F \cdot \vartheta(T, T_1, T_2)$$

q	=	heat of reaction	Gcal/t
k_0	=	frequency factor	1/h
E	=	activation energy	kcal/mol
R	=	gas constant	kcal/mol °C
T	=	gasification temperature	°K
γ	=	density of the fluidized bed	t/m³
V	=	volume of the fluidized bed	m³
h	=	overall heat transfer coeff.	kcal/m² h °C
F	=	heat transferring area	m²
ϑ	=	log. temperature difference	°K
T_1	=	helium inlet temperature	°K
T_2	=	helium outlet temperature	°K

Fig. 1: Heat balance of an allothermal gas generator

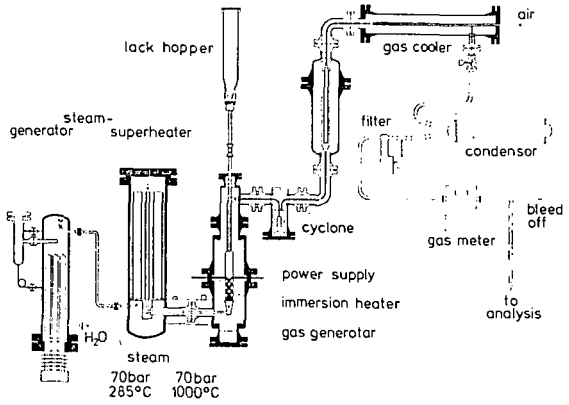

Fig. 2: Small scale pilot plant for steam gasification of coal

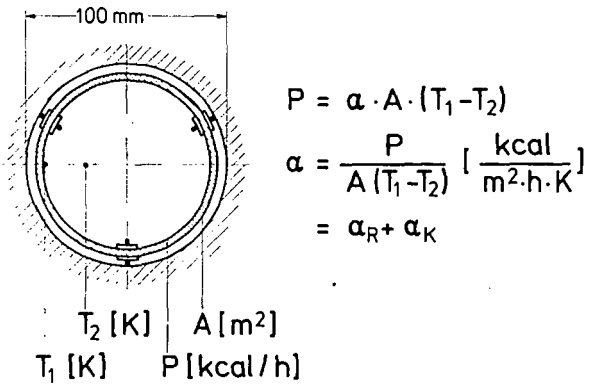

Fig. 3: Determination of the heat transfer coefficient from the heat exchanger into the fluidized bed

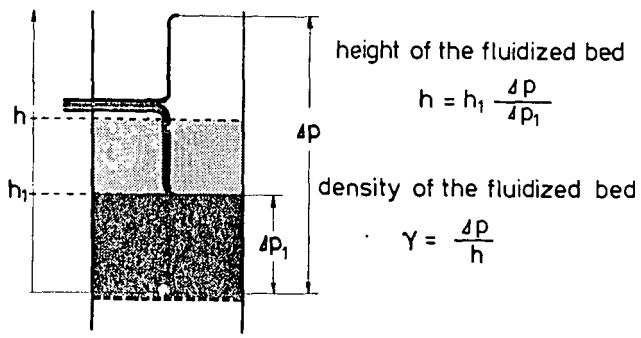

Fig. 4: Determination of the density of the fluidized bed

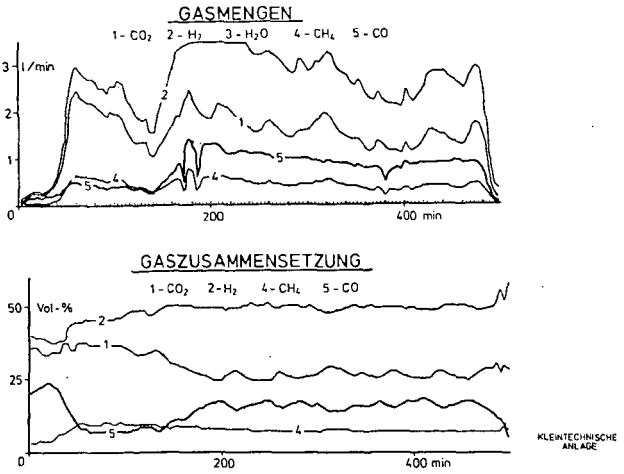

Fig. 5: Steam gasification of carbonized high volatile bituminous coal - gas production and gas composition -

H_2O^0/C / ϑ_R	10	30	100	150
700	27,57	23,27	12,40	8,84
750	21,83	17,15	7,21	4,41
800	16,36	11,67	3,55	1,78
850	11,47	7,18	1,45	0,61

CH_4
Vol % wf

Schwelkoks
Leopold
40 bar

Fig. 6: CH_4-content in the dry product gas (a), reaction heat (b), and steam decomposition (c) as function of reaction temperature and steam carbon ratio

H_2O^D/C / ϑ_R	10	30	100	150
700	338,7	374,6	733,1	916,3
750	528,9	591,7	1021,0	1209,8
800	748,8	842,8	1283,4	1427,6
850	988,5	1104,9	1465,0	1541,1

Utility
kcal/kg Koks

Schwelkoks
Leopold
40 bar

Fig. 6b

H_2O^D/C / ϑ_R	10	30	100	150
700	10,646	3,915	1,387	0,979
750	11,044	4,169	1,506	1,058
800	11,514	4,452	1,610	1,114
850	12,037	4,738	1,679	1,141

WDZ
%

Schwelkoks
Leopold
40 bar

Fig. 6c

Nr	Dauer h	T_{WB} °C	Umsatz %/min
2	5	750	0,5 (0,5)
3	23	800	1,9 (1,7)
4	9	860	4,2 (6,0)
7	18	820	2,5 (2,7)

Fig. 7: Comparison of reaction rate constants measured in a small scale pilot plant and in a fixed bed differential reactor ( )

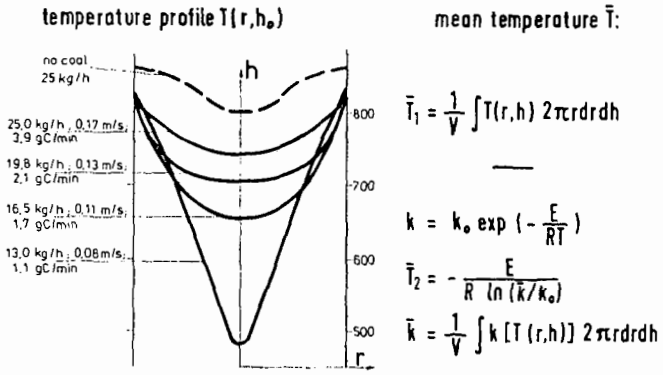

Fig. 8: Temperature profilesin the fluidized bed of the small scale pilot plant

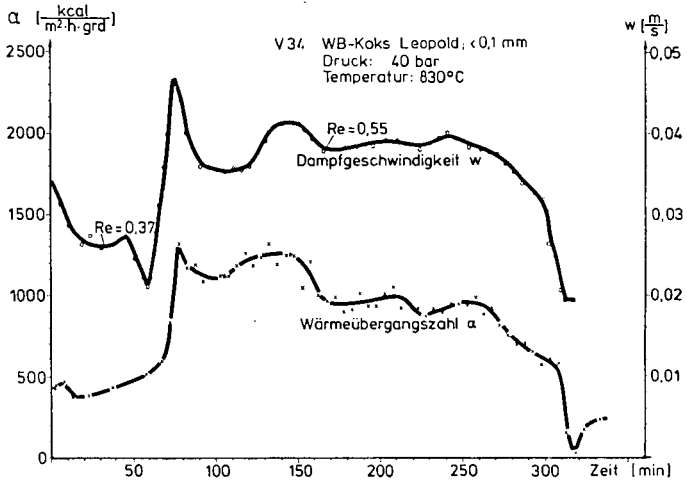

Fig. 9: Heat transfer coefficient and steam velocity as a function of time during a run at 40 bar and 830 °C

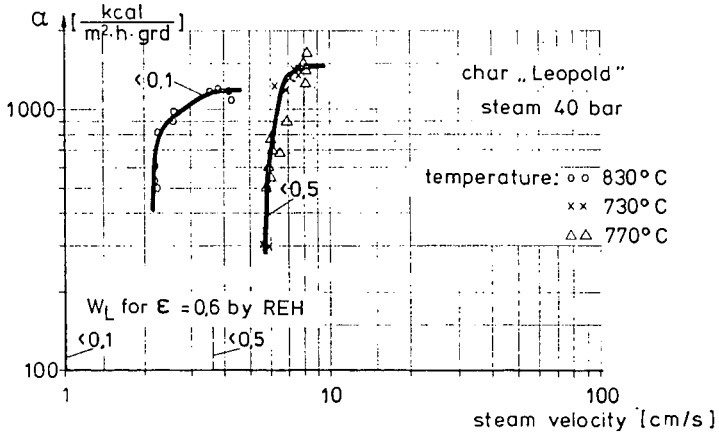

Fig. 10: Heat transfer coefficient as a function of steam velocity using two different particle sizes

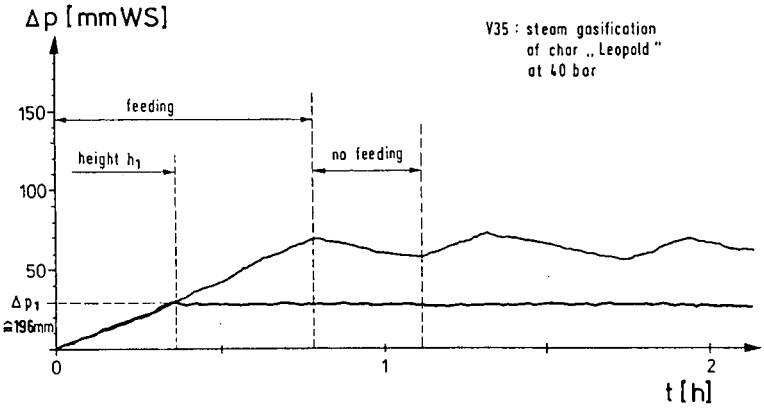

Fig. 11: Pressure differences within the fluidized bed as a function of time

MIXING AND REACTION OF PULVERIZED COAL IN AN ENTRAINED GASIFIER[1]

L. Douglas Smoot, F. Douglas Skinner, and Richard W. Hanks

Chemical Engineering Department, Brigham Young University, Provo, Utah 84602

INTRODUCTION

Several coal gasification processes under development include an entrained gasifier as one step in the process. In such cases, coal or char is contacted with a hot gas to cause particle combustion or gasification. Design and optimization of such units require an understanding of particle gasification kinetics, together with insight into turbulent mixing processes of the coal-laden streams with the hot gases. The present study is designed to develop an understanding of the physical and chemical rate processes that occur during gasification of entrained, pulverized coal particles.

Specific objectives are to measure locally: (1) the extent of mixing of primary and secondary gases, (2) the extent of particle dispersion, (3) the extent of particle reaction, and (4) the gaseous reaction products including pollutants. This study includes both non-reacting and reacting flow tests to be run at pressures from 1 to 20 atm. Key to the technical approach is particle and gas sampling from the reactor using water-cooled probes. Separate key components in primary and secondary streams will indicate directly the extent of gas phase mixing at the various sampling points. The particulate portion of each sample will be analyzed to determine ash, volatiles, and sulfur and nitrogen content.

TEST PROGRAM

Design of the coal gasification test program and test facility were based on review of the literature and discussions with agencies doing development work on entrained flow gasifiers. The baseline proportions of coal, oxygen and steam were determined by optimizing the theoretically computed cold gas efficiency based upon equilibrium gasification products of a typical high volatile Bituminous B coal. The baseline selected was 38 gm steam and 56 gm oxygen per 100 gm coal.

Experimental variables which were considered in establishing the test program included the particle feed rate, gas preheat temperature, primary and secondary stream velocities, secondary to primary injection angle, operating pressure, percent coal loading level, coal particle size and coal type. Table 1 summarizes the range of selected test conditions to be investigated in this study. A total of 50-60 tests are planned for the reacting test program.

TABLE 1. COAL GASIFIER TEST VARIABLES

VARIABLE	RANGE OF VARIATION
Pressure	1 - 20 atm
Coal Type	17 - 40% volatiles
Secondary Injection Angle	0 - 30°
Particle Size	30 - 60μ
Secondary Temp.	600 - 700°K
Secondary/Primary Velocity Ratio	1.25 - 2.0
Coal Feed Rate	70 - 140 kg/hr
Solids Loading	70 - 85%

1. This work is supported by U.S. ERDA, Washington, D.C., under Contract No. E(49-18)-1767, with Dr. Paul Scott, Technical Project Officer.

FACILITY DESIGN AND INSTALLATION

Figure 1 shows photographs of the reactor and a section of the reactor. Oxygen from a bank of high pressure gas cylinders flows through two automatic control valves which divide the flow between primary and secondary streams and maintain the desired pressure level upstream of choke flow nozzles, thus determining the mass flow rates of primary and secondary oxygen. The primary oxygen is preheated and entrains coal particles which are fed to the primary stream from a high pressure, double-auger feeder. The primary stream, consisting of O_2 and entrained coal, enters the reactor through the 1.27 cm diameter inner pipe of a concentric-pipe, annular burner.

The secondary oxygen flows to another preheater, where it mixes with saturated steam from an electric boiler. The steam and oxygen mixture is further heated to the desired temperature and then fed through the outer concentric annular pipe. The gasification reactions take place downstream of the burner jet exit in the 20 cm. diameter, ceramic-lined reactor chamber. The 1.2 m long reactor chamber, shown schematically in Figure 2 consists of several segments of 15 and 30 cm lengths, one of which is the test probe section. By changing the order in which these segments are bolted together, the test probe section may be placed at 15 cm axial increments along the length of the reactor chamber.

After leaving the reactor, the hot reaction gases and char residue are cooled and the solids are scrubbed out of the gas phase with water in a packed scrubber. The cooled gas is vented and the scrubbing liquid is reduced in pressure and disposed of in the sewer drain.

TEST PROCEDURES AND MEASUREMENTS

The variables to be measured include temperature, pressure, and gas and particle compositions. Reactor temperatures are measured with either ceramic-shielded Platinum/Platinum-6% Rhodium thermocouples or suction pyrometers. Each reactor section has three thermocouple ports equally spaced around the inside wall of the ceramic liner, so that temperature variations in both the axial and angular directions can be measured. In addition, radial temperatures will be measured in the probe section. Reactor pressures are measured with transducers. Thermocouple ports can be used as pressure ports if desired, so that pressures can be measured at several axial and angular locations in the reactor.

Particulate and gas samples are obtained with water-cooled probes which are located in several radial positions in the test section. Similar probes have been used successfully in reacting flow measurements by this laboratory in earlier studies (1,2). The gas samples are analyzed using a gas chromatograph to determine concentrations of CO, CO_2, H_2, O_2, light hydrocarbons, and a gaseous tracer. The solid char sample is analyzed to determine ash, volatiles, sulfur and nitrogen content, together with other elements. The ash content of the coal is used as the solid phase tracer in order to determine the dispersion rates of the coal or char particles. Recent work (3), has indicated that some ash components may vaporize and decompose in the flame, and this problem is being considered.

The final piping and facility assembly is completed and facility check-out and cold flow tests have been conducted. Available results from several cold flow tests will be presented and discussed. From several cold-flow test results at atmospheric pressure, the following observations have been made: (1) the coal particles disperse much more slowly than the gases; (2) increasing the secondary velocity or the injection angle both significantly increase the rates of gas and particle dispersion; (3) reducing the particle size significantly increases particle dispersion rates. Additional test results will be given in the presentation. It is anticipated that some test data for reacting gasification tests will also be included in the presentation.

ENTRAINED GASIFIER MODEL

A computerized model for predicting characteristics of pulverized coal combustion

and gasification uses the integrated or macroscopic form of the general conservation equations (4) for a volume element inside a gasifier or furnace, as illustrated in Figure 3. The following aspects of pulverized coal combustion have been included in the model: (1) mixing of primary and secondary streams; (2) recirculation of reacted products; (3) pyrolysis and swelling of coal; (4) oxidation of the char by oxygen, stream and carbon dioxide; (5) conductive heat transfer between the coal/char particles and gases; (6) variation in composition of inlet gases and solids; (7) variation in coal/char particle size; (8) oxidation of the hydrocrbons produced from coal pyrolysis; and (9) radiative heat transfer among the particles.

Key assumptions for this model are shown in Table 2, while differential mass, energy and momentum balances for particle and gas phases are summarized in Table 3. This set of first-order, non-linear equations also requires a large number of auxiliary, algebraic equations as component model parts. These equations describe the following aspects of the coal gasifier process: enthalpy-temperature relationships, physical properties including heat capacity, thermal conductivity, diffusivity, and viscosity; radiative interchange inside the gasifier; equations of state and mass flow continuity; convective and conductive heat interchange among the gases, particles and walls; rates of pyrolysis and oxidation of coal and char.

TABLE 2

Summary of Key Assumptions for Coal Model

1. Steady-state, compressible gas, with specified pressure variation.
2. Particles and gases in dynamic equilibrium.
3. Secondary gases and recirculated products input along reactor with instantaneous mixing.
4. Multiple particle sizes or types.
5. Particle phases and gas as separate phases.
6. Negligible gas conduction, diffusion, and thermal diffusion, gravity effects, particle interactions, wall friction, viscous dissipation, work on surroundings, gas phase radiation, particle-phase convective losses, kinetic energy.
7. Rate limiting steps include upstream radiation, gross oxidizer/fuel mixing, product recirculation, coal particle pyrolysis, char oxidation (with O_2, CO_2, H_2O).
8. Gas phase in local thermodynamic equilibrium.
9. Specified gas and particle ignition temperatures.
10. Coal pyrolysis by parallel activated processes.
11. Coal swelling proportional to extent of pyrolysis.
12. Spherical particles of uniform local particle temperature with specified char diameter and with internal and external reaction.
13. Irreversible particle reactions.
14. Ash inert and remains with the particle.
15. Moisture loss controlled by vapor diffusion.
16. Hydrocarbon volatiles produced from coal pyrolysis reactions, together with specified other chemical elements.
17. Char contains specified proportions of other elements which enter the gas phase at a rate proportional to the carbon reaction.
18. Char oxidation first order heterogeneous reaction, coupled with oxidizer diffusion to particle surface.

TABLE 3

Summary of Model Differential Equations

Type	Equation
Gas Element Continuity (k^{th})	$d(w_g\omega_k)/dx = A \sum_j r_{jk} + m_{sgk} + m_{\rho gk}$
j^{th} Particle Phase	$dw_j/dx = -Ar_j + m_{sj} + m_{\rho j}$
Gas Energy	$d(w_g h_g)/dx = h_{sg}m_{sg} + h_{\rho g}m_{\rho g} + A(\sum_j Q_j - Q_{cb} + \sum_j r_j h_{jg})$
Particle Energy (j^{th})	$d(w_j h_j)/dx = m_{sj}h_{sj} + m_{\rho j}h_{\rho j} + A(Q_{fj} - Q_{rb} - Q_j - r_j h_{jg})$
Gas Momentum	$d(w_g v)/dx + d(pA)/dx = m_s v_s + m_\rho v_\rho + vA\sum_j r_j$
Particle Number	$d(vn_j)/dx = (m_{\rho j}/\alpha_j A)$
Total Gas Continuity[1]	$d(w_g)/dx = A\sum_j r_j + m_{sg} + m_{\rho g}$
Coal Mass	$d(\alpha_{cj})/dx = -(r_{cj}/n_j v)$
Char Mass	$d(\alpha_{hj})/dx = -(r_{hj}/n_j v)$
Moisture Mass	$d(\alpha_{wj})/dx = -(r_{wj}/n_j v)$

1 Sum of Eqns 1 over k elements

A numerical solution has been developed for this entrained gasifier model. The model has been used to investigate effects of test variables on the extent of coal gasification and on the gas phase composition. Results indicate that the pyrolysis process is very fast and that oxygen in the gas phase is rapidly converted to CO_2. This is followed by the relatively slow CO_2-H_2O reactions with residual char. Specific predictive results will be presented in the paper and compared with available experimental results.

REFERENCES

1. Abbott, S.W., L.D. Smoot, and K. Schadow, "Direct Mixing and Combustion Efficiency Measurements in Ducted, Particle-Laden Jets," AIAA J., 12, No. 3, 275-282 (1974).

2. Smoot, L. Douglas, Horton, M. Duane and Williams, Gerald A., "Propagation of Laminar Pulverized Coal-Air Flames," 16th Symposium (International) on Combustion, Boston, Mass., August, 1976.

3. Padia, A.S., A.F. Sarofim, and J.B. Howard, "The Behavior of Ash in Pulverized Coal Under Simulated Combustion Conditions," Comb. Inst. (Central States Sect.), April (1976).

4. Bird, R.B. N.E. Stewart, and E.N. Lightfoot, "Transport Phenomena," John Wiley and Sons, New York, (1960).

NOMENCLATURE

m_s	rate of secondary flow into control volume	Q_{fj}	rate of radiative heat transfer in reactor
w_g	rate of gas flow into control volume	T_b	wall temperature
w_j	rate of particle flow into control volume	A	cross sectional flow area
m_ρ	rate of recirculation into control volume	w_k	mass fraction of k^{th} element
Q_j	heat conduction between gas & particles	x	axial coordinate
r_j	rate of pyrolysis and oxidation of coal/char	h	static enthalpy
r_i	rate of reaction of gas species	v	velocity
Q_{cb}	rate of heat loss by convection	p	pressure
Q_{rb}	rate of heat loss by radiation	n_j	particle number density
		α	mass of particle

Subscripts

g	gas	c	coal
κ	k^{th} element	h	char
s	secondary	a	ash
ρ	recirculation	w	moisture
j	j^{th} particle		

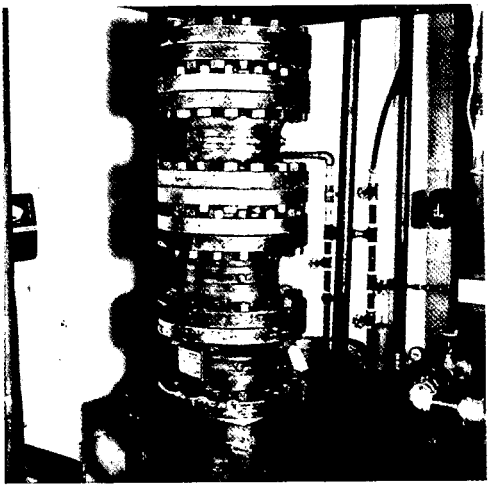

High Pressure Reactor

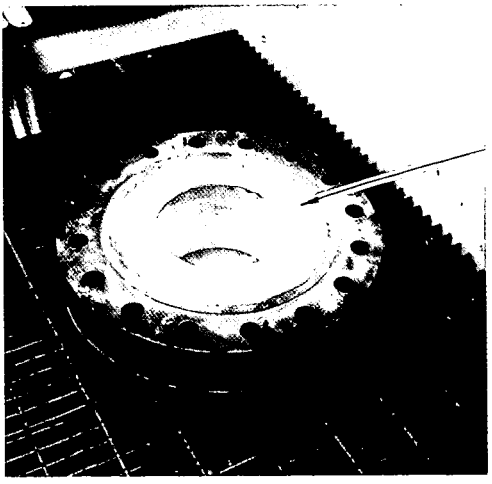

Typical 6" Reactor Section

Figure . High Pressure Reactor and Typical Section.

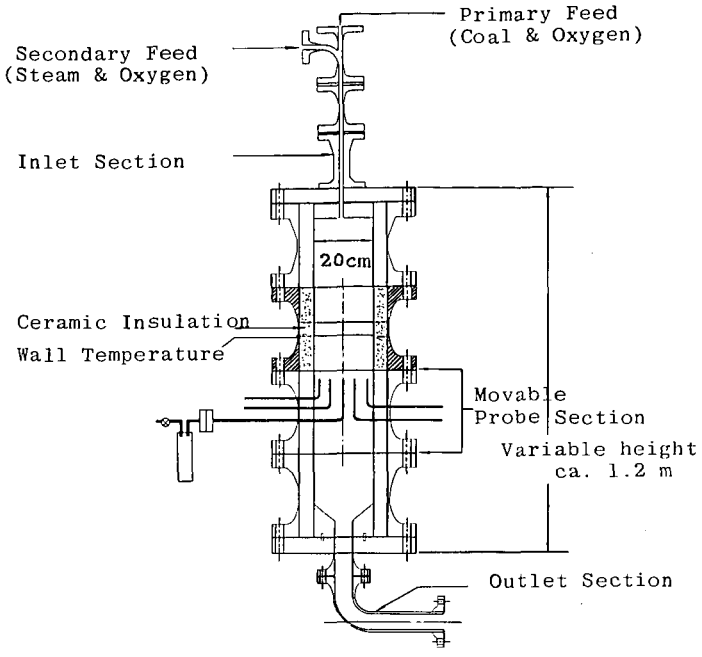

Figure 2. High Pressure Entrained Gasifier

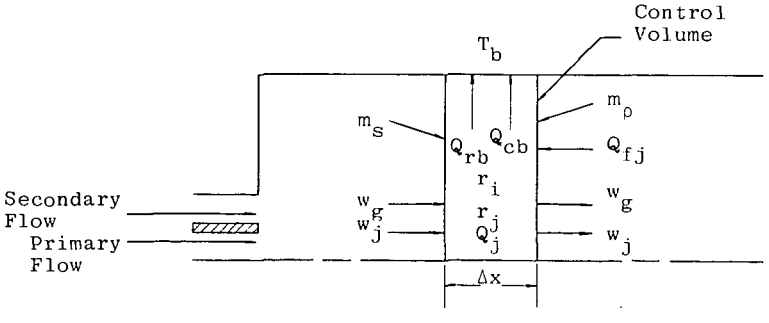

Figure 3. Schematic Diagram of Macroscopic Coal Gasification Model.

KINETIC DATA FROM A HIGH TEMPERATURE ENTRAINED FLOW GASIFIER

Ralph L. Coates

Chemical Engineering Department, Brigham Young University, Provo, Utah 84602

Introduction

An experimental program is currently being carried out at the Eyring Research Institute in which several different coals are being tested in a laboratory scale entrained flow gasifier. The design of the gasifier is essentially a scaled down version of an experimental gasifier operated at the Bureau of Mines Morgantown Coal Research Center (1, 2). This gasifier is being operated under contract with the Energy Research and Development Administration to obtain reaction rate and conversion efficiency data for several different coals and chars.

Description of Gasifier

A diagram of the gasifier is shown in Figure 1 and a flow diagram for the entire gasification system is presented in Figure 2. The reaction chamber, formed from silicon carbide is 7.6 cm I.D. and 28 cm in length. The coal, pulverized to 70-80 percent minus 200 mesh, is withdrawn with metering augers from a pressurized feed tank and blown into the top of the reaction chamber with recycled product gas. It enters the reactor through a water-cooled 8 mm I.D. nozzle. A preheated mixture of steam and oxygen is injected into the reactor through eight nozzles that closely surround the coal nozzle. These nozzles have rectangular openings, 1.1 x 1.5 mm in cross-section, and the oxygen-steam streams impinge on the coal stream at an angle of 30°.

The reactor effluent stream is cooled by radiation to the water-cooled walls fo the heat recovery unit which is attached to the base of the reactor. The heat recovered in this unit is used to generate the feed steam for the gasifier. Slag droplets and larger solid particles in the effluent stream are separated from the gases and they are then further cooled and cleaned by passage through a convective heat exchanger, a scrubber column, and fabric filters (Figure 2). Gas samples are withdrawn downstream of the filters. The cooled and cleaned gas is then metered and flared.

Gasifier Operating Conditions

High volatile, low sulfur, bituminous coal from the Deseret Mine in Carbon County, Utah, was used for these tests. This coal has a high heating value of 1430 kcal/kg. It is 70.1 percent carbon, 5.6 percent hydrogen, 11.7 percent oxygen, 1.4 percent nitrogen, 0.6 percent sulfur, and 10.6 percent ash (dry basis). The moisture of the coal as fed to the gasifier was approximately one percent.

To obtain the data reported here the gasifier was operated at a nominal pressure of 10 atmospheres and coal feed rates were 20 kg/hr. The volumetric flow rate of the recycle gas stream was 5 M^3/hr at STP. The oxygen and steam feed stream was preheated to 400°C for these test. The principal test variable was oxygen feed rate. The steam/coal feed ratio was 0.5 g/g. Product gas samples were not taken until steady-state operation was achieved, 20-30 minutes after start up.

Test Results

Results from a series of ten test runs in which the oxygen/coal feed rates were systematically varied are presented in Figures 3 and 4. Figure 3 shows the volume of dry gas produced per kg coal fed and the percent of carbon converted to gas. As observed during the Bureau of Mines studies (1,2)the carbon conversion increased markedly with increasing oxygen/coal ratio. Gas volume also increased with increases in this ratio. Figure 4 presents the corresponding gas composition

data. Carbon monoxide increased with increasing oxygen/coal ratio whereas the yield of hydrogen and methane decreased. The carbon dioxide concentration varied only slightly.

Data Analysis Procedure

After careful study of kinetic data available in the literature for the high temperature reaction of coal with oxygen and steam, it was concluded that the rate limiting reactions at the conditions employed in these tests were those of charred coal with steam and with carbon dioxide. The reactions of oxygen with coal volatiles and with char were calculated to be at least an order of magnitude faster. For example, the data of Kimber and Gray (3) indicate the specific reaction rate of both CO_2 and water vapor with 35 micron char particles to be less than 5 grams carbon/gram unreacted carbon per second per atmosphere partial pressure of the CO_2 or water. The data of Khitrin and Golovina (4) suggests rates of 3.3 sec^{-1} atm^{-1} and 1.9 sec^{-1} atm^{-1}, respectively, for water and CO_2 with char at 2000°K. On the other hand, the rate equation recommended by Field, et.al., (5) for the reaction of oxygen with char yields a specific rate of 1900 sec^{-1} atm^{-1} at this temperature.

Reaction rates of coal volatiles with available oxygen are even faster than the oxygen-char rates. Employing the rate equation suggested by Field (5). The specific reaction rate for the carbon monoxide-oxygen reaction is estimated to be of the order of 10^5 sec^{-1} for the conditions used in these experiments.

Mixing and diffusion rates were also considered in selecting a procedure for analyzing the data. The gasifier feed nozzle configuration used in these tests was selected after extensive tests of alternate configurations. These tests demonstrated that it provided rapid and efficient mixing of the feed streams. The recirculation rate near the point where the feed streams were injected was estimated to be approximately 150% of the mass flow of the feed streams. Consequently, it seems reasonable that as a first approximation the reactor might be considered as being well-mixed. Diffusion rates of steam and CO_2 to the surface of the char particles were considered by calculating the diffusion limited reaction rates. These were estimated to be of the order of 50-100 sec^{-1} at the experimental conditions of this study and were therefore considered to be of secondary importance in limiting the overall reaction rate.

On the basis of the above reasoning the data were analyzed assuming the reactor to be well stirred and that the gasification reactions could be represented by two simple reactions:

$$\text{Coal} + \text{Oxygen} \rightarrow CO_2 + H_2O + \text{Char} \qquad 1)$$

$$\text{Char} + CO_2 + H_2O \rightarrow CO + H_2 \qquad 2)$$

with reaction (1), which includes devolatilization of the coal, assumed to be fast relative to reaction (2).

The fraction of carbon gasified by equation (1), Y_1, may be calculated from the following stoichiometric equation:

$$Y_1 = \Phi - \tfrac{1}{2}(O/C)\ (\Phi - \varepsilon_O) + \tfrac{1}{4}(H/C)\ (\Phi - \varepsilon_H) \qquad 3)$$

In this equation, Φ is the equivalence ratio of the oxygen and coal feed streams, a value of one corresponding to a feed ratio such that sufficient oxygen is available to convert the carbon to CO_2 and the hydrogen to H_2O. The ratios (O/C) and (H/C) are the molar ratios of oxygen to carbon and hydrogen to carbon in the coal, and ε_O and ε_H are the fractions of oxygen and hydrogen that are gasified by reaction (1). The fraction of carbon gasified by reaction (2), Y_2, may then calculated from Y_1 and the total fraction of carbon gasified Y_T, which is available from the experimental data. Thus,

$$Y_2 = Y_T - Y_1 \qquad 4)$$

A further simplification is the assumption that the rate of reaction (2) is first order with respect to the amount of unreacted carbon.

$$\frac{dy}{dt} = k\ (1 - Y) \qquad 5)$$

The equation for the reaction rate constant resulting from integration of equation (5) is

$$k = -(1/t)\ \ln\ (1 - Y_T)/(1 - Y_1) \qquad 6)$$

This rate constant which is the specific reaction rate, can be utilized as a measure of the reactivity of the coal.

The reaction time was taken to be the ratio of the reactor volume to the volumetric flow rate of the reaction products at the outlet of the reactor. The density at the outlet was computed from the dry gas analysis and an overall oxygen balance and energy balance. The oxygen balance yielded the steam concentration and the overall energy balance yielded the outlet temperature. The temperature calculation was verified by thermocouple measurements that were made in several of the runs.

Specific Reaction Rates

The specific reaction rates that were computed from the experimental data are presented in Figure 5 versus the oxygen/coal equivalence ratio. Reactor outlet temperatures are also presented on this figure. It is noted that magnitudes of these rates are somewhat higher than the rates measured by Kimber and Gray (3) and by Khitrin and Golovina (4). A cross-plot of the rate constant and temperature data yielded the following correlating equation:

$$k = 1.4 \times 10^5\ \exp\ (-31{,}000/RT)\ \sec^{-1} \qquad 7)$$

The magnitude of the apparent activation energy, 31 kcal, is consistent with the assumption that the char surface reaction with CO_2 and steam is the rate limiting step in the gasification of this coal.

Aknowledgements

This study was funded by the Fossil Energy Divsion of the Energy Research and Development Administration under Contract No. E(49-18)-1548. The experimental work was carried out by Mr. Jay Bennion and Mr. Wiliam Liston.

References:

1. Holden, J.H., et al., "Operation of Pressure-Gasification Pilot Plant Utilizing Pulverized Coal and Oxygen: A Progress Report," Report of Investigations 5573, U.S. Dept. of the Interior, Bureau of Mines (1960).

2. Holden, J.H., K.D. Plants, et al., "Operating a Pressurized-Gasification Pilot Plant Using Pulverized Coal and Oxygen: Effect of Heat Loss of Economy," Report of Investigations 5956, U.S. Dept. of the Interior, Bureau of Mines (1962).

3. Kimber, G.M., and Gray, M.D., "Reaction of Charcoal Particles with Carbon Dioxide and Water at Temperatures up to 2800°K," Nature, Vol. 214, 1967.

4. Khitrin, L.N., and Golovina, E.S., in High Temperature Technology, Butterworths, London, 1964, pp. 485-496.

5. Field, M.A., Gil, D.W., Morgan, B.B., and Hawksley, P.G.W., Combustion of Pulverized Coal. The British Coal Utilisation Research Association, Leatherhead, 1967.

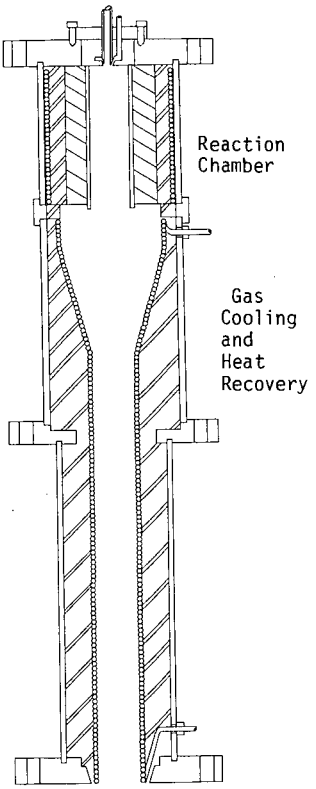

Figure 1. Diagram of laboratory gasifier.

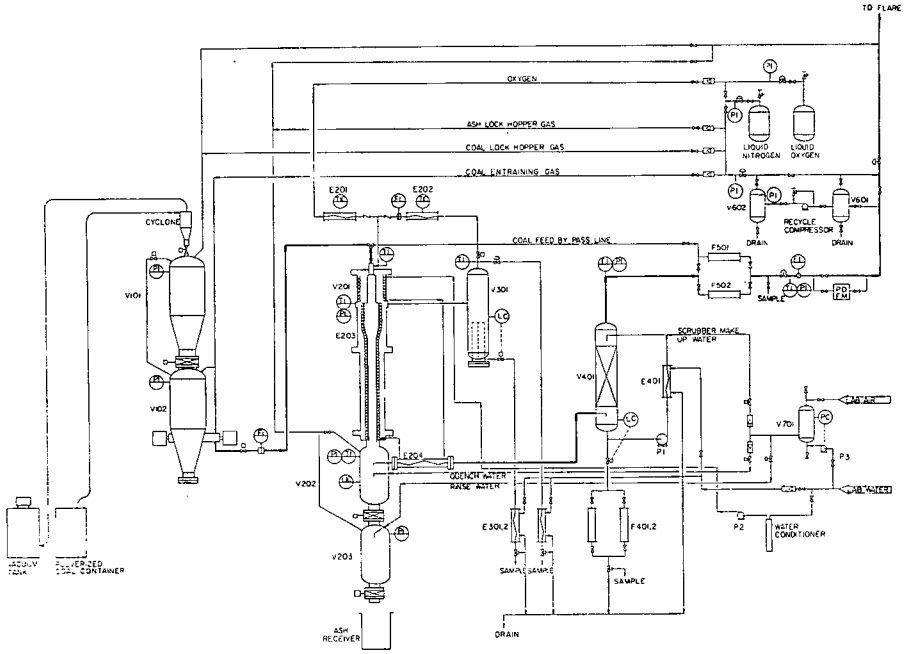

Figure 2. Flow diagram of laboratory gasification system.

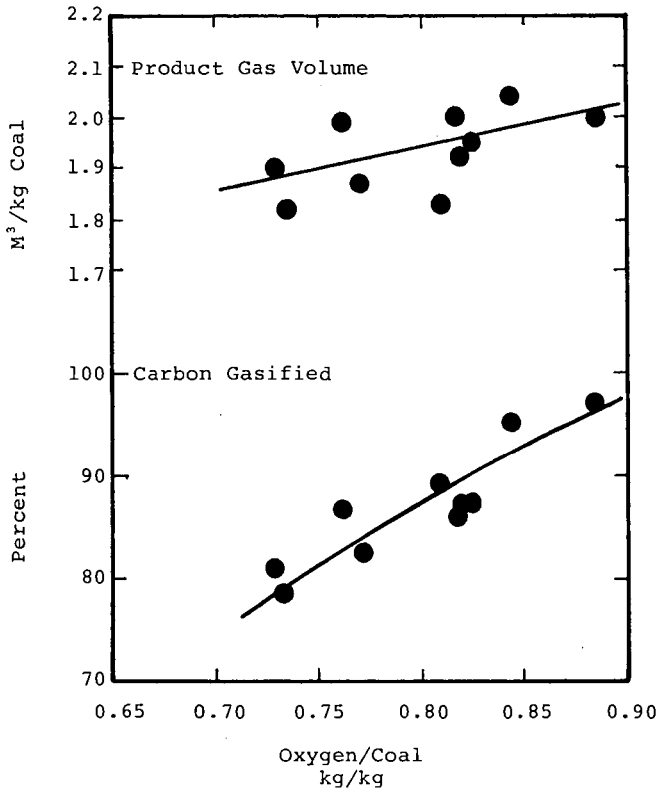

Figure 3. Gas volume and carbon conversion data from tests with Deseret Mine bituminous coal at 20 atm.

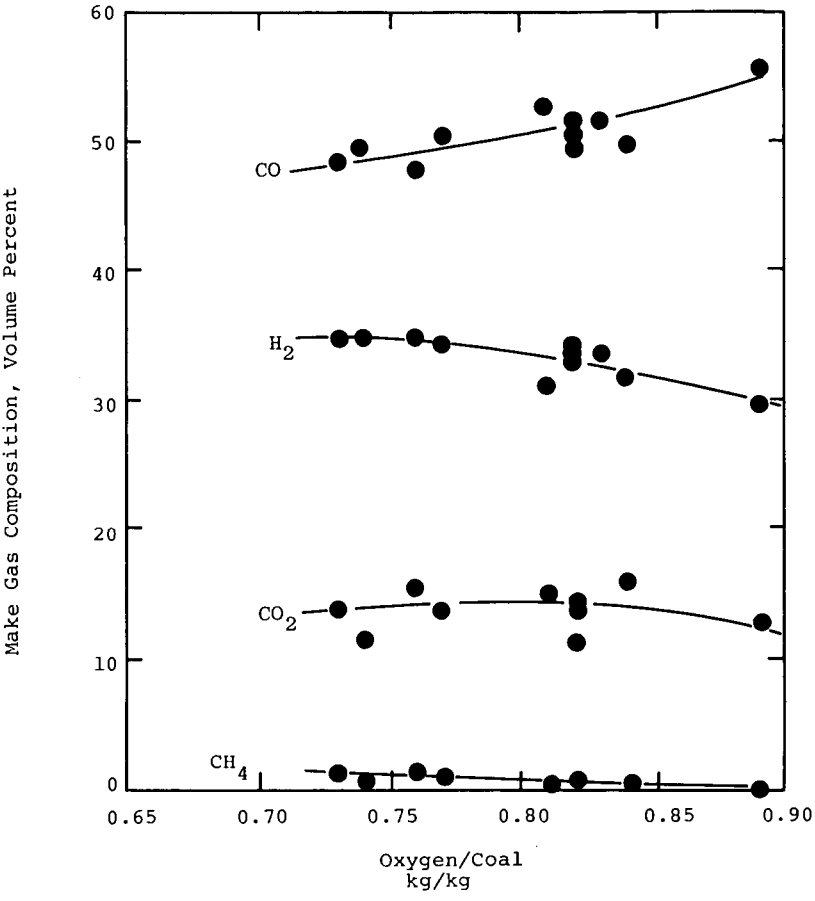

Figure 4. Gas composition data from tests with Deseret Mine bituminous coal at 20 atm.

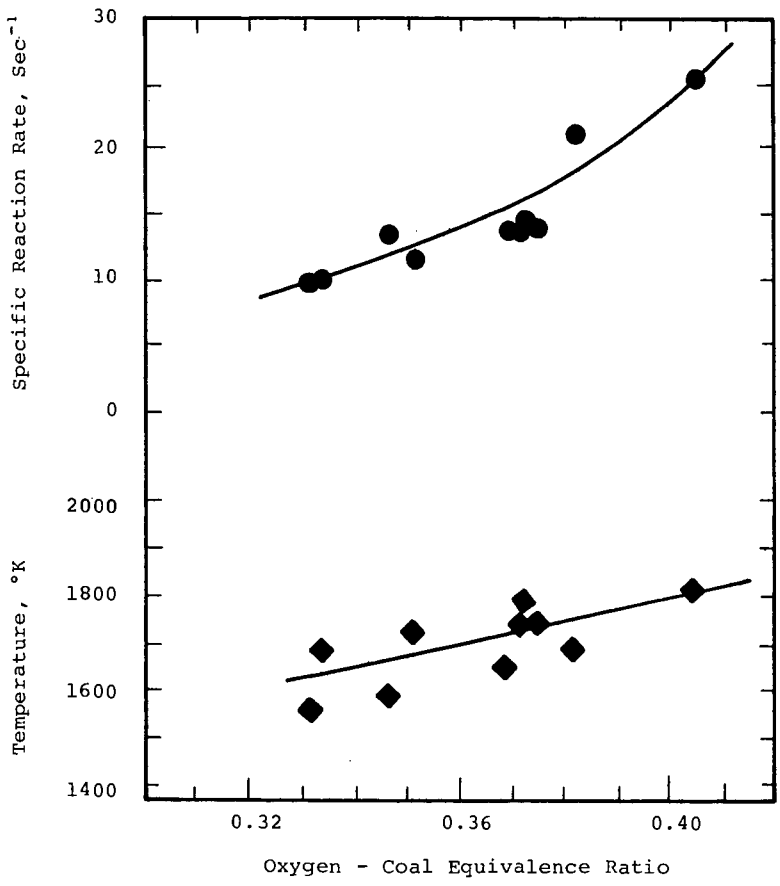

Figure 5. Specific reaction rates and reactor outlet temperatures calculated from Deseret Mine Coal test data.

PYROLYSIS OF LARGE COAL BLOCKS: IMPLICATIONS OF HEAT AND MASS TRANSPORT EFFECTS FOR IN SITU GASIFICATION*

Phillip R. Westmoreland and Richard C. Forrester III

Oak Ridge National Laboratory
Oak Ridge, Tennessee 37830

Gas production during pyrolysis of blocks of coal is strongly affected by heat and mass transfer resistances. Since large pieces of coal must be pyrolyzed during in situ gasification, these effects become important in modeling, production, and resource recovery. Experiments have shown that pyrolysis of subbituminous coal blocks, which are typically heated at 3.0 C°/min at the block surface and which have the high moisture content of in situ coal, evolves substantially more gas than does pyrolysis of powders.

Coal pyrolysis reactions are fundamental in all coal conversion processes. Coal chemical structures are thermally decomposed at 250°C or higher to produce liquid vapors, noncondensible gases, and a solid char residue. This decomposition may be utilized in coking or as part of the combustion, gasification, or liquefaction processes. For example, pyrolysis, partial combustion, and steam-char reactions combine in gasification to produce a combustible gas and an ash residue. Heat and mass transfer interferences with these chemical reactions are normally minimized in conventional coal conversion by crushing and drying the coal prior to processing.

Underground coal gasification (UCG) or in situ gasification represents a modeling challenge for coal pyrolysis because of three unusual characteristics: large particle size, high water content, and low heating rates. A typical UCG process feeds oxygen or air into a coal seam, supporting a moving, high-temperature reaction front (flame front). To permit flow of air to the front and flow of product gases away from it, seam permeability is increased by explosive fracturing, by burning a high-permeability path between injection and production pipes, or by other methods. Each of these methods leaves large blocks or sections of coal intact. Also, since seams are chosen to be below the water table, in situ coal reserves for UCG may be typically 30% moisture. Finally, the gasification front in several schemes moves at about 1 m/day, cocurrent with the faster gas flow. Hot product gases thus produce a slow-moving temperature gradient ahead of the front, slowly heating the coal.

Understanding of block pyrolysis and other aspects of UCG is important in its development toward being a significant, economical energy source. The concept of UCG was first proposed in 1868 by Sir William Siemans, and full-scale UCG operations in the U.S.S.R. have continued since the 1930's; however, despite large research programs immediately after World War II, no Western nation was able to develop an economical UCG process (1). The United States began UCG development in 1971, and results to date have been both technically and economically promising. Successful development of UCG would make an estimated 750 billion tons of coal available for energy production, as compared to the 297 billion tons of coal reserves listed by the Bureau of Mines as recoverable by strip or underground mining (2). In addition to utilizing otherwise inaccessible coal, UCG could have less of an environmental impact than either underground or strip mining and could improve resource recovery and personnel safety over that of underground mining.

Because of the potential of UCG and the unavailability of adequate data for process modeling, Oak Ridge National Laboratory began research in 1974 on pyrolysis of coal blocks at low heating rates. Primary variables in this study have been

*Research sponsored by the Energy Research and Development Administration under contract with Union Carbide Corporation Nuclear Division.

heating rate and final temperature, and these data have been compared to data on pyrolysis of powdered coal from the same source. Data and observations from these experiments have been shared with Energy Research and Development Administration UCG process developers at Laramie (Wyoming) Energy Research Center, Lawrence Livermore (California) Laboratory, and Morgantown (West Virginia) Energy Research Center, and have been incorporated into process models as deemed appropriate.

Equipment and Procedure

Figure 1 depicts the block pyrolysis equipment schematically. In the experiment, an approximately 15-cm-diam by 15-cm cylindrical block of coal was positioned on insulating blocks in the bottom of a 60-cm deep, thin-walled reactor vessel, fabricated from 8-in. Sched 10 304L stainless steel pipe. Protection of the reactor from external oxidation at high temperatures was afforded by a commercially prepared nickel-chromium-aluminum coating (Metco No. P443-10). Heat for pyrolysis was supplied by an electrical furnace, with reactor temperature controlled by an ORNL-fabricated temperature programmer. Control thermocouples, thermocouples for internal and external block temperature measurements, an inert gas purge line, and an exhaust line heated to 250°C were connected to the reactor through a flanged top. Condensibles (water and tars) were removed from the hot reactor exhaust by direct contact with water-cooled copper coils and by a fine glass-wool demister. A sufficient number of noncondensible gas samples were collected into evacuated sample bottles to describe gas evolution as a function of time. Finally, gases were metered and vented.

For these experiments, blocks of unweathered subbituminous coal were selected at the mine face from the Roland and Smith seams (Wyodak Resources Development Corporation, Wyodak, Wyoming). To prevent drying and breakage, these blocks were bagged in plastic and cushioned for shipping. Upon receipt at ORNL, coal was placed under water for storage until and after it was machined into cylinders. All machining operations were performed under a water spray for cooling and to prevent drying. Thermocouple holes (1.6-mm diam) were drilled through the top of the coal cylinder down to a middle, common plane. Hole patterns were chosen to minimize heat conduction through radially placed thermocouples (for example, spiraling outward from the block center); 1.0-mm-diam thermocouples were used for similar reasons. Standard analyses of the coal are reported in Table 1.

Table 1. Analyses of coal taken from the Roland-Smith seams, Wyodak Resources Development Corporation, Gillette, Wyoming

Moisture, wt %	30.0	Ultimate analysis, moisture-and-ash-free wt %	
Proximate analysis, dry wt %		Carbon	73.3
Ash	5.3	Hydrogen	5.2
Volatile matter	47.0	Nitrogen	1.1
Fixed carbon	47.7	Sulfur	0.56
		Oxygen	19.8
Standard calorific content, Btu/lb moisture-and-ash-free	12,800		

The experiment was preceded by an argon purge of air from the closed system. A constant flow of argon was maintained throughout the experiment, both to establish a tie element for calculating gas flowrates and to sweep gases and vapors from the reactor. The experiment itself consisted of elevating reactor temperature at a predetermined rate to a predetermined maximum, then holding it until the reaction was complete. Meanwhile, pressure, temperature, and flowrates were monitored, liquids were condensed and collected, and gas was sampled periodically. After completion,

the reactor was cooled to ambient temperature. Because pyrophoric chars were created in most experiments, the block of char (still dimensionally stable) was carefully removed and sampled under an argon blanket. Liquids were carefully removed and weighed, and gases were analyzed by a combination of low-resolution mass spectrometry and gas chromatography.

Data and Interpretation

General effects of heat and mass transfer resistances may be observed by comparison of block and powder pyrolysis data and by comparison of block pyrolysis data at different heating rates. Three representative experiments permit these analyses:

1. powder pyrolysis at 3.33 C°/min to 950°C (3),
2. block pyrolysis at 3.0 C°/min to 950°C, and
3. block pyrolysis at 2.0 C°/min to 1000°C.

Because of minimal heat and mass transfer effects indicated in the powder data of Campbell (3), a small heating-rate difference does not hinder comparison with the resistance-hindered second experiment. A satisfactory comparison may be made between experiments 2 and 3 since the effects of slightly different final temperatures are negligible compared to the effects of the different heating rates. The unimportant difference between powder heating rate and 3.0 C°/min may be eliminated and data at the two block heating rates may be compared directly by changing the ordinate from time to τ, a pseudo-temperature (°C) defined as:

$$\tau = T_o + \dot{T}_s \cdot t, \qquad 1)$$

where T_o is ambient starting temperature, $\dot{T}_s$ is the rate of temperature increase at the block surface, and t is elapsed time. It may be observed that τ is the same as surface temperature until maximum surface temperature is reached; from that point, it continues the same proportional relationship to time.

Heat transfer in block pyrolysis is most significantly affected by water content. In Fig. 2, temperatures at the block surface (radius ÷ block radius = 1), the equi-volume point ($r/R_o = 0.707$), and the block center ($r/R_o = 0$) are compared as functions of τ for the two block experiments. In a coal powder at these heating rates, particles are so small that the temperature is the same throughout a particle ($T = \tau$ to $T_{maximum}$ for all r). In a large, dried block, thermal conductivity would cause some temperature profile to build during heat up. However, in a realistically wet block, generation of steam soaks up a great deal of heat, resulting in high heating rates at the center and in sharp temperature profiles. Figure 2 shows that most of the block will heat up to 100°C as steady heating continues at the surface. A wet-dry interface gradually moves inward from the surface as steam is generated, creating a shrinking core of damp coal. This effect may be seen graphically in the temperature profiles of Fig. 3. (Placement of radial thermocouples in a central plane satisfactorily describes radial temperatures without heating effects from the cylinder top or bottom. These effects were further prevented by making the cylinder height greater than or equal to cylinder diameter.) Figure 2 also shows that at a lower block heating rate, internal block temperatures do not lag surface temperature as much (i.e., temperature profiles are not as steep), but that absorption of heat by steam generation still exerts a considerable resistance.

Gas evolution, the critical parameter for in situ gasification, is substantially greater in pyrolysis of blocks than of powders from the same coal. Figure 4 shows gas evolution and gas composition for powder pyrolysis and for block pyrolysis as functions of τ, again equivalent (up to 950°C) to block surface temperature; in this case, they correspond to approximately the same heating rate and elapsed time. Gas evolution rate (Fig. 4 only) is the sum of H_2, CO, CO_2, CH_4, C_2H_4, and C_2H_6 (those compounds cited by Campbell), normalized per gram of moisture-and-ash-free

coal (maf). Similarly, mole fraction refers to a fraction of the total volume of gases listed above (Fig. 4 only – all gases included in Fig. 5).

Most of the increased gas yield may be attributed to self-gasification of char by the generated steam. Initial evolution rates and compositions from block pyrolysis lagged those of the powder pyrolysis, but strongly resembled them. Since the fraction of coal block at pyrolysis temperatures (250°C or higher) gradually increased with τ, thus lagging the powder particles that were all at uniform temperature, this behavior is consistent with the occurrence of straightforward pyrolysis reactions. Beginning at about τ = 700°C, gas evolution from block pyrolysis produced more gas than would have been expected from powder pyrolysis data, in particular, more H_2 and CO. A reasonable explanation is that as steam diffused outward from the shrinking, damp core through the hot, outer char layer of the block, a form of the reaction

$$C_{(s)} + H_2O_{(g)} \rightarrow H_{2_{(g)}} + CO_{(g)} \qquad 2)$$

occurred. This explanation is particularly plausible considering that the reaction equilibrium constant, K_p, is greater than 1 for temperatures higher than 670°C.

Gas component evolutions in Table 2 suggest that steam-char reactions account for only a part of the increase in gas evolution observed in block pyrolysis. Increases in total evolution of H_2 and CO are 253 cm^3/g and 106 cm^3/g, respectively, while less marked changes occur in CO_2 (15 cm^3/g increase), CH_4 (11 cm^3 decrease), and C_2 compounds (3.9 cm^3 increase). If only steam self-gasification of carbon took place, stoichiometry dictates that the increased evolution of H_2 and CO would be the same, rather than 147 cm^3/g more of H_2 than of CO. Contribution from the water-gas shift reaction

$$CO_{(g)} + H_2O_{(g)} \rightleftarrows CO_{2_{(g)}} + H_{2_{(g)}} \qquad 3)$$

should be negligible or counterbalanced, since K_p exceeds 1 only for temperatures less than 810°C. It is reasonable to expect steam reduction of hydrocarbons ($K_p > 1$ for T > 610°C for CH_4), but hydrocarbon light gases are not greatly different; in any case, they could not contribute such a large amount of hydrogen. A likely explanation is that pyrolysis-generated tar and oil vapors, diffusing outward into hotter char, are themselves pyrolyzed or cracked to carbon and H_2.

Exothermic reactions in the center of the block were observed thermally in Fig. 3 near the end of the 3.0 C°/min block pyrolysis experiment. Since H_2 generated by the very high-heating rates at $r/R_o = 0$ was restricted in outward diffusion, it may have participated in highly exothermic hydrogenation reactions.

Comparison of block pyrolysis at different heating rates indicates that similar gas-evolution behavior occurred relative to powder pyrolysis. In each case (see Table 2), block pyrolysis produced more gas than powder pyrolysis, primarily because of increased H_2 and CO production. For block pyrolysis, as observed in Fig. 5, overall gas-evolution rates in the 3.0 C°/min experiment did not begin to increase beyond those of the 2.0 C°/min experiment until about at τ = 700°C; gas compositions in the two experiments remained quite similar. This difference reinforces the hypothesis that steam reactions in the hot outer layer produced extra H_2 and CO, since at τ = 700°C, approximately three-fourths of the 2.0 C°/min block had been dried, as compared to approximately one-half of the 3.0 C°/min block.

Table 2. Comparison of gas component evolution among three pyrolysis cases

	Gas evolution, cm^3 (STP)/g coal (maf)						
	H_2	CO	CO_2	CH_4	C_2's	C_3's	C_4's
Powder, 3.3 C°/min to 950°C (ref. 3)	134	48	60	71	8.5	--[a]	--[a]
Block, 3.0 C°/min to 950°C	387	154	75	60	12.4	6.4	1.2
Block, 2.0 C°/min to 1000°C	317	101	78	76	17.1	9.8	1.7

[a]Not reported.

Conclusions and Future Plans

Dewatering of coal blocks at in situ moisture levels was shown to markedly affect pyrolysis gas production by being the rate-limiting mechanism in heat transfer, and by causing self-gasification of the block as steam diffuses from a shrinking core of damp coal through a hot, outer layer of char. Cracking of product oil vapors as they diffuse outward may also contribute to the increased combustible gas evolution of block pyrolysis compared to powder pyrolysis.

These results influence modeling and design of in situ coal gasification. Since no data are available on coal-block pyrolysis, improved understanding of heat and mass transfer effects significantly improves semitheoretical models which have depended on powder pyrolysis data. For satisfactory resource recovery, the shrinking core of unreacted coal makes it critical to limit flame-front speed. If the flame front moves too fast, only an outer layer of any large masses of coal will be gasified, leaving damp, ungasified centers behind the front.

More experimentation is planned to quantify and expand these results. Specifically, a matrix of experiments is being performed at 0.3 C°/min and at 3.0 C°/min, proceeding to maximum temperatures of 500 to 1000°C. Analyses will be made of data on oil, char, and gas yields; oil, char, and gas compositions; thermal histories; and oil and gas physical properties. Later experiments are planned to investigate the effects of pressure, reducing gas atmospheres, and other coal ranks (lignites, caking and noncaking bituminous coals). The ultimate result is a satisfactorily accurate model of pyrolysis as it affects in situ coal gasification.

Acknowledgments

The authors gratefully acknowledge the technical assistance of K. Ladd and C. J. Golden. Guidance contributed by C. D. Scott, and the assistance of O. V. Gentry and W. F. England are also appreciated.

References

(1) A. D. Little, Inc., "A Current Appraisal of Underground Coal Gasification," PB 209 274, National Technical Information Service (1972).

(2) G. B. Glass, "The Applicability of United States Coal Resources to In Situ Gasification," presented at the First Annual Underground Coal Gasification Symposium, Laramie Energy Research Center, Wyoming, July 28-August 1, 1975.

(3) J. H. Campbell, "Pyrolysis of Subbituminous Coal as It Relates to In Situ Gasification (Part 1: Gas Evolution)," Lawrence Livermore Laboratory, UCRL-52035, March 11, 1976.

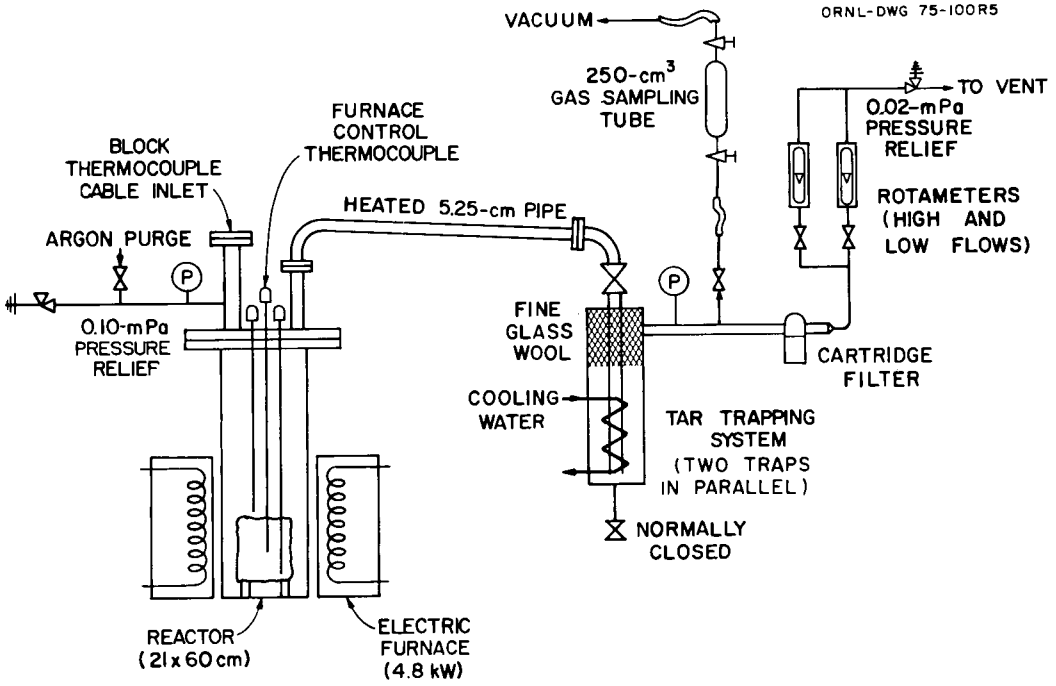

Fig. 1. Schematic diagram of block pyrolysis experiment.

ORNL DWG 76-14729

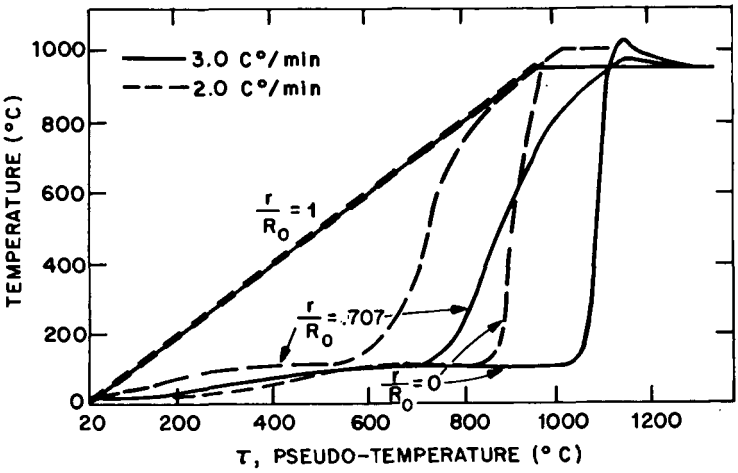

Fig. 2. Temperature changes at selected block radii in experiment BP1-4, pyrolysis at 3.0 C°/min to 950°C, and in BP1-13, pyrolysis at 2.0 C°/min to 1000°C.

ORNL-DWG 76-1456

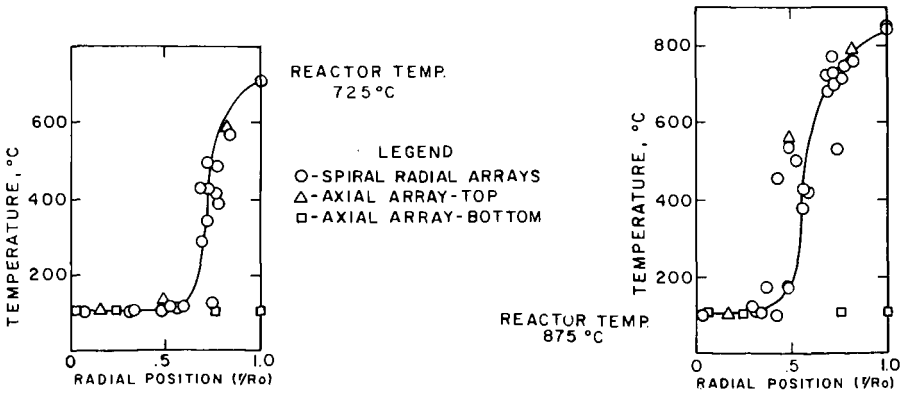

Fig. 3. Temperature profiles in experiment BP1-4, block pyrolysis at 3.0 C°/min to 950°C.

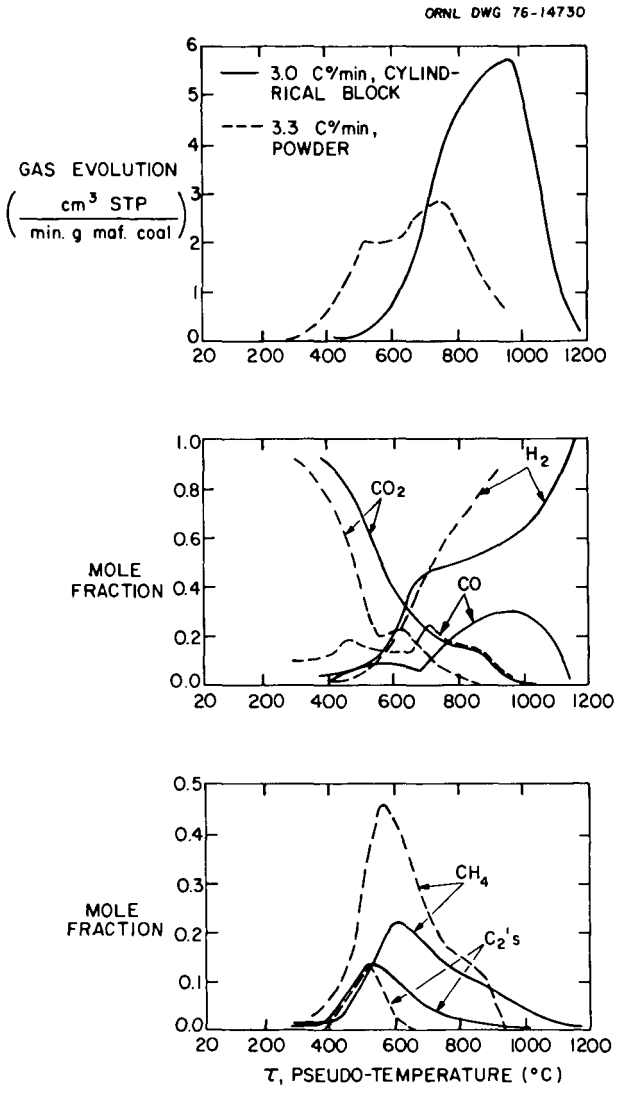

Fig. 4. Gas evolution rates and compositions in powder pyrolysis and block pyrolysis.

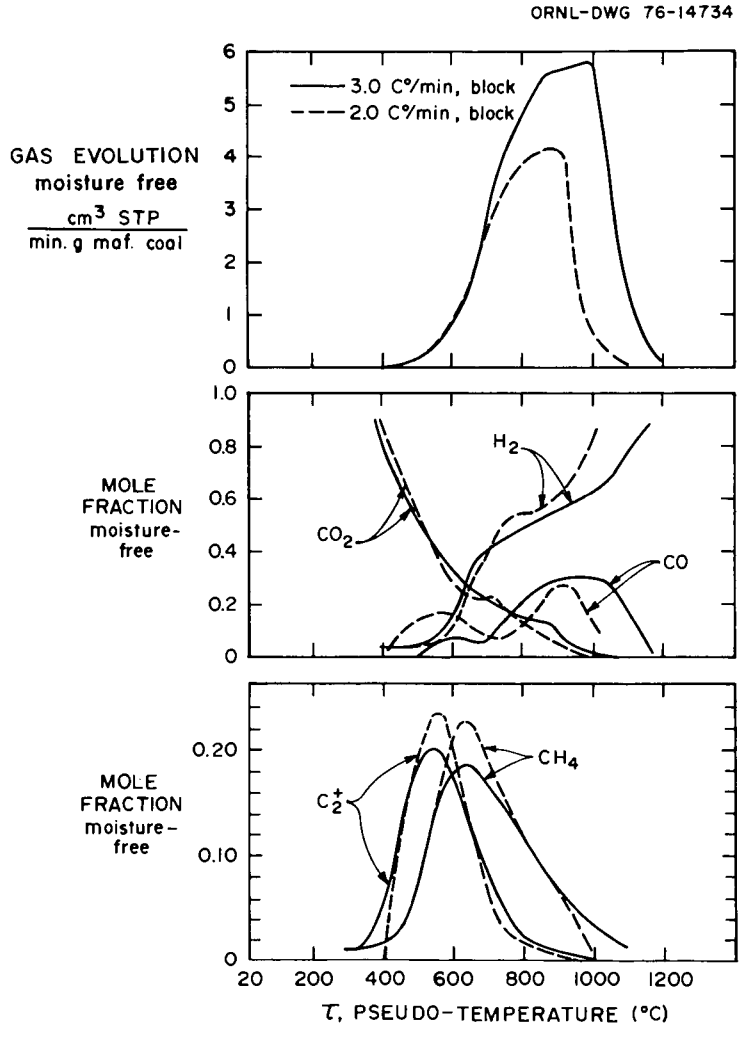

Fig. 5. Gas evolution rates and compositions in block pyrolysis at different heating rates.

CHARACTERISTICS OF CHARS PRODUCED BY PYROLYSIS FOLLOWING RAPID HEATING OF PULVERIZED COAL

N. Nsakala, R.H. Essenhigh, and P.L. Walker, Jr.

The Pennsylvania State University, Material Sciences Department, University Park, Pennsylvania 16802.

INTRODUCTION

Due at least partly to the dwindling native supplies of oil and natural gas, major research and development efforts aimed at converting coal into alternative fuels are currently underway in this country. During these various coal conversion processes two main events take place, namely: (i) evolution of the volatiles (pyrolysis) and (ii) gasification of the solid residue.

The understanding of the mechanisms of pyrolysis and gasification of coal is therefore important for achieving optimization of any conversion process. Nevertheless, the complexity of this subject matter is so great that it is always desirable to study pyrolysis separately from gasification. Accordingly, this paper describes experiments in which closely size graded pulverized coal particles were pyrolyzed (in a laminar flow pyrolysis furnace) follwoing a rapid rate of heating. The resulting chars were examined to determine the changes in physical characteristics due to rapid heating.

EXPERIMENTAL

Apparatus The apparatus built for studying pyrolysis following rapid heating of pulverized coal is, in principle, similar to that of Badzioch and Hawksley (1). It was specifically designed to accomplish the following major functions in the given order: (i) feed coal particles into the pyrolysis furnace at a known rate, (ii) raise the temperature of the particles as rapidly as possible (i.e. at a rate approaching 10^4 $^{o}C/sec$) to the predetermined temperature (i.e. that of the pyrolysis medium), (iii) allow the particles to be pyrolyzed at this temperature for a specific time, (iv) rapidly cool the products to suppress further pyrolysis reactions, and (v) separate solid (i.e. char) from the gaseous products.

The major components of this apparatus (Figure 1) are: a pyrolysis furnace, a gas preheat furnace, a fuel supply system, and a cyclone. All these components have been described in detail elsewhere (2). Following is a summary on the pyrolysis and gas preheat furnaces. The pyrolysis furnace consists of two concentric McDanel MV 30 mullite tubes. The inner, reaction tube is 5.08 cm id, 5.72 cm od, and 58.42 cm long; the outer, "winding" tube is 6.35 cm id, 6.985 cm od, and 50.8 cm long. The winding tube carries two different sizes of Kanthal A-1 heating elements with spacing of about 1.5 windings per centimeter over a total length of 45.72 cm. Six shunt taps were connected to the electrical circuit of the furnace to provide control over the shape of the gas temperature profile in the reaction zone. The space between the winding tube and the furnace housing (which was made of stainless steel sheet), was filled with fibrefrax insulation. The gas preheat furnace (or preheater) also consists of a McDanel MV 30 mullite tube of 1.905 cm id, 2.54 cm od, and 53.43 cm long. Silicon carbide (SiC) bars were used as the heating elements. The preheater was insulated as specified for the pyrolysis furnace. The wall temperatures of the furnace and preheater tubes were measured with chromel/alumel thermocouple beads placed along the tubes. The pyrolysis gas temperature profile in the reaction zone was measured with a small suction pyrometer also using a chromel/alumel thermocouple bead. The temperatures of the furnace and preheater tubes were each controlled by a TEM PRESS temperature controller.

Procedure With the temperature controllers of the pyrolysis and gas preheat furnaces

set at 955 and 965 ^{o}C, respectively, and at the total nitrogen gas (pyrolysis medium) flow rate selected, the temperature of nitrogen gas in the reaction zone was 808 ^{o}C. An appropriate arrangement of the shunts across the shunt taps rendered this nitrogen gas temperature profile reasonably flat (2). The gas flow in the pyrolysis furnace was laminar with a Reynolds number of 438. Laminar flow helps to keep the pyrolyzing coal particles in a narrow stream down the furnace axis.

Coal from the hopper (Fig. 1) was carried into the pyrolysis furnace through a water-cooled, and insulated feeder probe by a small flow of the primary nitrogen gas stream. This feeder was chosen such that its cold velocity was approximately isokinetic with the hot secondary stream; this has been found to disturb the particle stream the least (1). In the furnace,the particles were collected by an adjustable water-cooled, insulated probe. Adjustment of the probe altered the residence time in the furnace.

The coal particles in the furnace were in a dilute suspension (gas to solid ratio was about 80 to 1) and consequently were heated to the gas temperature at a rate of about 8000 ^{o}C/sec. The particles were allowed to pyrolyze at the reaction temperature for a specific time, determined by the collection probe position. To avoid disturbing the flow of gas in the pyrolysis furnace, the suction rate used for aspirating the solid and gasious products into this probe was kept essentially isokinetic with the flow stream in the furnace. Solid and gaseous products were separated in a small cyclone. The following conditions were kept constant throughout the investigation: (i) coal feed rate $\simeq$ 0.5 g/min, (ii) total nitrogen gas flow rate into the pyrolysis furnace = 31.72 ℓ/min [29.74 ℓ/min from the secondary stream and 1.98 ℓ/min from the primary stream], (iii) gas suction rate into the char collector probe = 16.99 ℓ/min, (iv) final pyrolysis temperature $\simeq$ 808 ^{o}C, and (v) pressure = normal atmospheric. The pyrolysis of coal particles was determined as a function of the mean particle size by weight (50 - 181 μm), isothermal pyrolysis time (0.018 - 1.025 seconds), and parent coal (three lignites, Table 1).

RESULTS

Weight Loss Coal particles flowing downwards in the pyrolysis furnace went through the heating, isothermal, and cooling periods. Based on the particle cooling rate of 2.72 x 10^{4} ^{o}C/sec in the char collection probe, it was concluded that pyrolysis during the cooling period was neglible compared to that occurring at the maximum temperature (2). Experimental results also showed that pyrolysis during the rapid heating period (the duration of which was about 0.095 sec for all the particle sizes studied) was negligible compared to that occurring at the maximum temperature (2). On the basis of these results it was concluded that pyrolysis in the laminar flow furnace occurred under essentially isothermal conditions.

Under the experimental conditions given above, the total residence time of nitrogen gas in the reaction zone of 30.48 cm in length was 0.3 second. Small coal particles were assumed to travel at the same velocity as the gas, implying therefore that their total residence time in the reaction zone was also 0.3 second. Since no appreciable pyrolysis occurred during the rapid heating period, the maximum isothermal pyrolysis time (τ_{iso}) could be obtained from the difference between the total residence time and heating time in the reaction zone, i.e. τ_{iso} = 0.3 - 0.095 = 0.205 second. Assuming that the temperature gradient between the center and the surface of coal particles was negligible, the heating rate of these particles was estimated, on the assumption of linear rise, to be 8000 ^{o}C/sec (2).

Due to the geometric configuration of the apparatus (Fig. 1) appreciable amounts of solids missed the char collection probe, rendering a direct materail balance unreliable. Therefore, weight loss (i.e. volatile yield) was determined using ash as a tracer. For each lignite studied, weight loss was expressed as function of mean particle size by weight and isothermal pyrolysis time. Some samples of one lignite (PSOC-246) were recycled into the pyrolysis furnace one or more times giving

a maximum cumulative isothermal pyrolysis time of 1.025 seconds. A subsidiary experiment showed that recycling the samples into the furnace had no measurable effect on the kinetics of the pyrolysis. A similar result was obtained by Anthony et al. (3).

Typical results on weight loss are presented in Figures 2 and 3. The solid/dashed curves in these figures are generated by the empirical Badzioch and Hawksley Equation, using the physical kinetic constants given in Table 2:

$$\Delta W = VM_o \cdot Q \cdot (1 - C)[1 - \exp(- k\tau_{iso})] \qquad 1)$$

where ΔW is the weight loss expressed as a percentage of the original dry-ash-free coal, VM_o is the proximate volatile matter of coal on dry-ash-free basis, Q is the so-called Q-factor, C is the Badzioch and Hawksley empirical constant, k is the reaction rate constant, and τ_{iso} is as defined above.

The results in Figures 2 and 3 show that: (i) weight loss depends on the particle size and pyrolysis time, smaller sizes and longer times giving greater weight loss, (ii) the agreement between the experimental and calculated weight losses is good for times shorter than about 0.2 second, but the disparity becomes great thereafter, and (iii) the extent of weight loss for the two lignites (PSOC-90 and PSOC-246) is comparable; this is perhaps due to the fact that these lignites are quite similar as far as chemical composition goes (Table 1). PSOC-140 exhibited a behavior similar to that of PSOC-90 and PSOC-246, and hence is omitted here.

Characteristics of Coals and Chars The following physical characteristics of both the original coals and the subsequent chars were determined as follows: (i) nitrogen and carbon dioxide specific surface areas calculated from the BET and Dubinin-Polanyi equations (4, 5), using the adsorption data at 77 and 298 ^{o}K, respectively; (ii) apparent and true densities obtained from mercury and helium displacements, assuming that samples were properly degassed (6); and (iii) total open pore volumes and porosities, calculated from mercury and helium densities.

For each lignite studied, the changes in the structural parameters were determined as a function of the mean particle size by weight and isothermal pyrolysis time. Typical results are given in Figures 4 and 5. The figures show that: (i) the specific surface areas increase with increasing pyrolysis time, the increase becoming more appreciable after times greater than about 0.2 second, (ii) the helium density gradually increases with increasing pyrolysis time, whereas the mercury density decreases with time, rapidly at first, then more slowly later; both densities tend to level off after about 0.6 second, and (iii) the total open pore volumes and porosities, which were calculated from the density data, rapidly increase with increasing pyrolysis time, tending to level off after about 0.6 second; this last result is given elsewhere (2).

Correlation Between Weight Loss and Some Physical Structural Parameters The release of volatile matter during pyrolysis results in a development in the internal porosity of the initial material. This is a direct result of one or a combination of the following: (i) opening of previously closed pores, (ii) opening of new pores, and (iii) enlargement of existing and/or newly developed pores. The development of the internal porosity can be followed by measuring the changes in the physical structural parameters given above. This type of information is important because the nature of pore structure of a particular coal determines to a large degree the extent of its reactivity during a given coal conversion process. The results given in Figures 6 and 7 show the development of the pore structure of PSOC-90 and PSOC-246 as a direct result of volatile matter release.

DISCUSSION

Experimental results showing negligible pyrolysis during the rapid heating period are supported by calculations based on first order non-isothermal kinetics.

Details on these calculations are given elsewhere (2). Briefly, assume that the rate of gas (i.e. volatiles) release during coal pyrolysis is (7)

$$dV/dt = k(V_o - V) \qquad 2)$$

where V_o is the volume of gas liberated at infinite time, V is the volume of gas liberated at time t, and $k = k_o \exp(-E/RT)$ where k_o is the frequency factor, E is the activation energy, R is the gas constant, and T is the temperature. Equation 2 was used to estimate the variation of fractional weight loss of volatiles (V/V_o) with time.

The values of k were determined experimentally (2) and that of k_o was estimated to be of the order of 10^{13} sec^{-1} (8). The relation $k = k_o \exp(-E/RT)$ was then used to estimate the values of activation energies (E). For example for $k = 2.6$ sec^{-1} and $T = 1081$ ^oK (Table 2), E was found to be $\sim$ 63 kcal/mole. The results from these calculations are given in Figure 8. It is clear from Figure 8 that the fractional weight loss of volatiles during the heating period is negligibly small (< 2%) for all values of E > 55 kcal/mole. If one accepts the value of 10^{13} sec^{-1} for k_o which, in this particular case, gives a value of 63 kcal/mole for E, then the results in Figure 8 are consistent with the experimental finding.

While Badzioch and Hawksley's empirical Equation 1 correlates fairly well with the experimental data at short isothermal pyrolysis times (Figures 2 and 3), it should be treated with some reserve. For example their assumption that C remains a positive constant value at infinite time for weakly swelling coals is contrary to kinetic expectations. It can be shown using the two-component hypothesis that C approaches zero at infinite time (2). Badzioch and Hawksley's value of 0.14 for C was nevetheless used in this investigation (2) since it gave results that closely approximated the expimental results at short times.

CONCLUSIONS

This study gives an insight into the pyrolysis behavior of pulverized coal following a rapid rate of heating in a laminar flow furnace. It is also helpful for the understanding of the reactivities of particular coals with common gasifying gases (e.g. steam, air, oxygen, carbon dioxide, hydrogen). For example, the results show that the change in the specific surface areas becomes appreciable only at total residence times greater than 0.3 second (i.e. at pyrolysis times greater that 0.2 second) at $\sim$ 808 ^oC. This type of information should be helpful in assessing the suitability of particular coals for gasification and/or determining the utilization processes for which they are most suitable.

ACKNOWLEDGEMENTS

The financial support of this work by the Energy Research Development and Administration [Contract No. E (49-18) - 2030] is appreciatively acknowledged.

REFERENCES

1. Badzioch, S., and Hawksley, P.G.W., Ind. Eng. Chem. Process Des. Develop., 9, 521 (1970).
2. Nsakala, N., PhD Thesis, The Pennsylvania State University, 1976.
3. Anthony, D.B., Howard, J.B., Hottel, H.C., and Meissner, H.P., Fuel, 55, 121 (1976).
4. Brunauer, S., Emmett, P.H., and Teller, E., J. Am. Chem. Soc., 60, 309 (1938).
5. Lamond, T.G., and Marsh, H., Carbon, 1, 281 (1964).
6. Franklin, R.E., Fuel, 27, 46 (1948)
7. Juntgen, H., and van Heek, K.H., Fuel, 47, 103 (1968).
8 Benson, S.W., Thermochemical Kinetics, Wiley, New York, 1968, p. 75.

Table 1

Chemical Analyses of Coals

Coal Identification			Chemical Analysis (in weight percent)					
Code No.	Origin or Source Area	ASTM Rank Range	Proximate Analysis+	(dry)	(daf)*	Ultimate Analysis**	(dry)	(daf)*
PSOC-140	Lignite Seam; Darco Mine, Texas	Lignite	Volatile Matter	46.0	50.4	C	65.0	71.7
			Fixed Carbon	45.3	49.6	H	4.7	5.2
			Ash	8.7	-	N	1.1	1.3
						S	0.7	0.7
						O	19.1	21.1
						Ash	9.4	-
PSOC-90	Lower Lignite Seam; Savage Mine, Montana	Lignite	Volatile Matter	39.9	43.5	C	64.8	71.6
			Fixed Carbon	51.7	56.5	H	4.4	4.9
			Ash	8.4	-	N	0.7	0.8
						S	0.3	0.3
						O	20.3	22.4
						Ash	9.5	-
PSOC-246	Coteau Seam; Glen Harold Mine, North Dakota	Lignite	Volatile Matter	43.7	47.5	C	64.1	71.0
			Fixed Carbon	48.3	52.5	H	4.4	4.9
			Ash	8.0	-	N	1.4	1.6
						S	0.6	0.6
						O	19.8	21.9
						Ash	9.7	-

* daf = dry-ash-free; ** Data obtained from the Penn State University Coal Data Base; + Proximate analysis for size graded materials (200x325 mesh for PSOC-140, 200x270 mesh for PSOC-90 and PSOC-246).

Table 2

Reaction Rate Constants for Pyrolysis of Coal

Constant	PSOC-140 200x325 mesh $\bar{x}$ = 50 μm*	PSOC-90 200x270 mesh $\bar{x}$ = 58 μm*	PSOC-246 200x270 mesh $\bar{x}$ = 64 μm*
T_f (°C)	770	808	808
Q	1.9	2.1	1.8
k (sec^{-1})	3.1	2.2	2.6

* $\bar{x}$ = mean particle size by weight

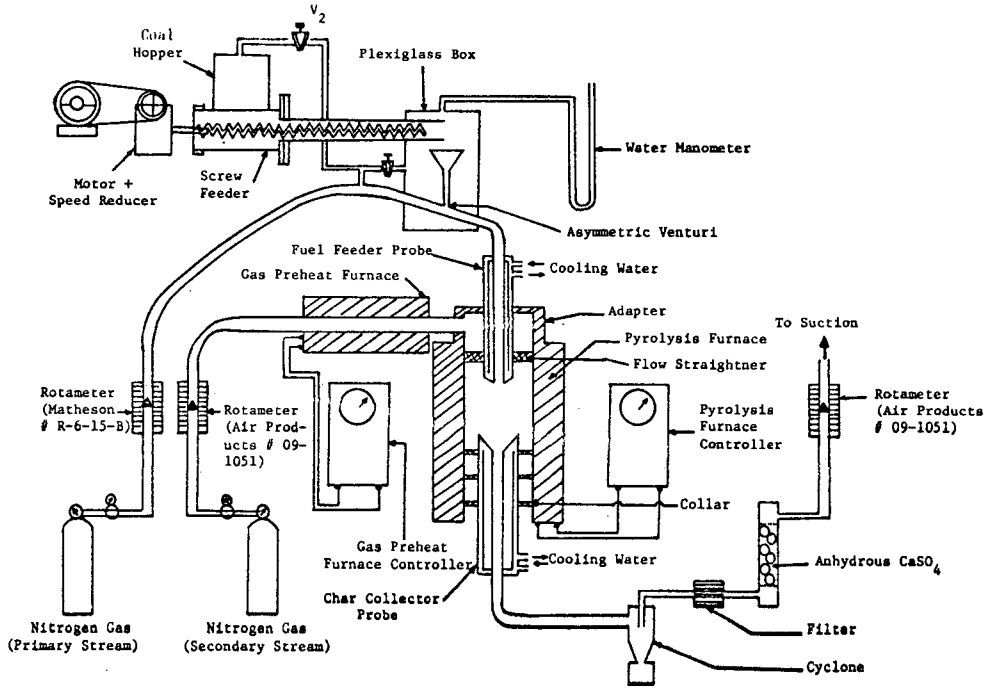

Fig. 1 - Experimental Equipment For Pyrolysis Following Rapid Heating of Pulverized Coal

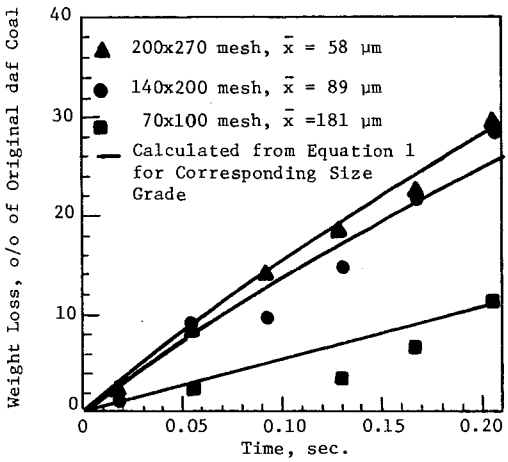

Fig. 2 - Variation of Weight Loss With Isothermal Pyrolysis Time For PSOC-90

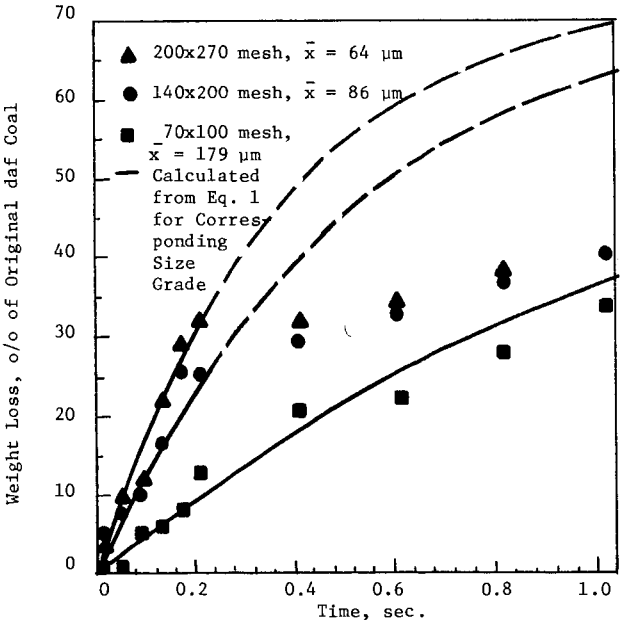

Fig. 3 - Variation of Weight Loss with Isothermal Pyrolysis Time for PSOC-246

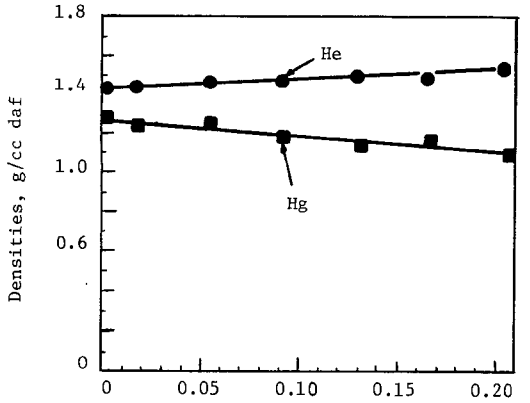

Fig. 4(a) - Variation of Hg and He Densities With Isothermal Pyrolysis Time For PSOC-90

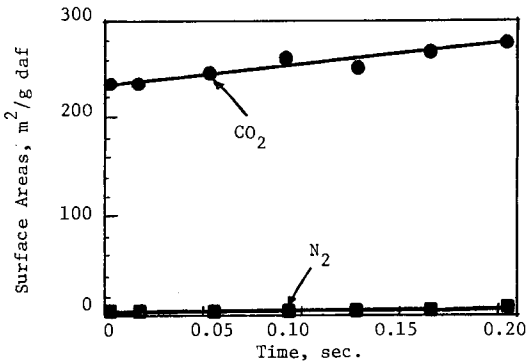

Fig. 4(b) - Variation of N_2 and CO_2 Specific Surface Areas With Isothermal Pyrolysis Time For PSOC-90

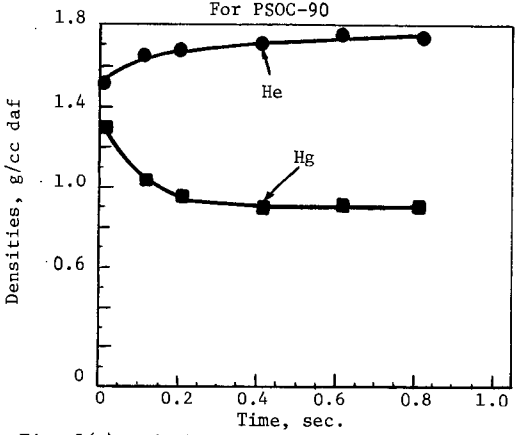

Fig. 5(a) - Variation of Hg and He Densities With Isothermal Pyrolysis Time For PSOC-246

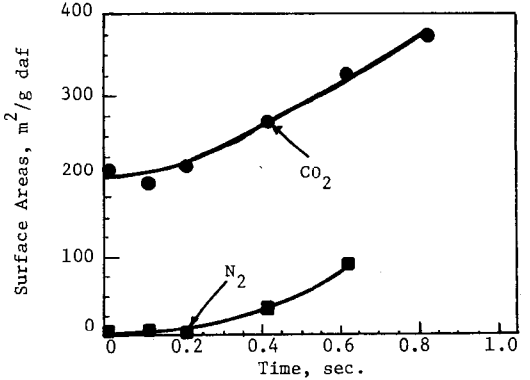

Fig. 5(b) - Variation of N_2 and CO_2 Specific Surface Areas For PSOC-246

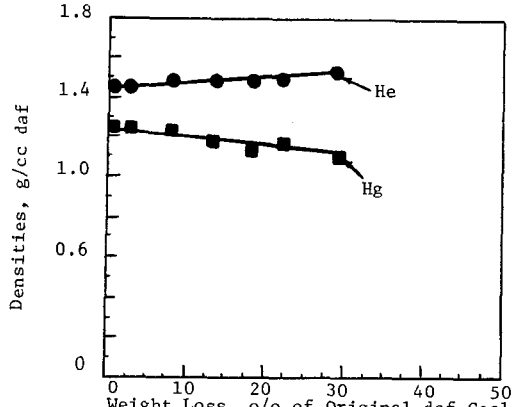

Fig. 6(a) - Correlation Between Weight Loss and Densities for PSOC-90

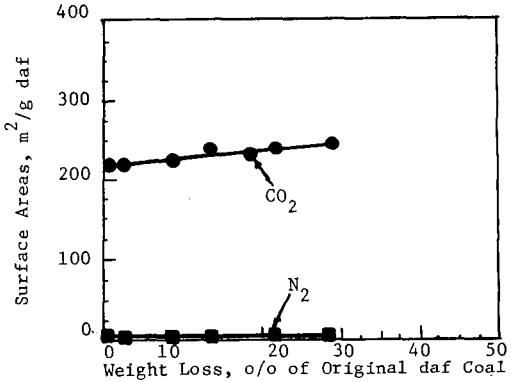

Fig. 6(b) - Correlation Between Weight Loss and Specific Surface Areas for PSOC-90

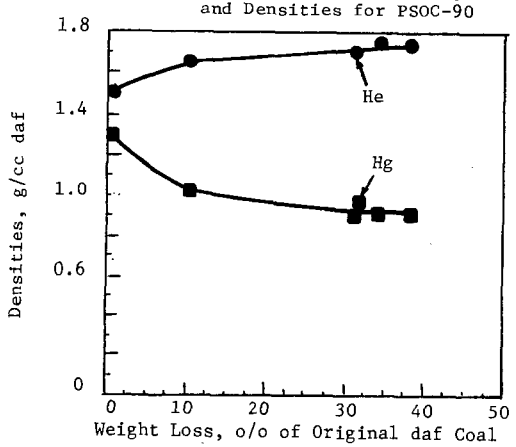

Fig. 7(a) - Correlation Between Weight Loss and Densities for PSOC-246

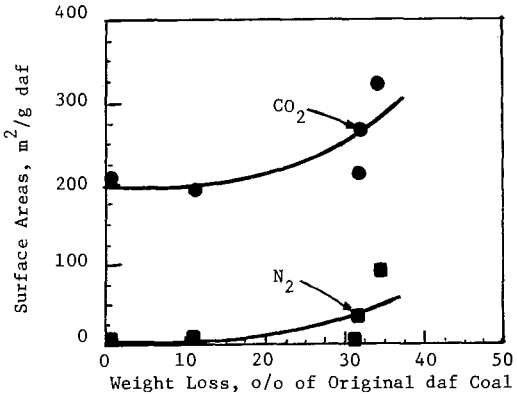

Fig. 7(b) - Correlation Between Weight Loss and Specific Surface Areas for PSOC-246

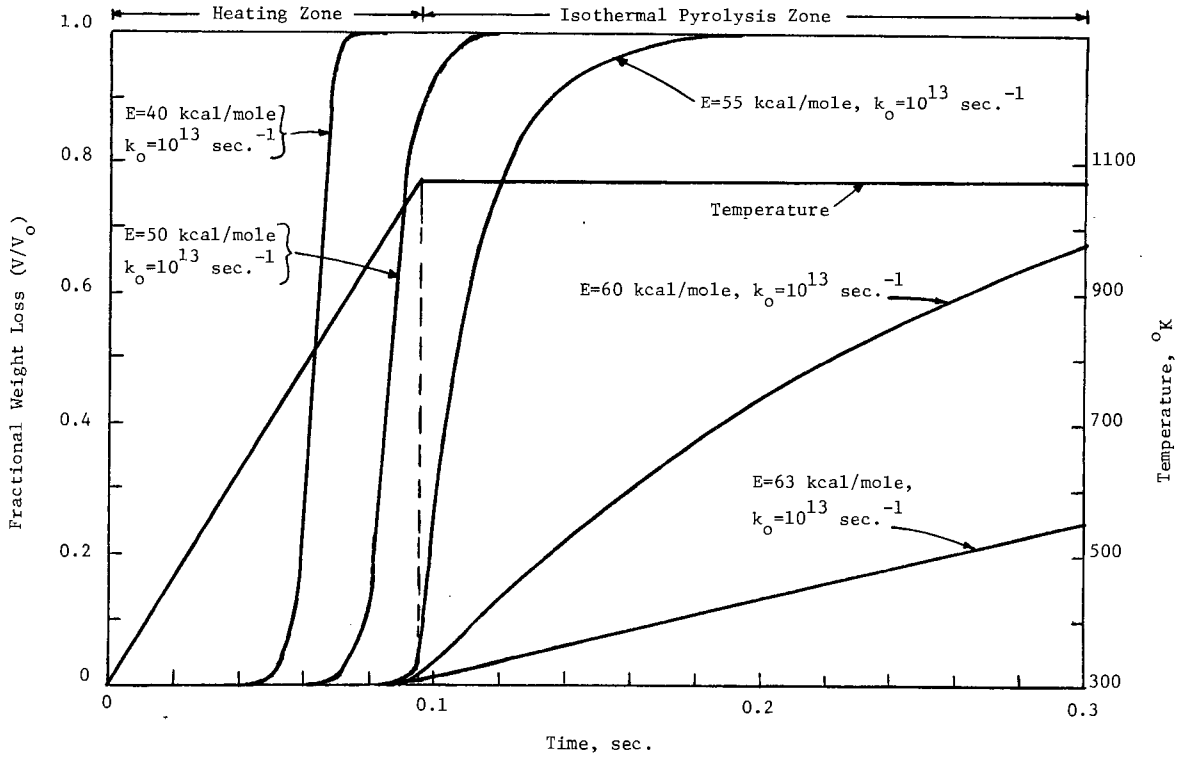

Fig. 8 - Variation of Fractional Weight Loss (V/V_o) of Volatiles With Time
[Calculated From Equations (6.33) & (6.36) of Ref. 2]

PRODUCT COMPOSITION AND KINETICS OF LIGNITE PYROLYSIS

Eric M. Suuberg, William A. Peters, and Jack B. Howard

Department of Chemical Engineering and Energy Laboratory
Massachusetts Institute of Technology
Cambridge, Massachusetts 02139

SUMMARY

The pyrolysis of pulverized Montana lignite by time-resolved measurement of the yields and compositions of products formed under controlled temperature-time histories was studied in a captive sample apparatus. A thin layer of particles held in a folded strip of stainless steel screen was electrically heated under both 1 atm helium and vacuum in a vessel connected to a series of product recovery traps. The temperature of the sample was measured with a thermocouple. Heating rate, peak temperature attained, and residence time at the peak temperature were independently varied in the ranges 100-10^4°C/s, 150-1100°C, and 0-10s. The yields of char and tar were determined gravimetrically and selected char samples were subjected to elemental analysis. The yields of water, carbon monoxide, carbon dioxide, hydrogen, and hydrocarbon gases and light liquids were determined by gas chromatography.

The yields of all the volatile products increase monotonically with temperature and approach asymptotic values at the higher temperatures. At 1000°C/s and 1 atm helium the ultimate yields, in percent by weight of the lignite (as-received), are 16.5 % water (including 6.8 % moisture), 9.5 % carbon dioxide, 9.4 % carbon monoxide, 5.4 % tar, 1.3 % methane, 0.6 % ethylene, 0.5 % hydrogen, and 0.9 % ethane, propylene, propane, benzene, and trace hydrocarbons. The total yield of 44.0 % is close to the ASTM volatile matter plus moisture (43.7 %). Pyrolysis at the higher temperatures volatilizes about 70 % of the sulfur and about 25 % of the nitrogen; the percent by weight of sulfur in the char is less than that in the lignite but the reverse is true for nitrogen.

The individual product yields vary with temperature in a series of steps indicative of the occurrence of five principal phases of devolatilization: moisture evolution at about 100°C; a large initial evolution of carbon dioxide beginning at about 450°C, probably from decarboxylations, and a small amount of tar formation; evolution of chemically formed water and a small amount of carbon dioxide at 500-700°C; rapid evolution of carbon monoxide, carbon dioxide, tar, hydrogen, hydrocarbon gases, and only little water at 700-900°C; high-temperature formation of carbon monoxide and carbon dioxide. The kinetics of the production of each product is modelled with one to three independent parallel first-order reactions. The frequency distribution of all the activation energies derived for the various products by fitting the present composition data agrees well with the Gaussian distribution obtained previously from weight loss data for the same lignite.

INTRODUCTION

Previous research at M.I.T. on coal pyrolysis in inert gas and in hydrogen was based on the measurement of coal weight loss, referred to as volatiles yield(1-5). The work is now being extended to include volatiles composition measurements and elemental analysis of the char for the same ranges of experimental conditions covered in the previous study. To this end, the previous apparatus has been modified to permit the collection and analysis of volatiles. This paper presents the first set of composition data, for lignite pyrolysis, and some initial interpretations of pyrolysis behavior in the light of the products formed.

APPARATUS AND PROCEDURE

The apparatus (Fig. 1) consists of five components: the reactor, designed to contain a coal sample in a gaseous environment of known pressure and composition; the electrical system, used to expose the sample to a controlled time-temperature history; the time-temperature monitoring system; the product collection system; and the product analysis system.

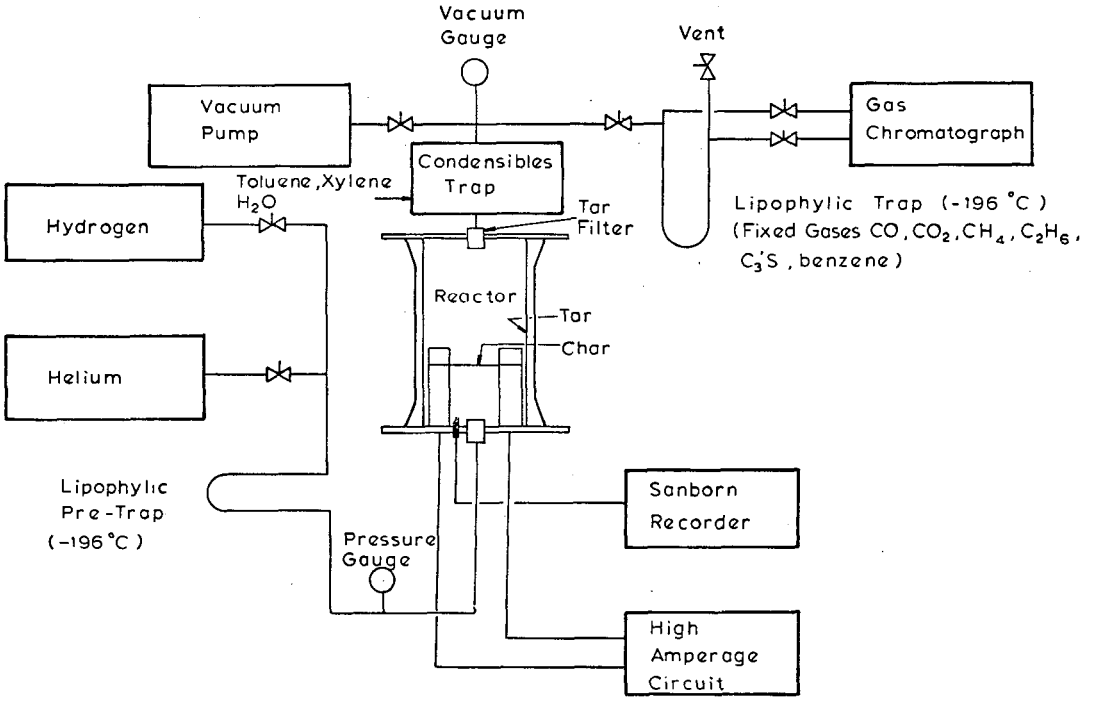

Figure 1. Captive Sample Apparatus and Analysis System.

The reactor, designed for atmospheric-pressure and vacuum pyrolysis work, consists of a 6-inch (15.24 cm) long, 3-inch (7.62 cm) diameter pyrex glass pipe, blind-flanged at both ends by stainless steel plates having electrical feedthroughs and gas inlet and outlet ports. The coal sample is held and heated in the vessel by a folded strip of 325 mesh stainless steel screen positioned between two relatively massive brass electrodes as shown in Fig. 2.

The electrical system consists of two automobile storage batteries connected in series to the reactor electrodes through a timer-controlled relay switch which cuts in either of two variable resistors at a predetermined time. This circuitry permits independent control of heating rate (10^2-10^4°C/s) and final sample holding time and temperature (150-1100°C for up to 30 s). The temperature-time history of coal is recorded by a chromel-alumel thermocouple (24 μm wire diam., 75 μm bead diameter) placed within the sample and connected to a Sanborn fast-response recorder.

Approximately 10-15 mg of powdered coal is spread in a layer one to two particles deep on a preweighed screen which is reweighed and inserted between the brass electrodes. The reactor is evacuated and flushed three to five times with helium and then set at the desired experimental pressure. The sample temperature is raised at a desired rate to a desired holding value which is then maintained until the circuit is broken. Sample cooling by convection and radiation then occurs rapidly since the electrodes, the vessel and its gaseous contents remain cold during the experiment, but not so rapidly as to avoid the occurrence of significant weight loss during cooling.

The yield of char, which remains on the screen, is determined gravimetrically. Products that condense at room temperature (tars and oils, hereafter defined as tars) are collected primarily on foil liners within the reactor and on a paper filter at the exit of the reactor. Any condensation on non-lined reactor surfaces is collected by washing with methylene chloride soaked filter paper. The tar from all three collections is measured gravimetrically.

Products in the vapor phase at room temperature are collected at the conclusion of a run by purging the reactor vapors through two lipophilic traps. The first trap consists of a 3 inch (7.62 cm) long, 1/4 inch (0.635 cm) diameter tube containing 50/80 mesh Porapak Q chromatographic packing. The trap is operated at room temperature, and collects intermediate weight oils such as benzene, toluene, and xylene. The second trap is a 15 inch long, 1/4 inch diameter tube (38.1 cm x 0.625 cm) also packed with Porapak Q but operated at -196°C in a dewar of liquid nitrogen. This trap collects all fixed gases produced by pyrolysis, with the exception of hydrogen which is determined by direct vapor phase sampling with a precision syringe.

Products are recovered for gas chromatographic analysis by warming the first trap to 240°C and the second to 100°C. The intermediate weight oils from the first trap are analyzed on either a 50/80 mesh, 3 % OV-17 or Porapak Q column, 6 ft x 1/8 in (183 cm x 0.318 cm). The fixed gases from the second trap are analyzed on a 12 ft x 1/4 in (366 cm x 0.635 cm) 50/80 mesh Porapak Q column, temperature programmed from -70 to 240°C at a rate of 16°C/min. The hydrogen is analyzed on a 10 ft x 1/8 in (305 cm x 0.318 cm) 80/100 mesh Spherocarb column at 0°C. A Perkin-Elmer Model 3920 B chromatograph with dual thermal conductivity/flame ionization detectors and a Perkin-Elmer Model 1 integrator are used for all the analyses.

Elemental analyses of the raw coal and char samples were performed by Galbraith Laboratories, Inc. of Knoxville, Tennessee.

The weight of the coal and screen was determined to within ±0.01 mg; hence, the uncertainty of the total weight loss measurement is about 0.1 % by weight of the coal. The products quantitated chromatographically (except H_2O) are subject to calibration uncertainties of 1 to 3 % of the mass of the species measured. The water measurements were somewhat more troublesome because of (1) moisture loss from the coal during the short time lapse between weighing the sample and performing the run and (2) moisture gain by the experimental system during assembly under high humidity conditions. The net uncertainty in the measured water yields caused by these opposing effects is about 2 % by weight of the coal. The tar measurement

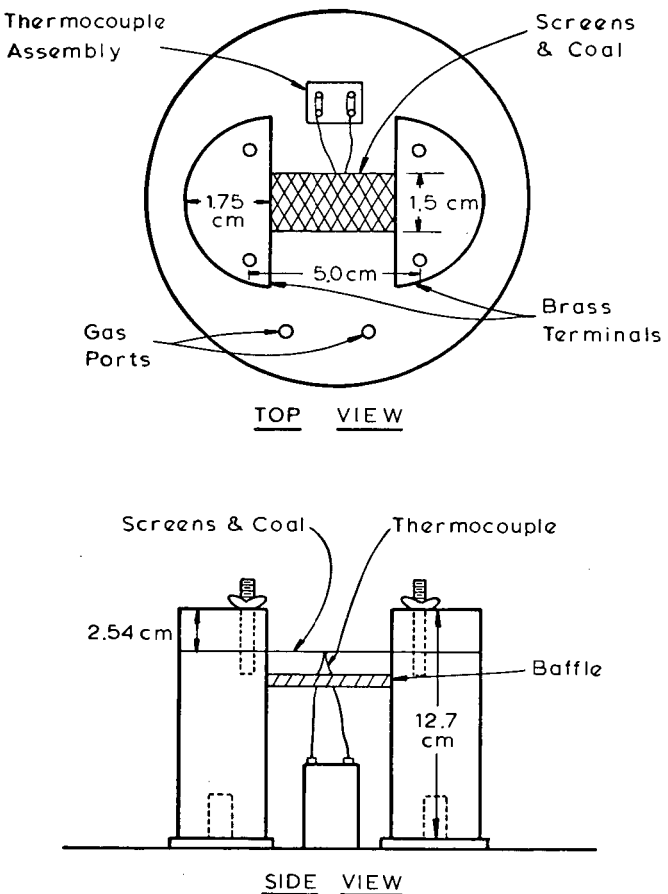

Figure 2. Sample Holding and Heating Assembly.

has its largest uncertainty in the washing procedure. The maximum error for atmospheric pressure runs is about 1 % by weight of the coal. The inherent uncertainty of the thermocouple measurements is about ± 8°C over the present range of temperatures. The ability of the selected thermocouple effectively to track the temperature of the sample at the highest heating rates was confirmed by experiments with thermocouples of different bead diameters.

Some discoloration of the screen used to hold the sample caused concern that the screen may be a source of error, for example through catalysis of primary pyrolysis or secondary cracking reactions. Experimental assessment of the role of the screen included passivation of the surface with a vacuum deposited layer of gold on some screens and copper on others, and variation of the number of layers of untreated screen through which the volatiles had to escape. Both gold and copper are less catalytic to cracking reactions than is stainless steel, and diffusion of these metals in stainless steel is too slow to destroy the integrity of the surface layer in even the longest residence times of this study. None of these cases lead to significant differences in the total yield of volatiles or in the composition of gaseous products included in the present study. Therefore, any error caused by the screen appears to be negligible for present purposes. This result is not surprising in view of the high escape velocity of volatiles from the sample and hence the low residence time of volatiles near hot screens. Nevertheless, untreated stainless steel screens in a similar apparatus are reported(6) to react significantly with hydrogen sulfide. This species is not of present concern.

RESULTS

All the results here reported are for a partially dried (as-received) Montana lignite (Savage Mine, Knife River Coal Co.) in the particle size range 53-88 μm (74 μm average diameter) (Table 1).

Table 1. Characteristics of the Partially Dried Lignite

Proximate Analysis, Wt.%(as-received)		Ultimate Analysis, Wt.%(as-received)		Petrographic Analysis (Wt.%(mineral-matter-free)	
Moisture	6.8	Carbon	59.3	Vitrinites	69.7
V.M.	36.9	Hydrogen+	4.5	Semi-Fusinite	15.2
F.C.	46.4	Nitrogen	0.9	Fusinite	7.9
Ash	9.9	Sulfur	1.1	Micronite	5.2
Total	100.0	Oxygen*+	17.5	Exinite	2.0

* By difference, using measurements of other elements, moisture and ash.
\+ Exclusive of moisture content.

Base Data With the exception of the data points carrying a double symbol (see below), the volatile product compositions shown in Fig. 3 were obtained when different samples of the lignite under 1 atm (101.3 kPa) of helium were heated at approximately 1000°C/s to various peak temperatures indicated on the abscissa. The samples were cooled at roughly 200°C/s beginning immediately when the peak temperature was attained. The total yield of any product or group of products is given on the ordinate as a weight percent of the partially dried lignite.

The lowest curve represents the yield of tar as defined above, which increases with increasing temperature to an asymptotic maximum of about 5.4 % by weight of the lignite at temperatures above 750 to 800°C. The tar appears to have two primary components. One is a heavy, tawny brown liquid-like material which deposits as a film on surfaces. The other consists of dark brown objects which give the impression of being solid pieces of lignite that were presumably broken off of the parent material and carried away with the volatiles. These "particles", some

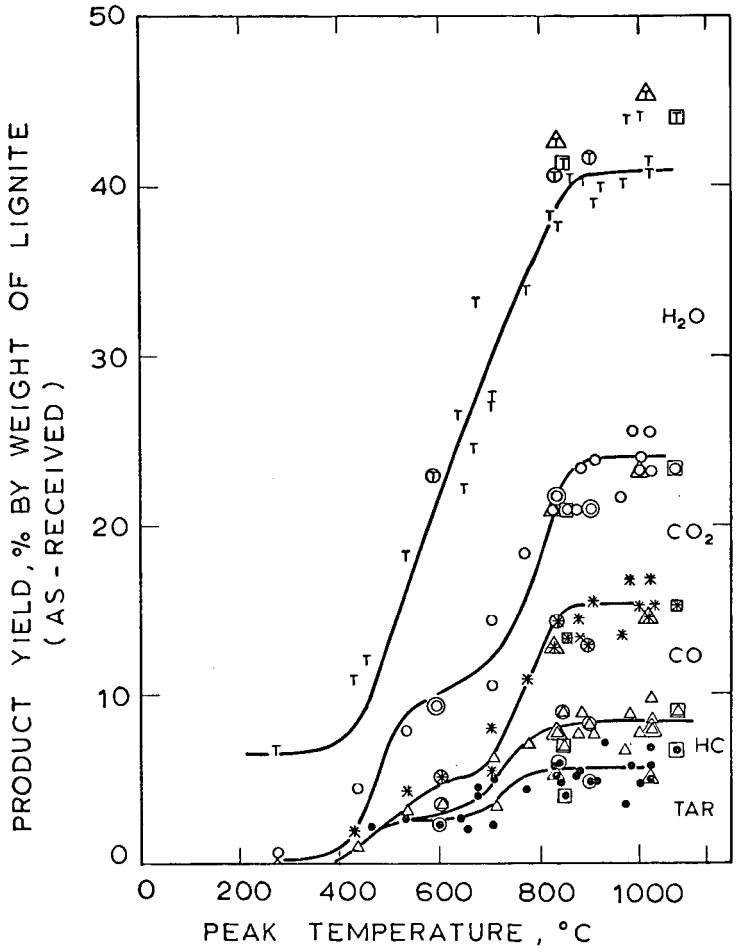

Figure 3. Pyrolysis Product Distributions from Lignite Heated to Different Peak Temperatures. [(●) tar; (Δ) tar and other hydrocarbons (HC); (*) tar, HC, and CO; (o) tar, HC, CO and CO_2; (T) total, i.e., tar, HC, CO, CO_2, and H_2O. Pressure = 1 atm (helium). Heating rate:(single points) 1000°C/s; (points inside O) 7,100 to 10,000°C/s; (points inside Δ) 270 to 470°C/s; (points inside □) 1000°C/s but two-step heating. (curves) First-order model using parameters shown in Table 5].

of which appear to be agglomerates, are for the most part smaller than 10 μm across but sometimes as large as 25 μm. About 75 % of the tar including most of the tawny liquid and a fraction of the particles appears to dissolve in methylene chloride. Extensive analysis of any one tar sample is difficult because of the small yields.

The distance between the tar curve and the next one above it represents hydrogen and all hydrocarbons lighter than tar. The maximum yield of these species occurs at the higher temperatures and is only about 3.3 % by weight of the lignite. The main components are methane (1.3 %), ethylene (0.6%), and hydrogen (0.5 %), with identified ethane, propylene, propane, and benzene and unidentified trace hydrocarbons making up the balance. The effect of temperature on yields of methane, hydrogen and ethylene is shown in Fig. 4. When the peak temperature is increased above 500°C the methane and ethylene yields increase rapidly to small asymptotic values in the range 600 - 700°C. Further increase in temperature beyond 700°C effects a dramatic increase in the yield of both species, and a second asymptote is reached at about 850°C for ethylene and about 900°C for methane. The yield of tar also exhibits a similar two-step behavior but hydrogen production, on the other hand, appears to occur in one step at relatively high temperatures.

The top curve in Fig. 3 represents the total yield of volatiles while, proceeding downward, the first, second and third regions between adjacent curves represent the yields of water, carbon dioxide, and carbon monoxide, respectively. The yields of these principal oxygenated species are shown in more detail in Fig. 5 where all three appear to approach high-temperature asymptotic yields of 16.5 % for water, 8.4 % for carbon dioxide, and 7.1 % for carbon monoxide. The carbon oxides each exhibit also a lower-temperature asymptote.

Although most of the pyrolysis is complete for peak temperatures above about 900 to 1000°C, there is in fact yet a third step in the curves for the carbon oxides which occurs at about 1100°C and therefore does not appear in Fig. 5. Since this temperature is the upper limit of the apparatus, investigation of this third step was accomplished by use of a longer residence time technique. The coal was heated at 1000°C/s to 1000°C and there held for 5 to 10 s rather than being immediately cooled as before. The resulting carbon monoxide yield exhibits a final asymptote of 9.4 % while that of carbon dioxide is 9.5 %. The yields of the other species were not changed by the additional residence time. Thus prolonged heating at 1000°C gave a total volatiles yield of 44.0 % by weight of the lignite which is close to the ASTM volatile matter plus moisture (43.7 %).

Elemental analyses of selected char samples are shown in Fig. 6. Although over 40 % by weight of the lignite is volatilized at the higher temperatures, only 22 % of the carbon is volatilized. Most of the volatile material comes from hydrogen and oxygen, which is consistent with the observed predominance of water among the volatile products. Pyrolysis at the higher temperatures removes about 70 % of the sulfur from the solid material, but the nitrogen is reduced by only about 25 %. Consequently, the sulfur content (percent by weight) in the char is lower than that of the lignite, but the reverse is true for nitrogen. Similar data obtained by Kobayashi et al.(7,8) in an entrained flow reactor show that the fractional evolutions of sulfur and nitrogen are increased to at least 85 % and 65 %, respectively, as the pyrolysis of Montana lignite is extended to 1800°C. The weight of ASTM ash in the char from most of the present experiments is less than that in the raw lignite, which is qualitatively similar to a previous observation(7,8).

Elemental balances were calculated for runs in which both volatile products and char were analyzed. For estimation purposes, tar and trace hydrocarbons (total less then 1 % by weight of the lignite) were assumed to be 90 % carbon and 10 % hydrogen by weight. Typical results for four runs to different peak temperatures are presented in Table 2 along with total mass balances. Whereas the mass balances are excellent and the carbon and hydrogen balances are satisfactory, the oxygen balances are marginal. Since oxygen in char is determined by

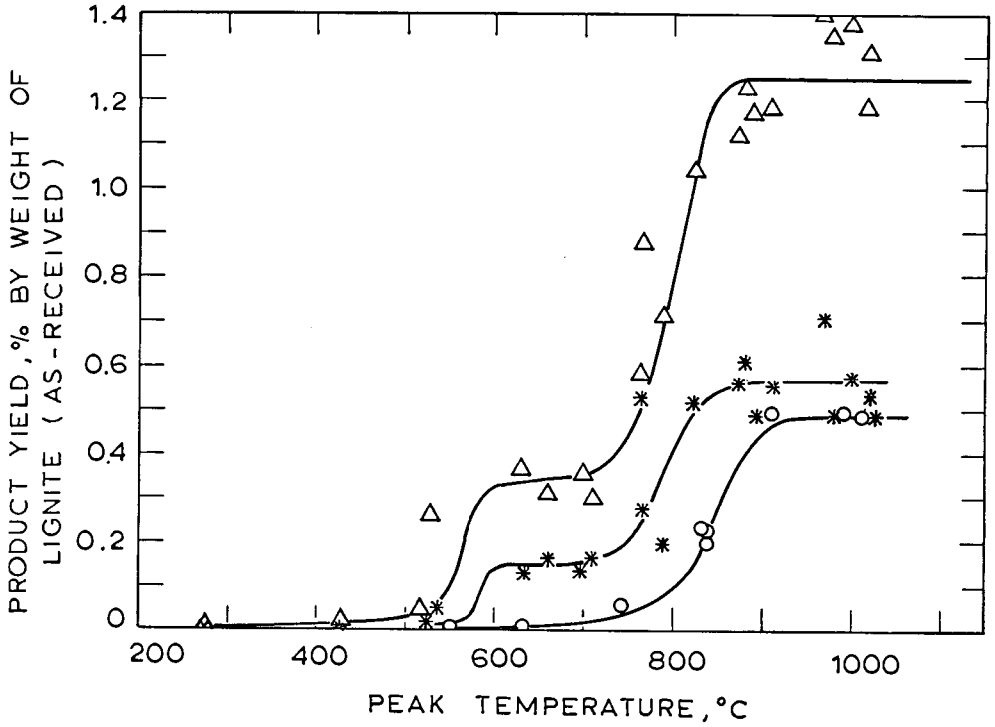

Figure 4. Yields of Methane, Ethylene and Hydrogen from Lignite Pyrolysis to Different Peak Temperatures [(Δ) CH_4; (*) C_2H_4; (o) H_2. Pressure = 1 atm (helium). Heating rate = 1000°C/s].

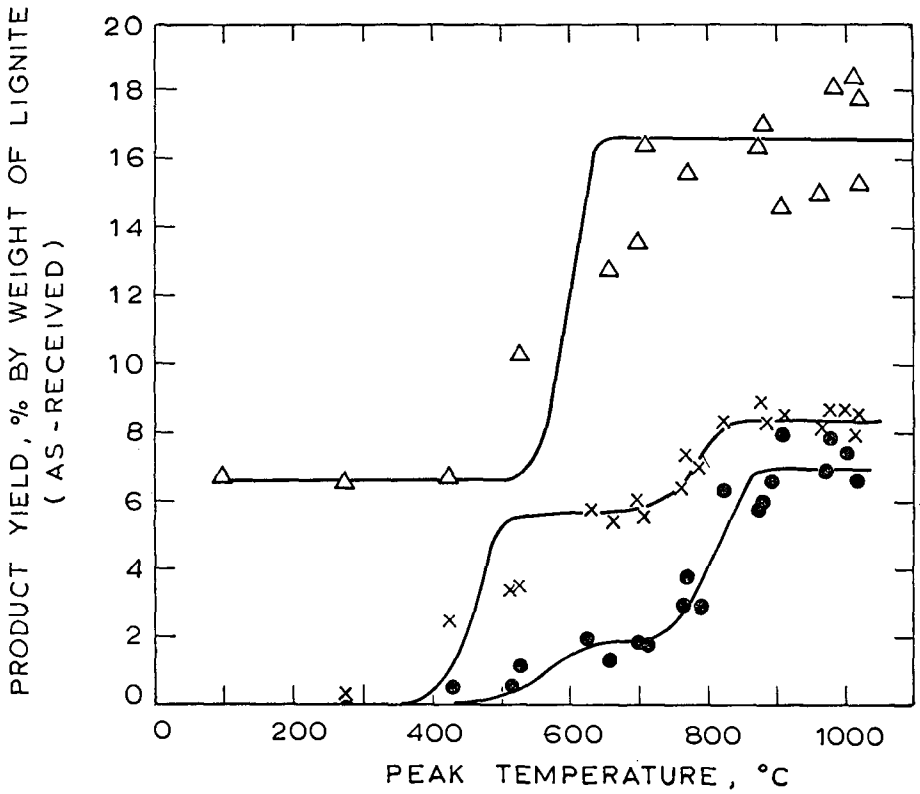

Figure 5. Yields of Water, Carbon Monoxide, and Carbon Dioxide from Lignite Pyrolysis to Different Peak Temperatures [(Δ) H_2O; (x) CO_2; (●) CO. Pressure = 1 atm (helium). Heating rate = 1000°C/s].

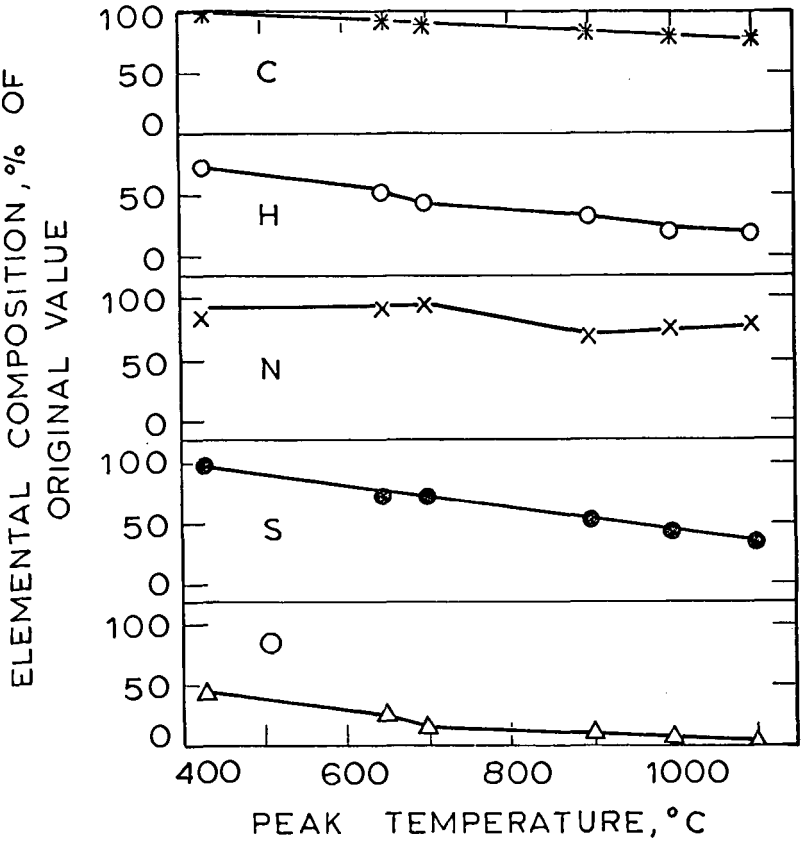

Figure 6. Elemental Compositions of Chars from Lignite Pyrolysis to Different Peak Temperatures [(*) C; (o) H; (x) N; (●) S; (Δ) O. Pressure = 1 atm (helium). Heating rate = 1000°C/s].

Table 2. Carbon, Oxygen, Hydrogen and Total Mass Balances

Product	Yield, weight % of Lignite (as-received)+, in Four Runs to Different Peak Temperatures															
	430°C				710°C				910°C				1000°C			
	Total	C	H	O	Total	C	H	O	Total	C	H	O	Total	C	H	O
CO_2	2.5	0.68	-	1.8	5.5	1.5	-	4.0	8.6	2.3	-	6.3	8.7	2.4	-	6.3
CO	0.46	0.20	-	0.26	1.8	0.77	-	1.0	8.0	3.4	-	4.6	7.5	3.2	-	4.3
HC*	0.02	0.02	0.0	-	0.95	0.79	0.17	-	2.6	2.1	0.49	-	3.0	2.4	0.58	-
Tar	1.5	1.3	0.15	-	2.3	2.1	0.23	-	4.9	4.4	0.49	-	4.7	4.3	0.47	-
H_2O	6.6	-	0.73	5.9	16	-	1.8	14	15	-	1.7	13	19	-	2.1	17
H_2	0.0	-	0.0	-	0.01	-	0.01	-	0.50	-	0.50	-	0.50	-	0.50	-
Char	89.0	64.0	3.9	10.9	73.9	53.6	2.3	2.9	60.9	47.5	1.8	2.9	55.8	44.2	1.0	1.1
Total	100	66.2	4.78	18.0	99.9	58.8	4.51	21.9	101	59.7	4.98	25.9	99.2	56.5	4.65	28.7
Closure	100%	112%	90%	77%	100%	99%	85%	93%	101%	101%	94%	110%	99%	95%	88%	122%

*Hydrocarbons other than tar.

+Lignite (as-received) is 59.3%C, 5.29%H, and 23.5%O, including H and O in lignite moisture.

difference, uncertainties inherent in the other measurements are absorbed in the oxygen values.

Product heating value contents -- i.e., mass yield x net (lower) heating value on a mass basis -- shown in Fig. 7 were estimated from the product yields in Table 2 and some additional tar and gas measurements. Heating values of the lignite and char were calculated from the elemental analyses (Table 1 and Fig. 6) using the correlation of Mott and Spooner (9) here adjusted to a net-heating value, as-received basis. The net heating value of the tar and that of hydrocarbons other than methane, ethylene and tar were assumed to be 16,000 and 19,700 Btu (37.2 and 45.8 KJ/g) respectively. The heating values of the methane, ethylene, hydrogen and carbon monoxide were, of course, known.

The heating value contents of the gas and tar follow the two-step behavior associated with the appearance of many of the individual components. At the higher temperatures, the gas accounts for a maximum of almost 15 % of the heating value content initially in the lignite, and the tar for about 8 %. At a temperature of about 1000°C, the char retains almost 70 % of the heating value on the same basis. The volumetric net heating value of the gas produced at peak temperatures above about 900°C is about 380 Btu/std. cu. ft. (14.2 MJ/m^3) on a dry basis.

The total heating value content of all products appears first to increase and then to decrease as the peak temperature increases. Pyrolysis appears to be endothermic over a range of lower to intermediate temperatures where the total heating value content of all the products is greater than that of the starting material. At higher temperatures, however, the total becomes less than the initial value and therefore pyrolysis to those temperatures may be thermally neutral or exothermic. The approximations used in this analysis preclude quantitative assessment of heats of pyrolysis.

Effect of Temperature-Time History Data points inside squares in Fig. 3 were obtained with the base conditions given above but modified as follows. The lignite was first heated to an intermediate temperature and then cooled to room temperature as before. The resulting char was then heated to a higher temperature and again cooled. The figure shows cumulative product yields for both cycles. The intermediate temperatures for the points at 855°C and 1970°C are 480°C and 670°C, respectively. The yields of all products in both cases are not significantly different from those obtained when the lignite is heated directly to the final peak temperature. This observation is consistent with the previous conclusion from weight loss data (3,4) that the pyrolysis reactions occurring at higher temperatures are largely independent of those occurring at lower temperatures. Such behavior is indicative of multiple parallel independent reactions as opposed to competitive reactions.

The encircled data points in Fig. 3 were obtained at heating rates of 7,100 to 10,000°C/s which is approximately ten-times higher than that of the base data. The points in triangles represent data taken at 270 to 470°C/s. No clear effect of heating rate is observed over the range here used. It is shown below that this behavior is expected for independent parallel, rather than competitive reactions.

Effect of Pressure Some runs were conducted under vacuum conditions (0.05 mm Hg; 7 Pa). Up to a temperature of 800°C, the total yield of volatiles and their composition are indistinguishable from those produced under 1 atm (101.3 kPa) of helium at roughly the same heating rates. Above 800°C, however, observable differences are noted in both total yield and product composition. The differences occurring at a peak temperature of 1000°C can be seen in Table 3. The temperature dependence of the pressure effect on the yields of some key components is shown in Fig. 8. Collection of all the tar formed under vacuum is difficult. Whereas at atmospheric pressures most of the tar stays suspended as an aerosol until it is purged through the filter, tar produced under vacuum deposits uniformly across all

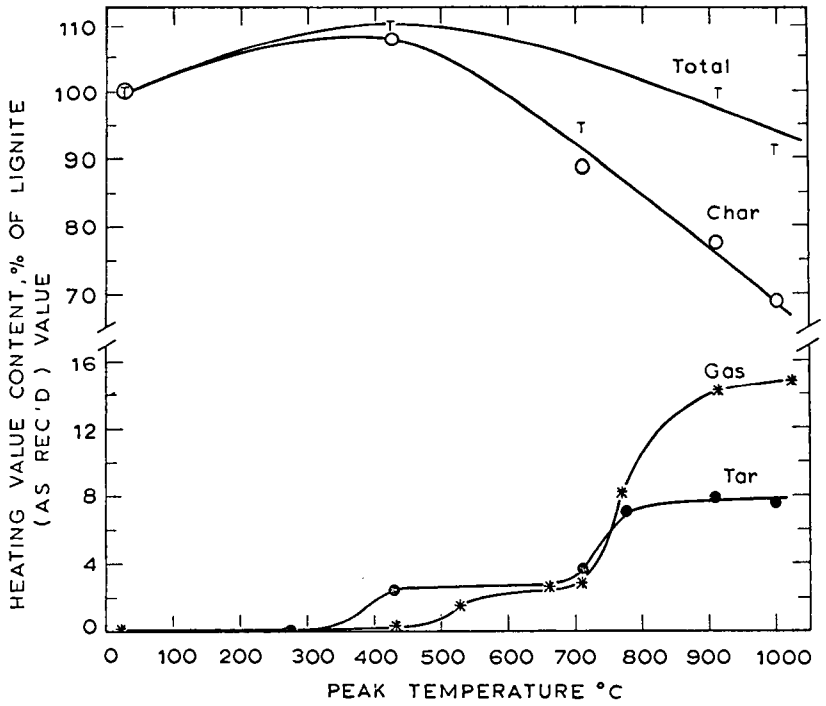

Figure 7. Distribution of Heating Value Content of Products from Lignite Pyrolysis to Different Peak Temperatures [(T) total, all products including char; (o) char; (*) gas; (●) tar. Pressure = 1 atm (helium). Heating rate = 1000°C/s. Basis: 100% on ordinate corresponds to 9,900 Btu/lb (23 KJ/g) lignite (as-received), the initial net (lower) heating value].

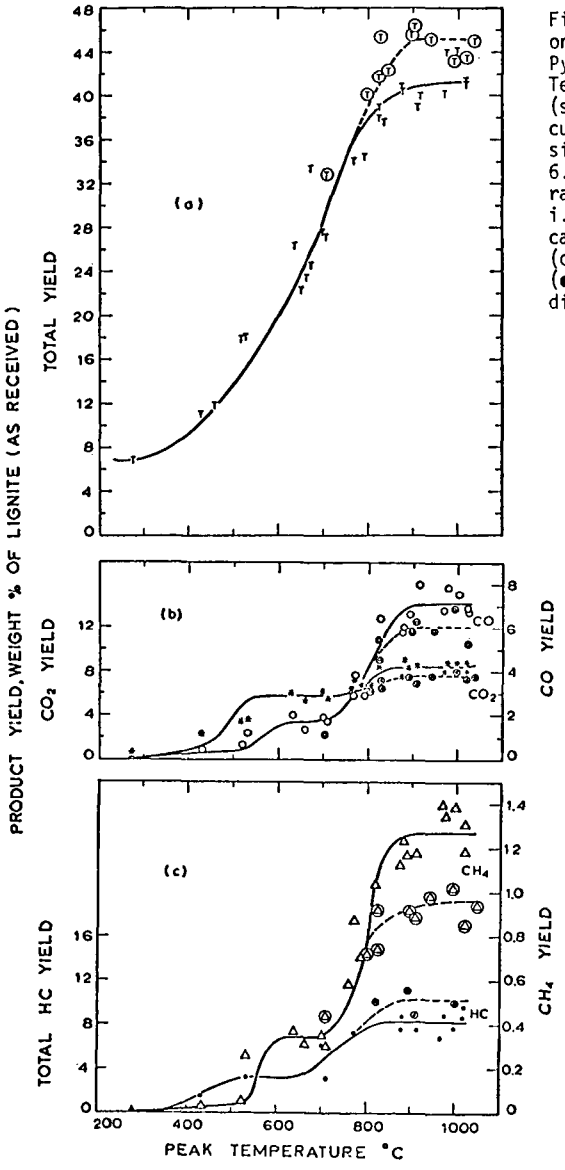

Figure 8. Effect of Pressure on Product Yields from Lignite Pyrolyzed to Different Peak Temperatures [Pressure: (single points and solid curves) 1 atm; (points inside 0 and dashed curves) 6.6×10^{-5} atm. Heating rate = 1000°C/s. (T) total, i.e., tar, all other hydrocarbons, H_2O, CO_2 and CO; (o) CO; (*) CO_2; (Δ) CH_4; (•) total hydrocarbons including tar].

Table 3. Effect of Pressure on Lignite Pyrolysis Product Yields (Peak temperature, 1000°C; heating rate, 1000°C/s)

Product	Yield, wt% of lignite (as received)	
	1 atm. He	vacuum
CO	7.1	6.1
CO_2	8.4	7.6
CH_4	1.3	0.95
C_2H_4	0.56	0.45
HC*	0.95	2.0
Tar	5.4	6.9
H_2O	16.5	18.1
H_2	0.50	N.M.**
Total Products	40.7	42.1
Measured Wt. Loss	41.3	44.7

*All hydrocarbons other than Tar, CH_4, and C_2H_4.
**Not measured

reactor surfaces upon initiation of the purge. Recovery of the thin tar film by the methylene chloride washing procudure is somewhat inefficient. Thus the total mass balance is poorer at vacuum than at 1 atm. A carbon balance conducted as described for Table 2 shows a carbon dificit of about 3 % for the vacuum data in Table 3. Therefore the actual vacuum tar yield at 1000°C may be about 9 % of the lignite weight.

The main conclusion from Table 3 and Fig. 8 is that vacuum pyrolysis of lignite produces higher yields of heavy hydrocarbon products and lower yields of light gases than are obtained at 1 atm. Since also the total weight loss is higher under vacuum, it appears that secondary cracking and char forming reactions play a role in determining product yields. In view of the thin layer of coal employed, the main contribution of the secondary reactions in this experiment presumably occurs within the particles. A similar but quantitatively more significant effect of secondary reactions on total weight loss from a bituminous coal was observed by Anthony et al.(3,4). Other workers(10,11) also have observed increased yields of low-volatile species in vacuum pyrolysis of coal.

MODEL

The modelling of coal pyrolysis as a set of independent parallel reactions having a statistical distribution of activation energies has been shown to provide valuable insight into the overall or global kinetics of the process(3). With the products in the present study dominated by a few individual species and classes of species, e.g. tar, there is interest in determining whether pyrolysis can be effectively modelled as only a few reactions representing the production of these key products.

As a first test of this approach, the appearance of product i is modelled as a reaction first-order in the amount of i yet to be produced. Thus for the reaction

$$\text{Coal} \rightarrow \text{Product}_i \qquad (1)$$

the assumed first-order rate is

$$dV_i/dt = k_i(V_i^* - V_i) \qquad (2)$$

and the rate constant is assumed to be

$$k_i = k_{io} \exp(-E_i/RT) \qquad (3)$$

where k_{io} is the pre-exponential factor, E_i is the activation energy of reaction i, V_i is the amount of product i produced up to time t, V_i^* is the amount of product i which could potentially be produced, (i.e., at $t = \infty$), T is the absolute temperature, and R is the gas constant. Assuming that temperature increases linearly with time, as it does in our experiments, with the constant rate $dT/dt = m$, solution of the above equations gives

$$\int_0^{V_i} dV_i/(V_i^* - V_i) = \int_0^T (k_{io}/m) \exp(-E_i/RT)dT \quad (4)$$

Since $E_i/RT \gg 1$ is a good approximation for coal decomposition reactions, the solution becomes

$$(V_i^* - V_i)/V_i^* = \exp[-(k_{io}RT^2/mE_i)\exp(-E_i/RT)] \quad (5)$$

This equation is plotted in Fig. 9 for activation energies typical of organic decomposition reactions (see Table 4) and a typical pre-exponential factor of $k_{io} = 1.67 \times 10^{13} s^{-1}$. The inadequacy of the single-reaction model in fitting the data on total yield of volatiles is evident from this figure; nevertheless, this approach has been taken by many workers for correlating pyrolysis data.

It can be seen from the wide range of materials listed in Table 4 that organic decomposition reactions encompass a wide range of activation energies and pre-exponentials. It is not surprising that coal, the chemical structure of which is far more complex than that of the materials in Table 4, decomposes thermally to produce numerous products and that these products exhibit different activation energies. When a single first-order reaction is used to model coal pyrolysis, the activation energy and pre-exponential factor are forced to be very low in order to fit the overall temperature dependence that actually results from the occurrence of different reactions in different temperature intervals. The results are sometimes interpreted as reflecting transport limitations because the parameters are too low for organic decompositions. This point is further discussed elsewhere(5).

Considerably more success is attained when the first-order model is applied to the appearance of single products. As is implied in Figs. 3 to 5, many individual species are not adequately described by one first-order process. Rather than utilizing a large number of parallel reactions with a distribution of activation energies for individual species(18), a simplifying assumption is made that one, two or three parallel reactions, depending on the observed behavior, describes the formation of certain key products. The mechanistic implication is that a given species may arise from more than one type of reactant, or from more than one reaction pathway.

The first-order model was used with the measured time-temperature history of each experimental run to construct best fit curves for the yield data. The resulting kinetic parameters are summarized in Table 5. The curves shown in Figs. 3,4, and 5 were calculated using these parameters and the model, for a standardized experiment in which coal is heated at 1000°C/s to the peak temperature, and then cooled at 200°C/s back to room temperature. The curves fit the data well for most species, and modelling with only one or two reactions appears sufficient in all cases except the carbon oxides which require a third reaction for data above about 1000°C (not shown here). Figure 3 shows how the various individual reactions cooperate to give a smooth total weight loss curve. Again, this figure emphasizes that a large fraction of the total weight loss is due to the oxygenated species.

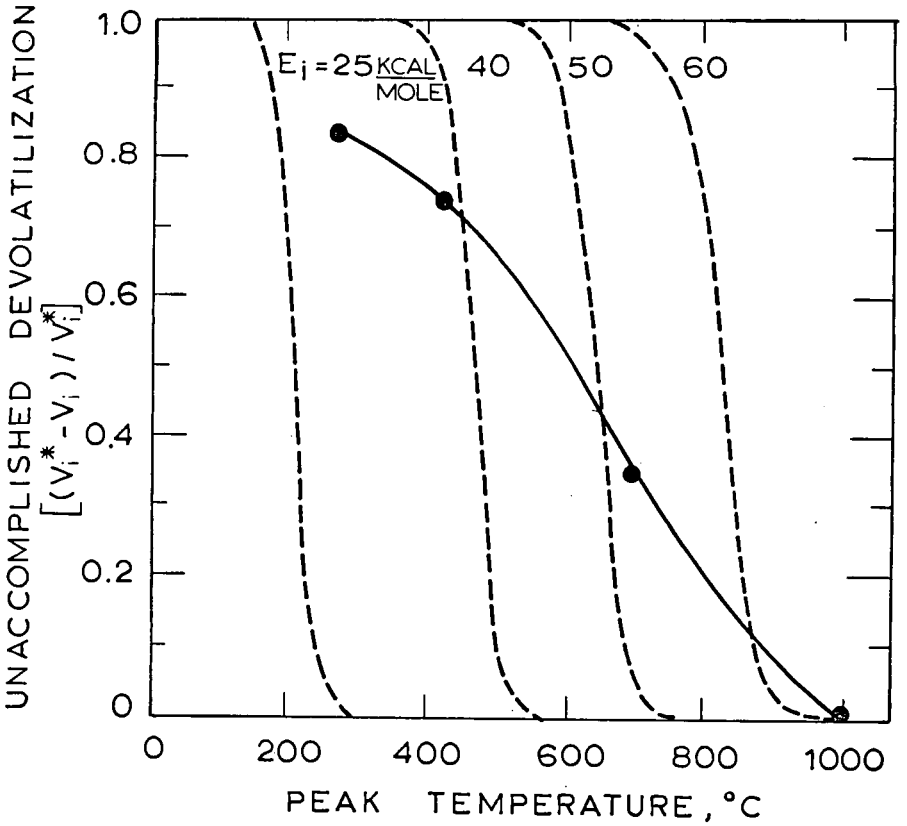

Figure 9. Comparison of Data on Overall Conversion of Lignite to Volatiles with Predictions from Single-Step First-Order Pyrolysis Model [(•) data; (dashed curves) predictions from model].

Table 4. Kinetic Parameters for Pyrolysis of Various Organic Materials

Material Pyrolyzed	Product[a]	Experimental Temp., °C	Activation Energy, kcal/mole	Pre-Exponential Factor, s^{-1}	Ref.
Ferulic Acid ($C_{10}H_{10}O_4$)	CO_2	150-250	27.7	6.0×10^{9}	12, 13
Perylene Tetracarboxylic Acid Anhydride ($C_{24}H_8O_6$)	CO_2	400-600	71.5	5.2×10^{17}	12, 13
	CO	400-600	64.9	5.0×10^{16}	12, 13
Protocatechuic Acid ($C_7H_6O_4$)	$(H_2O)_1$	50-300	18.8	2.7×10^{8}	12, 13
	$(H_2O)_2$	50-300	42.4	2.3×10^{5}	12, 13
	CO_2	50-300	40.4	1.6×10^{15}	12, 13
Naphthalene Tetracarboxylic Acid ($C_{14}H_8O_8$)	H_2O	100-250	33.5	1.2×10^{13}	12, 13
Mellitic Acid ($C_{12}H_6O_{12}$)	H_2O	230[b]	16.6	2.3×10^{5}	13
Tartaric Acid ($C_4H_6O_6$)	H_2O	195[b]	42.9	6.7×10^{17}	13
Polystyrene $(C_8H_8)_n$	overall	394[b]	77	8.3×10^{22}	13
	overall	335-355[b]	58	9.0×10^{15}	14
Teflon $(C_2F_4)_n$	overall	575[b]	67-69	4.3×10^{14}	13
Polyethylene $(C_2H_4)_n$ "Phase 1"	overall	385-405	48	5.2×10^{11}	14
"Phase 2"	overall	385-405	71	8.7×10^{18}	14
Hydrogenated Polystyrene $(C_8H_{14})_n$	overall	335-350	52	1.4×10^{14}	15
Polymeta-methylstyrene $(C_9H_{10})_n$	overall	333-353	50	7.2×10^{16}	15
Polyalpha-methylstyrene $(C_9H_{10})_n$	overall	273-288	58	8.3×10^{18}	15
Polymethyl-methacrylate $(C_5H_8O_2)_n$					
Avg. Molecular Wt. 150,000	overall	240-270	33	3.6×10^{9}	15
Avg. Molecular Wt. 5,100,000	overall	310-325	55	1.8×10^{16}	15
Polymethylacrylate $(C_4H_6O_2)_n$	overall	285-300	37	1.4×10^{10}	15
Cellulose $(C_6H_{10}O_5)_n$	overall	250-1000	33.4	6.8×10^{9}	16
		250-350	35	3.3×10^{11}	13, 17

a. Denotes species whose evolution is described by the parameters given. Two different stages of water evolution are denoted by $(H_2O)_1$ and $(H_2O)_2$. Overall refers to all products combined.

b. Temperature of maximum pyrolysis rate.

Table 5. Kinetic Parameters for Lignite Pyrolysis

Product	Stage	E_i, kcal/mole	log (k_{io}/s^{-1})	V_i^*, Wt.% of lignite (as-received)
CO_2	1	36.2	11.33	5.70
	2	64.3	13.71	2.70
	3	42.0	6.74	1.09
CO	1	44.4	12.26	1.77
	2	59.5	12.42	5.35
	3	58.4	9.77	2.26
CH_4	1	51.6	14.21	0.34
	2	69.4	14.67	0.92
C_2H_4	1	74.8	20.25	0.15
	2	60.4	12.85	0.41
HC[a]		70.1	16.23	0.95
Tar	1	37.4	11.88	2.45
	2	75.3	17.30	2.93
H_2O		51.4	13.90	16.5
H_2		88.8	18.20	0.50
Total				44.0

a. Hydrocarbons other than CH_4, C_2H_4 and Tar

Examination of Fig. 3 also reveals that there are apparently five principal phases of devolatilization. The first occurs at very low temperatures (~100°C) and is associated with moisture evolution. The second phase at 1000°C/s heating rate begins at about 450°C and is associated with a large initial evolution of carbon dioxide, probably from low-activation energy decarboxylations. The loss of carboxyl groups as carbon dioxide at relatively low temperatures has been reported for lignites(10). A small amount of tar is also evolved at this stage. This material may contain not only real tar (e.g., asphaltenes and heavy oils) but also small particles of lignite broken off the parent particles by the escaping gases as mentioned above. The third phase involves evolution of water chemically formed in the range 500-700°C where the only other significant product is carbon dioxide. It can be seen from Fig. 6 that carbon, nitrogen and sulfur during this phase remain largely in the char while the oxygen and hydrogen contents of the char sharply decrease. The fourth phase involves a final rapid evolution of carbon containing species. Carbon oxides, tar, hydrogen, and hydrocarbon gases are all rapidly evolved in the temperature range 700-900°C, where little water is produced. The fifth phase is the previously discussed high temperature formation of carbon oxides. To be compared with the foregoing, Chukhanov(19) suggests that coal pyrolysis involves three stages: evolution of carbon oxides and water (450-550°C); formation of tar and hydrocarbon gases; and residue degasification.

In order to compare the present kinetic parameters with those obtained before using a distributed activation energy model(1,3-5), the frequency distribution of the present activation energies is derived from Table 5 as follows. Data points in Fig. 10 represent the cumulative ultimate yields of all volatile components having activation energies less than or equal to those of the indicated points. Each point is labelled with the component whose ultimate yield is added to those

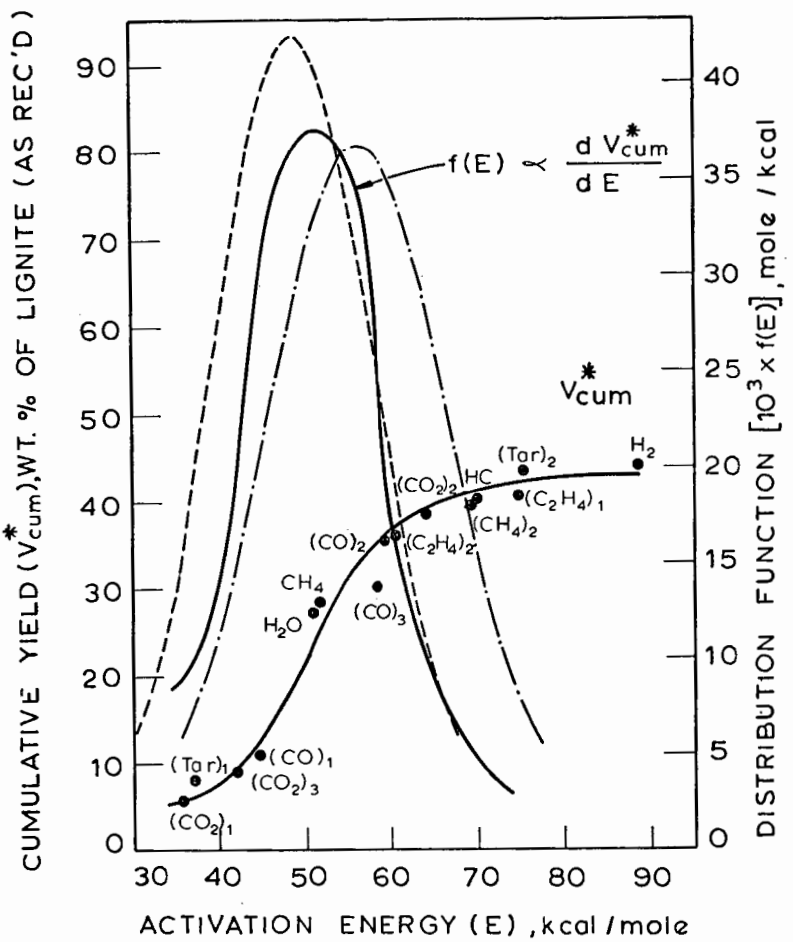

Figure 10. Distribution of Activation Energies of Pyrolysis Reactions [(●) cumulative yields, from present base data, of components indicated to left of and including a given point; (solid curves) present results based on volatiles yields; (broken curves) previous results [1,5] based on weight loss data and two different sets of kinetic parameters].

of all other components shown on points to the left to give the indicated cumulative yield; e.g., the vertical distance between two adjacent points represents the ultimate yield of the component specified on the higher point. The slope of the smooth curve drawn through the data gives the frequency distribution curve $dV^*_{cum}/V^*_{tot}dE$, which is here normalized so that the area under a segment of the curve between two values of activation energy is the percentage of the total ultimate volatile yield that is associated with activation energies in the specified interval.

Figure 10 also presents two distributions (broken curves) obtained previously(1,5) for the same lignite as was used here, but from a kinetic analysis of weight loss data using a statistically large number of reactions having a Gaussian distribution of activation energies and all having the same pre-exponential factor. The left-hand curve was obtained when the pre-exponential factor (k_o=$1.07x10^{10}s^{-1}$) was evaluated as one of the adjustible parameters, while the right-hand curve was obtained using a preferred fixed value of k_o($1.67x10^{13}s^{-1}$). The mean activation energies (E_o) and standard deviations (σ) of the previous distributions are, in kcal/mole, (left) E_o=48.7 and σ=9.38 and (right) E_o=56.3 and σ=10.9. Statistical analysis shows that the present data are not significantly different from a Gaussian distribution with E_o and σ being 53.3 and 11.5 kcal/mole, respectively. The similarity of the present distribution derived from product compositions to the previous results based on weight loss is especially encouraging since k_o, which does influence E_o, was here allowed to assume a different value for each reaction whereas previously a single k_o was used for all reactions.

DISCUSSION

Since coal is always "hydrogen-starved" in the sense that its empirical formula is usually $CH_{0.6}$ to CH (the present lignite is roughly $CH_{0.9}$) while the desired products are in the range CH to CH_4, it is desirable to use the coal hydrogen as efficiently as possible. The oxygen in the coal removes most of the hydrogen at temperatures below those at which the principal hydrocarbon forming reactions can occur; thus, by the time the coal is hot enough for the latter reactions to occur, there is too little hydrogen left to produce stable, volatile fragments. The addition of hydrogen from outside the particle, e.g., as in the case of hydrogasification, enhances the yield of volatiles perhaps by stabilizing some reactive sites or species that would otherwise form char(4,5,20-23). This hypothesis will be tested with future experiments in a hydrogen atmosphere.

If the pyrolysis reactions that form water and hydrocarbons are in competition for hydrogen, then the hydrocarbon yield could perhaps be increased by subjecting the coal to a favorable time-temperature history. For example, in the present results tar forming reactions have a higher activation energy than the water forming reactions (75.3 kcal/mole compared to 51.4 kcal/mole) and hence are favored by going to higher temperatures. According to the present model, very high rates of heating would be required to attain these higher temperatures without the water forming reactions first reaching completion. At 1000°C/s, the water forming reactions are about 90 % complete before the onset (defined as 1 % completion) of the tar forming reactions. This analysis neglects the low temperature tar forming reactions and also assumes that the water and tar forming reactions are independent. At 6090°C/s, the water forming reaction are predicted to be 75 % complete when the onset of tar formation occurs (at 700°C), and at $2.8x10^5$°C/s, the water reactions are only 35 % complete at the onset of tar formation (at 800°C). Total volatile yields significantly larger than those of the present study were in fact observed(7,8) from Montana lignite heated at about $2x10^5$°C/s to about 1800°C.

It is interesting to compare the observed product distributions with those that would be obtained if all the volatiles generated in a run were in mutual equilibrium in the presence of char at the final temperature of the particles. For approximation purposes the char is assumed to be graphite and the mole fraction of the ambient helium adjacent to and within the particles is assumed to be negligible. Equilibrium relations for the reactions

$$CO + H_2O = CO_2 + H_2 \quad (6)$$

$$C + H_2O = CO + H_2 \quad (7)$$

$$C + 2H_2 = CH_4 \quad (8)$$

$$CH_4 + H_2O = CO + 3H_2 \quad (9)$$

in the presence of excess solid carbon are shown as curves in Fig. 11 where the base data are given as points. Two cases are considered, one including water from the lignite moisture in the volatiles (points) and the other including only the chemically formed water (not shown). The latter case covers the possibility that moisture is lost early enough so as to be absent from the reacting mixture. The complete or partial loss of others products could also be considered but this was not done since moisture loss, which appears to offer the largest potential for an effect, is found to be of little significance in this rough analysis.

Figure 11 shows that the data tend toward less disagreement with the equilibrium values as temperature increases. When the total pressure of volatiles is assumed to be 1 atm, which is the experimental pressure under which the data were taken, all the reactions are far from equilibrium with the exception of Reaction 6 at the higher temperatures, where a rather close approach to equilibrium cannot be excluded within the large uncertainty of this calculation. Reaction 6 is the only one of the four that is independent of pressure. The equilibrium values for the other reactions also agree roughly with the data if the assumed total pressure of the volatiles is increased substantially, the values for Reactions 7,8, and 9 depending on pressure to the powers -1, +1, and -2, respectively.

Volatiles pressures much larger than 1 atm within the pores of the particles are not inconsistent with calculated pressure drops associated with volatiles explusion under the present conditions of rapid pyrolysis. The agreement in Fig. 11 between the equilibrium values and the data for an assumed pressure of 1000 atm is intriguing. We do not know to what extent such a high pressure properly reflects conditions developed within rapidly pyrolyzing lignite, but we note that internal pressures of this order of magnitude (a) would be calculated if it is assumed that the formation of volatiles within the pores largely precedes the escape therefrom, and (b) would appear to be required to fracture the particles based on the strength of the material. Lignites rapidly heated are known to exhibit fracturing or "sparking", a phenomenon that could account for the particulate material here found in the tar as noted above.

Although the foregoing equilibrium analysis is far from definitive, it is probably safe to conclude that the final mixture of volatiles is closer to equilibrium than are the primary volatiles and, therefore, that mass transport and secondary reactions within the particles do play some role in determining product distributions. Thus, at temperatures above about 800°C, the enhanced mass transport condition provided by vacuum pyrolysis leads to somewhat higher yields of hydrocarbon liquids and tars and correspondingly lower yields of light hydrocarbon and carbon oxide gases. The behavior indicates that more volatiles cracking within particles occurs at 1 atm than under vacuum, but the difference affects no more than about 5 % of the total lignite material. The fact that this effect is small supports the picture that the pressure inside lignite particles during rapid pyrolysis is indeed high and therefore not strongly dependent on external pressure in

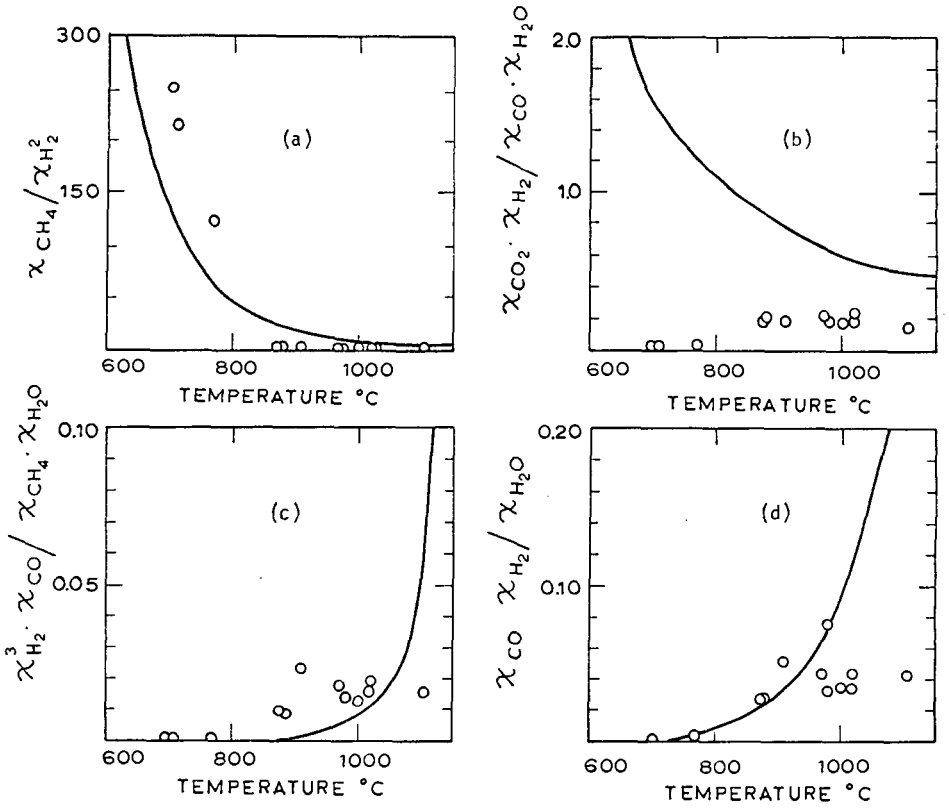

Figure 11. Comparison of Gas Composition Data for Different Peak Temperatures with Calculated Equilibrium Values under Simplified Conditions [χ_i = mole fraction of i. (o) base data; (curves) equilibrium values multiplied by 10^3 in (a), 1 in (b), 10^{-6} in (c) and 10^{-3} in (d), all these factors being equivalent to the assumption that the total partial pressure of volatiles is 10^3 atm].

the range 0 to 1 atm. Accordingly, the absolute amount of volatiles cracking within the pores may be much larger than the change observed in going from 1 atm to vacuum conditions.

The suggested role of mass transport and secondary reactions points up the empirical nature of pyrolysis models, such as the one employed here, that do not explicitly account for these effects. The kinetic parameters obtained by application of the present multiple parallel reaction model to species originating in some combination of primary and secondary reactions are clearly overall properties. Derivation from the present data of fundamental properties of the primary pyrolysis reactions must await a better understanding of mass transfer and secondary reactions in the particles. Nevertheless, the demonstrated success of the present model in correlating the data means that the multiple parallel reaction picture together with the identification from the data of key "reactions" (e.g., stages in the evolution of a given product species) is an effective representation of primary reactions as modified by the effects of mass transport and secondary reactions.

ACKNOWLEDGEMENT

We are grateful to the National Science Foundation, Research Applied to National Needs (RANN), for funding under Contract AER 75-13673; to Kevin E. Bennet, Richard N. Caron, Karen J. Hladik and Scott Free for valuable laboratory work; to William DuBroff of Inland Steel Research Laboratories for petrographic analysis for the lignite; and to the Institute of Gas Technology and Knife River Coal Company for lignite samples. One of us (E.S.) gratefully acknowledges personal support through the N.S.F. Energy Trainsceship program.

NOMENCLATURE

E = activation energy, kcal/mole

E_i = activation energy of reaction forming product i, kcal/mole

E_0 = mean of activation energy distribution, kcal/mole

$f(E)$ = activation energy distribution function, mole/kcal

k_i = first-order rate constant of reaction forming product i, s^{-1}

k_{io} = pre-exponential factor in k_i, s^{-1}

k_o = pre-exponential factor when all k_{io} are assumed equal, s^{-1}

m = constant heating rate, °C/s

R = gas constant, kcal/mole K

t = time, s

T = absolute temperature, K

V_i = amount of product i generated up to time t, fraction of the original coal weight

V_i^* = value of V_i at $t = \infty$ (ultimate yield), approximated by measurements at long reaction times, fraction of the original coal weight

V_{cum}^* = sum of V_i^* for all i with $E_i \leq E$, fraction of the original coal weight

V_{tot}^* = sum of all V_i^*, fraction of the original coal weight

σ = standard deviation of activation energy distribution, kcal/mole

x_i = mole fraction of component i

REFERENCES

1. Anthony, D.B., "Rapid Devolatilization and Hydrogasification of Pulverized Coal," Sc. D. thesis, Massachusetts Institute of Technology, Cambridge, Mass., 1974.

2. Anthony, D.B., J.B. Howard, H.P. Meissner, and H.C. Hottel, "Apparatus for Determining High Pressure Coal-Hydrogen Reaction Kinetics under Rapid Heating Conditions," Rev. Sci. Instrum. 45, 992 (1974).

3. Anthony, D.B., J.B. Howard, H.C. Hottel, and H.P. Meissner, "Rapid Devolatilization of Pulverized Coal," Fifteenth Symposium (International) on Combustion, p. 1303, The Combustion Institute, Pittsburgh, Pa. (1975).

4. Anthony, D.B., J.B. Howard, H.C. Hottel, and H.P. Meissner, "Rapid Devolatilization and Hydrogasification of Bituminous Coal," Fuel 55, 121 (1976).

5. Anthony, D.B. and J.B. Howard, "Coal Devolatilization and Hydrogasification," A.I. Ch.E. J. 22, 625 (1976).

6. Solomon, P.R., personal Communication (1976).

7. Kobayashi, H., "Devolatilization of Pulverized Coal at High Temperatures," Sc.D. thesis, Department of Mechanical Engineering, Massachusetts Institute of Technology, Cambridge, Mass., 1976.

8. Kobayashi, H., J.B. Howard, and A.F. Sarofim, "Coal Devolatilization at High Temperatures," Sixteenth Symposium (International) on Combustion, The Combustion Institute, Pittsburgh, Pa. (in press).

9. Mott, R.A., and C.E. Spooner, "The Calorific Value of Carbon in Coal: The Dulong Relationship," Fuel 19, 226, 242 (1940).

10. Howard, H.C., "Pyrolytic Reactions of Coal," in Chemistry of Coal Utilization, pp. 340-394, Supplementary Volume, H.H. Lowry, ed., Wiley, New York (1963).

11. Loison, R., and F. Chauvin, "Pyrolyse Rapide du Charbon," Chem. Ind. (Paris) 91, 269 (1964).

12. Jüntgen, H. and K.H. Van Heek, "Gas Release from Coal as a Function of the Rate of Heating," Fuel 47, 103 (1968).

13. Jüntgen, H. and K.H. Van Heek, "Reaktionsablaufe unter nichtisothermen Bedingungen," in Fortschritte der chemischen Forschung, vol. 13, pp. 601-699, Springer-Verlag, Berlin (1970).

14. Madorsky, S.L., "Rates of Thermal Degradation of Polystyrene and Polyethylene in a Vacuum," J. Polymer Science IX (2), 133 (1952).

15. Madorsky, S.L., "Rates and Activation Energies of Thermal Degradation of Styrene and Acrylate Polymers in a Vacuum, J. Polymer Science XI (5), 491 (1953).

16. Lewellen, P.C., W.A. Peters, and J.B. Howard, "Cellulose Pyrolysis Kinetics and Char Formation Mechanism" Sixteenth Symposium (International) on Combustion, The Combustion Institute, Pittsburgh, Pa. (in press).

17. Van Krevelen, D.W., C. Van Heerden, and F.J. Huntjens, "Physiochemical Aspects of the Pyrolysis of Coal and Related Organic Compounds," Fuel 30, 253 (1951). [Numerical results modified by Jüntgen and Van Heek (13)].

18. Hanbaba, P., H. Juntgen, and W. Peters, "Nicht-isotherme Reaktionskinetik der Kohlenpyrolyse, Teil II: Erweiterung der Theorie der Gasabspaltung und experimentelle Bestätigung an Steinkohlen," Brennstoff-Chem. 49, 368 (1968).

19. Chukhanov, Z.F., Izvest. Akad Nauk S.S.S.R., Otdel Tekh. Nauk, No. 8, pp. 7-22 (1954); Chem Abs. 49, 5808 (1955).

20. Moseley, F., and D. Paterson, "Rapid High-Temperature Hydrogenation of Coal Chars, Part 1," J. Inst. Fuel 38, 13 (1965).

21. Zahradnik, R.L. and R.A. Glenn, "Direct Methanation of Coal," Fuel 50, 77 (1971).

22. Johnson, J.L., "Kinetics of Bituminous Coal Char Gasification with Gases Containing Steam and Hydrogen," in Coal Gasification, p. 145, Advances in Chemistry Series, No. 131, Am. Chem. Soc., Washington, D.C., (1974).

23. Johnson, J.L., "Gasification of Montana Lignite in Hydrogen and in Helium during Initial Reaction Stages," Am. Chem. Soc., Div. of Fuel Chem. Preprints 20, No. 3, 61 (1975).

RECENT PROGRESS IN KINETIC MODELS FOR COAL PYROLYSIS

M.J. Antal, E.G. Plett, T.P. Chung,
and M. Summerfield
Princeton University
Princeton, New Jersey

INTRODUCTION

Two mathematical models for the hypothesized kinetic mechanisms of coal pyrolysis have attracted attention in the recent literature. The first model uses a distributed activation energy to simulate the pyrolysis mechanism (1-4); whereas the second uses a set of six competitive/consecutive reactions to model the observed results of coal pyrolysis (5). These models have been developed to assist in the design of improved pyrolytic reactor systems for synthetic fuel production. They may also offer an insight into the more complicated physical-chemical processes occuring during hyrogasification of the coal.

The models are expected to be useful for studying two distinct types of situations. The first type involves the prediction of reactor performance for pyrolysis conditions within the range of conditions studied in the laboratory. This situation exercises the model's interpolative capability. The second type of situation uses the model to predict reactor performance under conditions which have not yet been carefully studied in the laboratory. This situation is inherently more risky, and exercises the model's predictive capabilities.

In this paper we examine the two models from the standpoint of their interpolative and potential predictive capabilities. We attempt to offer an insight into the special set of properties which make each model attractive. More experimental data is required before a meaningful comparison of the two models' capabilities can be made.

MODELS EMPLOYING A DISTRIBUTED ACTIVATION ENERGY

The concept of a distributed activation energy as originally proposed by Vand (6) was adapted to the problem of coal devolatilization by Pitt (7), and later used by Hanbaba and his coworkers (8), and Anthony (1-4). The model postulates the decomposition mechanism take a large number of independent, parallel, first order chemical reactions with different activation energies reflecting variations in the bond strengths of species composing the coal molecule. Following this postulate, the rate of evolution of volatiles V_i by reaction i is given by

$$\frac{dV_i}{dt} = -k_i \, (V_i^* - V_i) \qquad (1)$$

where V_i^* represents the effective volatile content of the coal (1) due to reaction i, and k_i has the customary Arrhenius form

$$k_i = A_i \exp(-E_i/RT). \tag{2}$$

In Eq. (2) A_i is a constant, E_i the activation energy, R the universal gas constant, and T the temperature. The total rate of evolution of volatiles is then given by

$$\frac{dV}{dt} = \sum_i \frac{dV_i}{dt} = \sum_i - k_i(V_i^* - V_i). \tag{3}$$

Returning to Eq. (1) we have

$$\frac{dV_i}{V_i^* - V_i} = -k_i dt \tag{4}$$

which can be integrated to give

$$V_i^* - V_i = V_i^* \exp(-\int_o^t k_i dt) \tag{5}$$

Summing both sides of Eq. (5) over all reactions i we have

$$V^* - V = \sum_i V_i^* \exp(-\int_o^t k_i dt) \tag{6}$$

where $V^* = \sum_i V_i^*$ and $V = \sum_i V_i$.

Now suppose that the fraction V_i^* of the total effective volatile content of the coal V^* is evolved by reactions with activation energies between $E_i - (1/2)\delta E_i$ and $E_i + (1/2)\delta E_i$, so that

$$V_i^* = V^* f^*(E_i)\delta E_i \tag{7}$$

and $\sum_i f^*(E_i)\delta E_i = 1$. Substituting Eq. (7) into Eq. (6) we have

$$V^* - V = \sum_i V^* f^*(E_i) \exp(-\int_o^t k_i dt)\delta E_i \tag{8}$$

Finally, if the total number of parallel reactions i is large enough, Eq. (8) can be approximated by the integral equation

$$V^* - V = \int_o^\infty V^* f^*(E) \exp(-\int_o^t k\, dt)dE \tag{9}$$

where $\int f^*(E)dE = 1$.

In order to make Eq. (9) mathematically more tractable, Anthony (4) assumed $f^*(E)$ to be a Gaussian distribution with mean activation energy E_o and standard deviation σ:

$$f^*(E) = [\sqrt{2\pi}\,\sigma]^{-1} \exp(-(E-E_o)^2/2\sigma^2). \quad (10)$$

With this definition, Eq. (9) becomes

$$V^* - V = [\sqrt{2\pi}\sigma]^{-1} V^* \int_o^\infty \exp(-\int_o^t k\,dt) \exp\left\{-\frac{(E-E_o)^2}{2\sigma^2}\right\} dE \quad (11)$$

To simplify the mathematics Anthony evaluated the expression

$$[\sqrt{2\pi}\,\sigma]^{-1} V^* \int_{-\infty}^\infty \exp(-\int_o^t k\,dt) \exp\left\{-\frac{(E-E_o)^2}{2\sigma^2}\right\} dE \approx V^* - V \quad (12)$$

numerically, choosing the adjustable parameters A, E_o, σ and V^* so as to achieve a "best fit" with experimental data. Although equation (12) contains only one more adjustable parameter than that required by a single reaction model, Anthony was able to obtain surprizingly good agreement with experiment (4). In a recent publication Anthony and Howard (1) attribute this agreement to the model's ability to realistically describe multiple decomposition reactions, such as are supposed to occur during coal pyrolysis. However, the following paragraphs suggest that another interpretation of the model's success is also possible.

We first adapt the concept of a distributed activation energy to systems of equations describing irreversible chemical reactions such as the Reidelbach-Summerfield reaction set. These equations have the general form

$$\frac{d}{dt} P_i = \sum_j X_{ij}\, k_{ij}\, R_j \quad (13)$$

where P_i is the i^{th} product, X_{ij} are the appropriate stoichiometric coefficients, k_{ij} the Arrhenius rate constants, and R_j the relevant reactants. Integrating Eq. (13) from time t = 0 to t = τ yields

$$P_i(\tau) - P_i(0) = \sum_j X_{ij} \int_o^\tau k_{ij}\, R_j(t)dt. \quad (14)$$

Using the distributed activation energy concept, we suppose that at time t each product has been evolved by reactions with a distributed activation energy, so that Eq. (13) becomes

$$\frac{d}{dt} (\delta P_{ik}) = \sum_j X_{ij}\, k_{ijk}\, (\delta R_{jk}) \quad (15)$$

Integrating Eq. (15) from 0 to τ with the relation $P_i = \sum_k \delta P_{ik}$, and the distributed activation energy hypothesis

$$\delta R_{jk} = R_j f(E_{ijk})\,\delta E_{ijk} \quad (16)$$

we have

$$P_i(\tau) - P_i(0) = \sum_j X_{ij} \int_o^\tau dt\ R_j(t) \sum_k k_{ijk} f(E_{ijk})\ \delta E_{ijk}. \qquad (17)$$

Taking the limit $\delta E_{ijk} \to 0$, Eq. (17) becomes

$$P_i(\tau) - P_i(0) = \sum_j X_{ij} \int_o^\tau dt R_j(t) \int_o^\infty k_{ijk} f(E) dE \qquad (18)$$

where $k_{ijk} = A_{ijk} \exp(E/RT)$. The integral $\int_o^\infty k_{ijk} f(E) dE \equiv K_{ij}$ serves as an effective rate constant, so that Eq. (18) can be written

$$P_i(\tau) - P_i(0) = \sum_j X_{ij} \int_o^\tau K_{ij}\ R_j\ dt \qquad (19)$$

If f(E) is chosen to be the Gaussiar distribution given by Eq. (10), K_{ij} becomes

$$K_{ij} = A'_{ij} \int_o^\infty \exp -\left(\frac{E}{RT} - \frac{(E - E_{ij}^o)^2}{2\sigma^2} \right) dE \qquad (20)$$

with $A_{ij}' = A_{ijk}/(\sqrt{2\pi}\,\sigma)$ for all k. The integral in Eq. (20) can be evaluated analytically, with the result

$$K_{ij} = A'_{ij} \exp\left[\frac{-E_{ij}^o}{RT} + \frac{\sigma^2}{2R^2T^2} \right] \left[1 - (1/2)\operatorname{erfc}\left(\frac{\sqrt{2}E_{ij}^o}{2\sigma} - \frac{2\sigma}{2RT} \right) \right] \qquad (21)$$

If $\sigma << E_{ij}^o$ Eq. (21) can be approximated by the relation

$$K_{ij} \approx A_{ij}' \exp\left(\frac{-E_{ij}^o}{RT} + \frac{\sigma^2}{2R^2T^2} \right) \qquad (22)$$

Equation (22) offers an insight into the power of the distributed activation energy concept. A graph of log k vs 1/T need not be straight in order to be fitted by the effective reaction rate K_{ij}. This is because the distributed activation energy introduces a $(T^{-1})^2$ dependence in the exponent. Thus the distributed activation energy can be viewed as a clever device for introducing a second term in the power series expansion of log k. From this one could justifiably conclude that the distributed activation energy is no more than a sophisticated curve fitting technique, as opposed to a model which offers a realistic description of the coal devolatilization process (1).

Unfortunately, Eq. (1) used by Anthony cannot be interpreted as easily as Eq. (18). If we set $\delta V^* = V_i^*$ and

$\delta V = V_i$, Eq. (1) becomes

$$\frac{d}{dt}(\delta V) = -k_i (\delta V^* - \delta V) . \tag{23}$$

But $\delta V^* = V^* f^*(E)\delta E$ (see Eq. (7)); hence

$$\frac{d}{dt}(\delta V) = -k_i (V^* f^*(E)\delta E - \delta V) \tag{24}$$

or $$\frac{d}{dt}\left(\frac{\delta V}{\delta E}\right) = -k_i V^* f^*(E) + k_i \left(\frac{\delta V}{\delta E}\right) . \tag{25}$$

In the limit $\delta E \to 0$ we have

$$\frac{\partial}{\partial t}\left(\frac{\partial V}{\partial E}\right) - k_i \left(\frac{\partial V}{\partial E}\right) = -k_i V^* f^*(E) \tag{26}$$

where $V(t) = \int_o^\infty \left(\frac{\partial V}{\partial E}\right) dE$. If we integrate Eq. (26) over E we obtain

$$\frac{d}{dt}(V) - \int_o^\infty k_i \left(\frac{\partial V}{\partial E}\right) dE = -V^* \int_o^\infty k_i f^*(E) dE \tag{27}$$

which compares with Eq. (1) written without a distributed activation energy:

$$\frac{d}{dt}(V) - kV = -V^* k. \tag{28}$$

The term $\int_o^\infty k_i f^*(E)dE$ on the right hand side of Eq. (27) plays the role of k on the right hand side of Eq. (28) and may be regarded as an effective rate constant K as before. Unfortunately, the role of kV on the left hand side of Eq. (28) is played by the term

$$\int_o^\infty k_i \left(\frac{\partial V}{\partial E}\right) dE \tag{29}$$

and no particularly meaningful interpretation exists.

Eq. (27) governs the time evolution of the expression $\frac{\partial V}{\partial E} \equiv V(t,E)f(t,E)$, where $\lim_{t\to\infty} f(t,E) = f^*(E)$. From this it is clear that the distribution function is not independent of time in this setting, but evolves in a manner governed by Eq. (26).

If the distribution function were independent of time, the expression $\frac{\partial V}{\partial E}$ would become $\frac{\partial V}{\partial E} = V(t)f^*(E)$ and Eq. (27) would change to.

$$\frac{d}{dt}(V) - V\int_o^\infty k_i f^*(E)dE = - V^*\int_o^\infty k_i f^*(E)dE \qquad (30)$$

For this case the integral on the left hand side of Eq. (30) could also be interpreted as an effective rate constant K, and all the preceding remarks about distributed activation energies would also be true here.

The physical meaning and implications of a time dependent distributed activation energy are not clear at the present time. It would be interesting to see if solutions to Eq. (30), which assume a time independent distributed activation energy, give better agreement with experiment than solutions to Eq. (26). In any case, certain aspects of Eq. (26) suggest that it too can be interpreted as little more than a very sophisticated curve fitting technique.

MODELS EMPLOYING A SET OF PARALLEL AND CONSECUTIVE REACTIONS

Modeling at Princeton has emphasized the development of a reaction scheme involving a set of competitive/consecutive reactions chosen to simulate observed experimental trends. The goal of this research has been the creation of a model which simulates the gross fundamental mechanisms of pyrolysis. Such a model is anticipated to have reliable predictive capabilities, as well as the more easily obtained interpolative capability.

Recent research has focused on a critical re-examination of the Reidelbach-Summerfield (R-S) model (5) for coal pyrolysis. Table I summarizes the kinetic mechanisms present in this model. A detailed discussion of the reasoning which lead to this model can be found in the literature (5). Reaction 1 was proposed to limit the decomposition of coal at low temperatures. Chemically, this step can be considered to be a reaction in which bond scissions occur and free radicals are produced. After the coal has been activated, devolatilization can proceed by two routes, depending on the heating rate and final temperature. Since tar has always been reported as being driven off first, the tar formation step was chosen to have a low activation energy. In order to satisfy the experimental observation that the gas to tar yield ratio increases with increasing temperature, the primary gas formation reaction was chosen to have a high activation energy. Reaction 4 accounts for the observation that gas evolution occurs up to 900°C during pyrolysis. Finally, reaction 5 accounts for results of the high temperature experiments of Kimber and Gray. In this

model, reactions 1, 2 and 4 constitute the low temperature devolatilization route, and reactions 1, 3 and 5 give the high temperature route.

Stoichiometric factors for the R-S model were chosen to yield results which agreed with experimental data available in the literature. Values for the activation energies and frequency factors were obtained by fitting theoretical predictions of the R-S model to experimental data. Results calculated using the R-S model with the stoichiometric factors, frequency factors, and activation energies given in Table I enjoyed good agreement with experiment. However, the activation step employed an activation energy with a surprizingly large value of 75 kcal/mole. Due to the magnitude of this number, an experimental program was undertaken to study the activation step and to critically evaluate the other steps in the model.

Since the activation step, by definition, cannot be accompanied by weight loss, some other physical change had to be measured in order to determine the reaction rate and order. Measurements of heat release on the differential scanning calorimeter (DSC) proved to be useful in this case, assuming the activation step to be a single discrete reaction. Results of several experiments (9) on the DSC indicated that the reaction was first order with an activation energy of 28 kcal/mole and a frequency factor of 2.0×10^8 1/sec. Using these values, the R-S model no longer yielded results which agreed with experiment, and further modifications to the model were necessary.

Table 2 summarizes the modified R-S model now being studied at Princeton. Reaction 1 describes the formation of activated coal AC and an inert solid S_1. The activated coal may be viewed as a viscous liquid bitumen, which exists in equilibrium with a polymerized solid S_2. The activated coal can be vaporized at low temperatures to form a gaseous tar and an intermediate solid S_3, or it can be cracked at higher temperatures to form a primary gas PG and another intermediate solid S_4. Reactions 5 and 6 correspond to reactions 4 and 5 in the original R-S model.

The differential equations given by this model have been integrated numerically and the results compared with experiment. As indicated in Fig. 1, the calculated results enjoy good agreement with the experimental data of Badzioch and Hawksley (10). Although this agreement is encouraging, it cannot be regarded as providing sufficient evidence to assert the "correctness" of the model. Evidently, at least two models of the R-S type exist which agree with available experimental data. There are potentially many more. In order to determine if a "correct" reaction scheme exists within this formalism, thus defining a model with true predictive capability, more experimental results are required.

These experiments should be designed to emphasize chemical effects and minimize the effects of heat and mass transfer. Presently, TGA and DSC studies on Wyodak coal are being made at Princeton to generate experimental rate data needed to thoroughly exercise the models discussed in this paper. Results of these studies will be reported as they become available.

CONCLUSIONS

Both the distributed activation energy model and R-S model yield results which enjoy good agreement with experiment. From this we conclude that both models have good interpolative capabilities for the limited range of experimental conditions examined to date. However, research reported in this paper suggests that the success of the distributed activation energy model may be due to its mathematical ability to fit experimental values of log k with a power series expression in T^{-1}. The predictive capability of such a model is open to question.

The R-S model represents an attempt to define a reaction scheme which simulates the gross fundamental pyrolysis reactions. If this attempt is successful, the model should enjoy good predictive capabilities. Presently, two models of the R-S type exist and both agree with experiment. It is concluded that more experimental data is required to fully exercise the models' capabilities and determine their "correctness". Experimental work to generate the required rate data is underway at Princeton and other universities.

ACKNOWLEDGEMENTS

The authors are grateful to Dr. F. E. Rogers for many helpful discussions.

Prepared for the U. S. Energy Research and Development Administration, under Contract No. E(49-18)-2253.

REFERENCES

1 Anthony, D. B. and Howard, J. B., AIChE Journal, Vol. 22, No. 4 (1976), p. 625.

2 Anthony, D. B., Howard, J. B., Hottel, H. C. and Meissner, H. P., Fuel, Vol.55, No. 2 (1976), p.121.

3 Anthony, D. B., Howard, J. B., Hottel, H. C. and Meissner, H. P. 15th Symp. (International) on Combustion, The Combustion Institute, Pittsburgh, 1975, p. 1303.

4 Anthony, D. B., Sc.D thesis, Massachusetts Institute of Technology, 1974.

5 Reidelbach, H. and Summerfield, M., "Kinetic Model for Coal Pyrolysis Optimization", Am. Chem. Soc. Dir. Fuel Chem. Preprints, Vol. 20, No. 1 (1975), p. 161.

6 Vand, V., Proc. Phys. Soc., Vol. A55, (1943) p. 222.

7 Pitt G. J., Fuel, Lond., Vol. 41 (1962), p. 267.

8 Hanbaba, P. H., Jüntgen, H., and Peters, W., Brennstoff-Chem., Vol. 49, 1968, p. 368.

9 Chung, T. P., "Kinetic Modeling of the Primary Devolatilization of Coal in Pyrolytic Processes", Senior Thesis, Princeton University, Princeton, N.J. , 1976.

10 Badzioch, S. and Hawksley, P. G. W., Ind. Eng. Chem. Process Des. Develop., Vol. 9, No. 4 (1970), p. 521.

Table 1

General hypothetical scheme for coal pyrolysis of the Reidelbach-Summerfield model

$C \xrightarrow{k_1} AC$	Activation Step (high E)
$AC \xrightarrow{k_2} x_2 PT_L + (1 - x_2) S_1$	primary decomposition — low E
$AC \xrightarrow{k_3} x_3 PG_2 + (1 - x_3) S_2$	primary decomposition — medium E
$S_1 \xrightarrow{k_4} x_4 PG_2 + (1 - x_4) S_3$	primary decomposition — high E
$S_2 \xrightarrow{k_5} x_5 PG_3 + (1 - x_5) S_4$	primary decomposition — high E
$AC \xrightarrow{k_6} DAC$	Deactivation Step (DAC ≠ C)
$PT_L \xrightarrow{k_7} x_7 SG_1 + y_7 S_5$	Polymerization in the liquid phase inside the particle (yields mainly solid).
$PT_L \xrightarrow{k_8} x_8 SG_2 + y_8 S_6$	Depolymerization in the liquid phase inside the particle (yields mainly gas).
$PT_L \underset{k_9}{\overset{k_9'}{\rightleftharpoons}} PT_G$	Vaporization (depending on heat and mass diffusion)
$PT_G \xrightarrow{k_{10}} x_{10} SG_3 + y_{10} S_7$	Polymerization in the gas phase
$PT_G \xrightarrow{k_{11}} x_{11} SG_4 + y_{11} S_8$	Cracking in the gas phase

where

C	=	Initial coal
AC	=	Activated coal
PT_L	=	Liquid primary tar
PT_G	=	Gaseous primary tar
PG	=	Primary gas
SG	=	Secondary gas
S	=	Solid intermediate or residue
x,y	=	Stoichiometric coefficients
E	=	Activation energy

Table 2

Proposed Mechanism for primary devolatilization

$$C \xrightarrow{k_1} x_1 \cdot AC + (1 - x_1) \cdot S_1$$

$$AC \underset{k_{22}}{\overset{k_{21}}{\rightleftharpoons}} S_2$$

$$AC \xrightarrow{k_3} x_3 \cdot PT + (1 - x_3) \cdot S_3$$

$$AC \xrightarrow{k_4} x_4 \cdot PG + (1 - x_4) \cdot S_4$$

$$S_3 \xrightarrow{k_5} x_5 \cdot PG + (1 - x_5) \cdot S_5$$

$$S_4 \xrightarrow{k_6} x_6 \cdot PG + (1 - x_6) \cdot S_6$$

Best Fit Parameters

Reaction	x_i	Activation Energy	Pre-exponential Factor
1	0.80	28000 cal/g-mole	2×10^{8} 1/sec
2	1.00	4900 cal/g-mole	135
	1.00	52000 cal/g-mole	2.6×10^{13} 1/sec
3	0.45	11700 cal/g-mole	1.24×10^{4} 1/sec
4	0.60	36700 cal/g-mole	5.44×10^{7} 1/sec
5	0.30	23000 cal/g-mole	1.30×10^{6} 1/sec
6	0.69	55000 cal/g-mole	1.00×10^{10} 1/sec

C	coal
AC	activated coal
PT	primary tar (volatilized)
PG	primary gas
S_i	solids
x_i	stoichiometric coefficients
k_i	Arrhenius rate constants

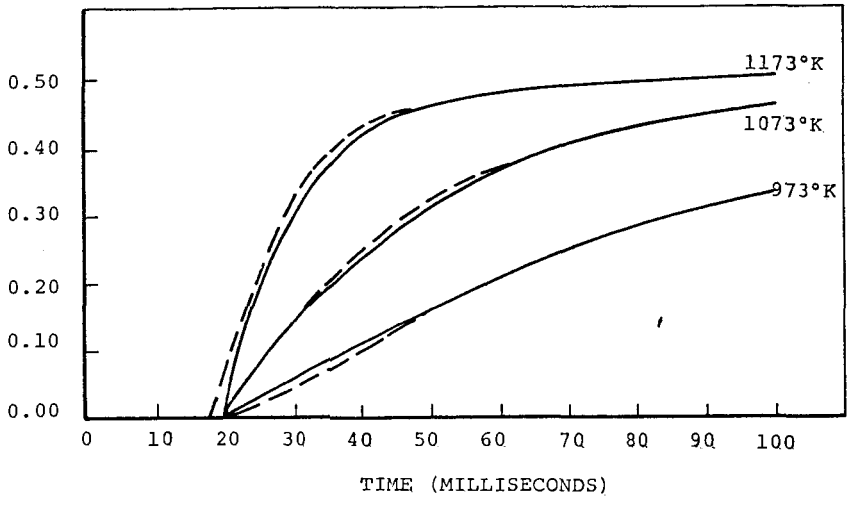

Figure 1 Primary decomposition of a hvAb coal at different temperatures as a function of time.

--------Theoretical curve obtained with the new primary decomposition scheme proposed in this study.

————Experimental results obtained by Badzioch and Hawksley for coal D.

THE COMBINED INFLUENCE OF CHEMICAL AND PHYSICAL FACTORS UPON COAL PARTICLE TEMPERATURE PROFILES DURING RAPID HEATING PYROLYSIS

James D. Freihaut, Alan A. Leff, and Francis J. Vastola

Dept. of Mat. Sci, Fuel Sci. Sec., The Penn. State Univ., Univ. Pk., PA 16802

INTRODUCTION

Wide variation in reported kinetic parameters for the pyrolytic decomposition of coal particles in varying experimental conditions causes considerable speculation as to whether coal particle behaviour is capable of generalization. Taking into account the precision and sensitivity of the experimental work performed, with respect to weight loss, the temptation is to attribute the differences in kinetic parameters to the chemical and physical nature of coal itself. The complexity of coal structure is then said to impart to coal a chameleon-like behaviour.

Assuming first order mechanisms for the decomposition of coal, some results indicate pyrolytic decomposition with a singular value for the activation energy and frequency factor, whereas others display behaviour corresponding to distributions of kinetic parameters (1,2). With varying results, apparently related to the unique apparatus and design used in each study, the question naturally arises as to whether sufficient attention is being given to transport processes involved in pyrolytic decomposition.

In particular, it might be asked as to what combination of chemical and physical parameters could influence the internal temperature profile of the coal particles such that the temperature can not be said to be identical to that of the external driving system during the time of initial pyrolysis? In other words, can the initial pyrolytic reactions themselves significantly influence the temperature profile of the particle, and if so, what combination of physical and chemical parameters would be needed to produce or maintain a significant temperature gradient within the particle during initial pyrolysis? If a combination of such capability exists, and the range of parameter values lies within those employed in decomposition studies, then results from studies dealing with coupled transport and reaction principles may aid in the understanding of observed pyrolytic behavior.

PHYSICAL MODEL USED AS THE BASIS OF NUMERICAL CALCULATIONS

In order to numerically determine the effect of chemical and physical parameters upon particle temperature profiles during pyrolysis, a basic composition model of coal itself needs to be postulated. It is desirable to make the model as straightforward and general as possible in order to more clearly ascertain the effects of systematic parametric changes upon results. Keeping the model initially general also allows maximum freedom in refining the model to take into account additional processes which may change the form of the original transport equation.

The basic model proposed here for calculation purposes views coal as consisting of two "fractions."- a pyrolytic fraction and an inert fraction. The "pyrolytic" fraction is taken to mean the thermally active or responsive material present in the coal matrix. The response is assumed to take the form of a first order expression of the Arrehenius type. The pyrolytic fraction exists uniformly throughout the particle. "Inert" is taken to mean the part of the coal matrix which is not subject to thermal decomposition but only to simple heat absorption. Although proposed here for the sake of clarity in calculations, hypotheses of the two-part type are certainly not novices in coal structure studies. Note that "two fraction" here is taken to refer to the inert and pyrolytic parts of the coal matrix to distinguish from similar terms used elsewhere which refer to the thermally responsive material alone (3).

NUMERICAL FORMULATION AND SOLUTION TECHNIQUES

A heat balance for concentric shells within spherical, isotropic particles takes the following form when consideration is given for possible heat absorption by pyrolytic reactions:

$$\dot{q}_{in} - \dot{q}_{out} = \dot{q}_m + \dot{q}_p \qquad 1)$$

where m refers to the absorption by unreacting solid matrix and p refers to heat absorption due to the pyrolysis process. The balance leads to the unsteady-state partial differential equation for conductive heat transport of the form:

$$\frac{\partial T}{\partial t} = \left(\frac{k}{\rho C_p}\right)\left[\frac{\partial^2 T}{\partial r^2} + \left(\frac{2}{r}\right)\frac{\partial T}{\partial r}\right] - \beta(\text{Pyrolysis Reaction Rate}) \qquad 2)$$

where, k= thermal conductivity, cal/cm-sec-^{o}K

ρ= solid matrix density, g/cc

C_p= solid matrix heat capacity, cal/g-^{o}K

$\beta = \frac{\text{heat of reaction, cal/g of P(s).}}{k \cdot C_p}$

As noted above, the initial global pyrolytic process is assumed to follow a first order Arrehenius type of expression and, consequently, has the form:

$$\frac{d(P_{(s)})}{dt} = k \cdot P_{(s)} \qquad 3)$$

where, $P_{(s)}$ is in g/cc, density of pyrolytic material,

$k = k_o \times \exp(-Eact/RxT)$

with k_o in sec^{-1},

Eact in cal/"mole",

R= 1.99 cal/"mole"-^{o}K,

T in ^{o}K.

One of several boundary conditions could be chosen for the numerical process:

$$Tr_o = T_e = C,\ C \text{ a constant in } {}^oK; \qquad 4)$$

$$\frac{dT}{dt})r_o = m,\ m \text{ a linear heating rate in } {}^oK/sec; \qquad 5)$$

$$\frac{dT}{dt})r_o = H(T_e - T_s),\ H \text{ a postulated, combined heat transfer coefficient;} \qquad 6)$$

$$\frac{dQ}{dt})r_o = F,\ F \text{ a constant heat flux in } cal/cm^2\text{-}sec \qquad 7)$$

where "ro" refers to particle surface and "e" refers to the external, driving environment.

The results shown in this study are obtained using the first type of boundary condition noted above. Results for the other type of boundary conditions are to be compared in a subsequent study.

Initial conditions within the particle need also to be specified before the calculation process begins. In this case the initial temperature distribution is assumed to be flat, and at 298°K. A uniform concentration of pyrolytic material, such as 40% of total particle mass and expressed in g/cc, is postulated and assumed to be present uniformly throughout the particle.

Since the reaction rate term of the transport equation contains the temperature variable in an exponential manner, no analytical solution exists and recourse to numerical methods is appropriate. Results were obtained using both explicit and implicit finite difference schemes. Displayed results are from an implicit Crank-Nicholson scheme with iterative solution of the node equations obtained at each time step. Inclusion of a floating time step, whose value is decreased at large heat flux conditions, aids in reducing time required to reach the predetermined tolerance in the iterative process. Integration of the transport equation is accompanied by integration of the first order equation describing the decay of condensed pyrolytic material within the particle matrix.

RESULTS AND DISCUSSION

Given the computational model and scheme above, it remains to determine what parametric value sets, for a given particle size, lead to chemical control of particle decomposition and what value sets lead to heat transport control. Or, given a set of kinetic parameters and reaction conditions, can a change in particle size lead to a transition from chemical control to heat transport control of the initial pyrolytic process?

In chemical control, the process is pictured as taking place uniformly throughout the particle and at, or very near, the stated external driving temperature. In heat transport control, the pyrolytic process is viewed as taking place in a relatively thin-shell, reaction zone. The reaction zone shrinks toward the particle center as the pyrolytic process depletes the concentration of pyrolytic material. Both types of process have been postulated to explain behaviour of coal particles (1,4). Experimental conditions and particle sizes varied considerably, however, and the results shown below indicate that such extreme variation in behaviour is indeed plausible, even for the same coal type.

Ideally the shrinking core process can be described by means of the following limit definitions:

$$\lim_{\Delta r \to 0} \left[\frac{(P_{(s)})_r - (P_{(s)})_{r+\Delta r}}{\Delta r}\right] = \infty, \text{ and } \lim_{\Delta r \to 0} \left[\frac{(T_{r+\Delta r} - T_r}{\Delta r}\right] = \infty \quad 8,9)$$

at the reaction front, corresponding to infinite gradients for the remaining solid pyrolytic material and the temperature of the solid matrix. The isothermal-volumetric, chemical control case might be described by:

$$\lim_{\Delta r \to 0} \left[\frac{P_{(s)})_r - (P_{(s)})_{r+\Delta r}}{\Delta r}\right] = 0, \text{ and } \lim_{\Delta r \to 0} \left[\frac{(T_{r+\Delta r}) - (T_r)}{\Delta r}\right] = 0 \quad 10,11)$$

corresponding to flat concentration and temperature gradients within the particle during the pyrolytic process.

In practice, one must decide in advance upon some finite gradient values which approximate the ideals. It would seem desirable to specify operational gradients for the classification of decomposition type in terms of P_o, concentration of original pyrolytic material present, and r_o, particle radius. In the case of heat transfer control, working gradient indices could be specified as follows:

$$\text{Let, } \Delta(P_{(s)}) = (P_{(s)})_r - (P_{(s)})_{r+\Delta r} = (0.5)\, P_o$$

within a radial displacement, Δr, of $0.2r_o$. This would give a concentration gradient at the reaction front of $\frac{0.5P_o}{(0.2r_o)}$, or $\frac{2.5P_o}{r_o}$. An analogous, operational gradient index could be derived for the temperature denoting heat transfer control. Similar indices can also be formulated for the chemical control case, but in this case radial displacement would be taken as $1.0r_o$. As a result a working table might have the form:

	Heat Transport Control	Chemical Control
Concentration Gradient	$\geq 2.5 \frac{(P_o)}{r_o}$	$\leq 0.1 \frac{(P_o)}{r_o}$
Temperature Gradient	$\geq \frac{500°K}{r_o}$	$\leq \frac{10°K}{r_o}$

In figures 1, 2, and 3 below are shown the results of the numerical calculations for two different particle sizes held under the same surface boundary conditions and made to decompose by the same set of chemical parameters. Clearly, the 500μm particle approximates the transport control ideal during the major part of the initial pyrolytic process whereas the 25μm particle approximates the chemical control limit. Examination of the figures indicate, that, in the case of heat transport control, the reaction process is taking place across a temperature

range significantly different from the stated driving temperature. Figure 4 shows the temperature-time history of the center of the 500μm particle. It can be seen that the endothermicity of the pyrolytic process introduces an appreciable time lag in the particle's response to the driving temperature.

Calculations performed with variation of allowed chemical and physical parameters for the same particle size indicate there is a wide range of experimental conditions in which the initial pyrolytic process is non-isothermal and non-uniform within the particle, depending upon the parameters chosen for the thermal decomposition process. These results are being examined more closely in conjunction with various boundary conditions.

REFERENCES

1. S. Badzioch and Peter G. W. Hawksley, IEC Process Des. and Dev., 9, 521 (1970).

2. D. B. Anthony, J. B. Howard, H. C. Hottel, and H. P. Meissner, Fifteenth Symposium (International) on Combustion, 1303, The Combustion Institute, Pittsburgh, Pa. (1975).

3. R. H. Essenhigh and J. B. Howard, Penn State Studies No. 31, Administrative Committee on Research, Pennsylvania State University, University Park, PA (1971).

4. W. Peters and H. Bertling, Fuel, 44, 317 (1965).

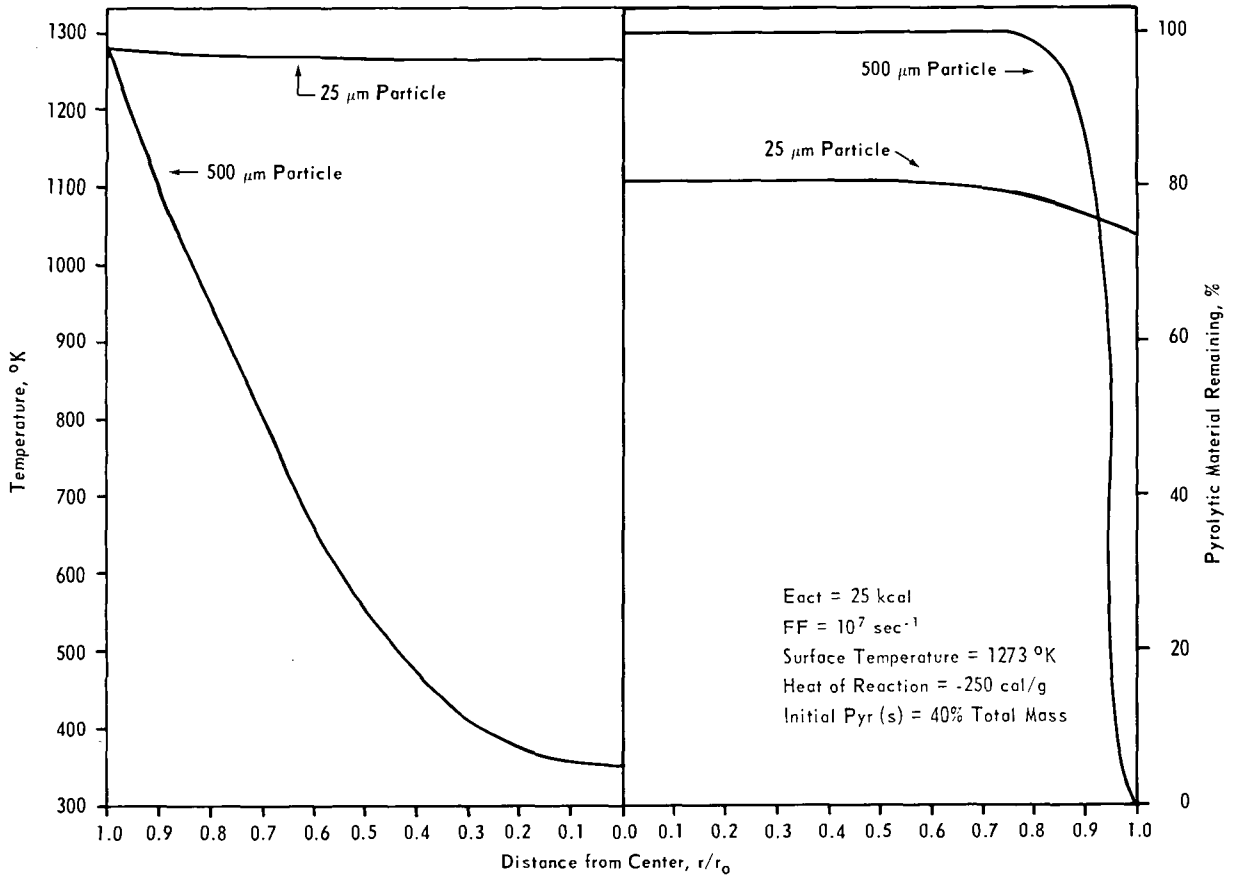

Figure 1. TEMPERATURE AND PYROLYTIC MATERIAL PROFILES AT 25% REACTION COMPLETION

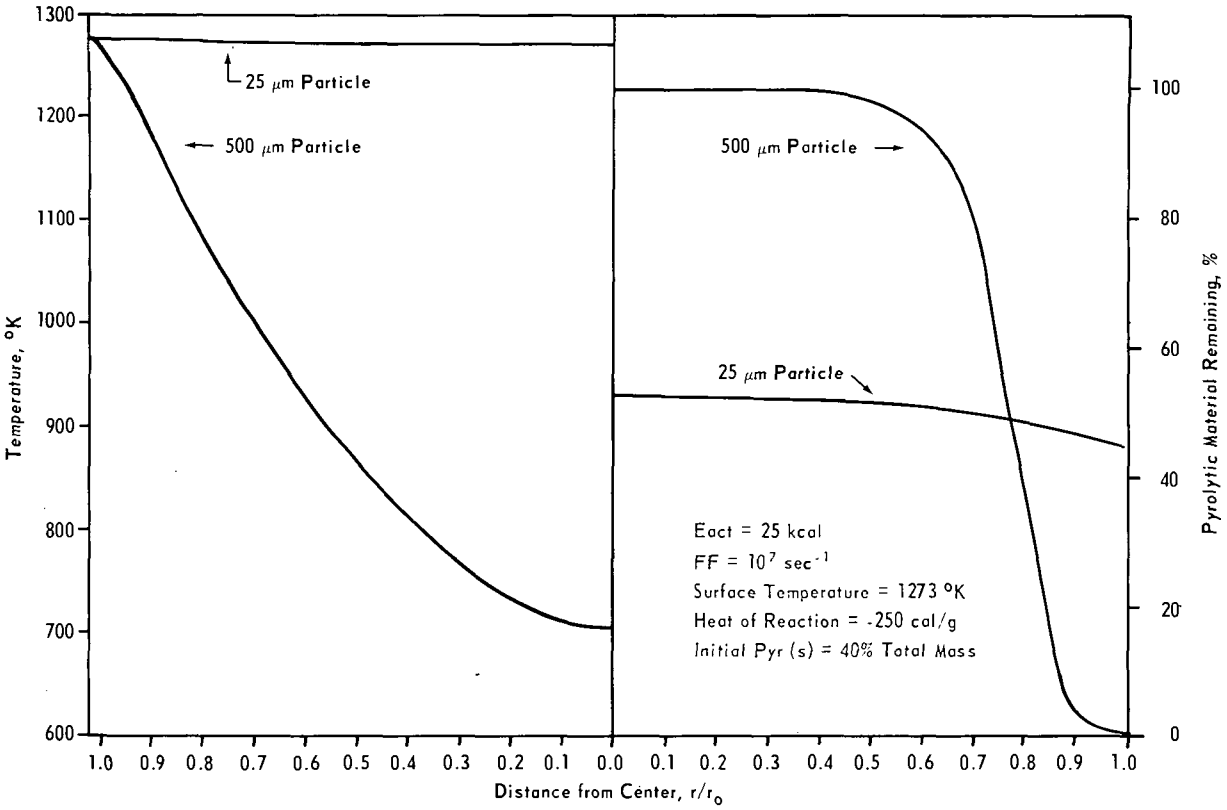

Figure 2. TEMPERATURE AND PYROLYTIC MATERIAL PROFILES AT 50% REACTION COMPLETION

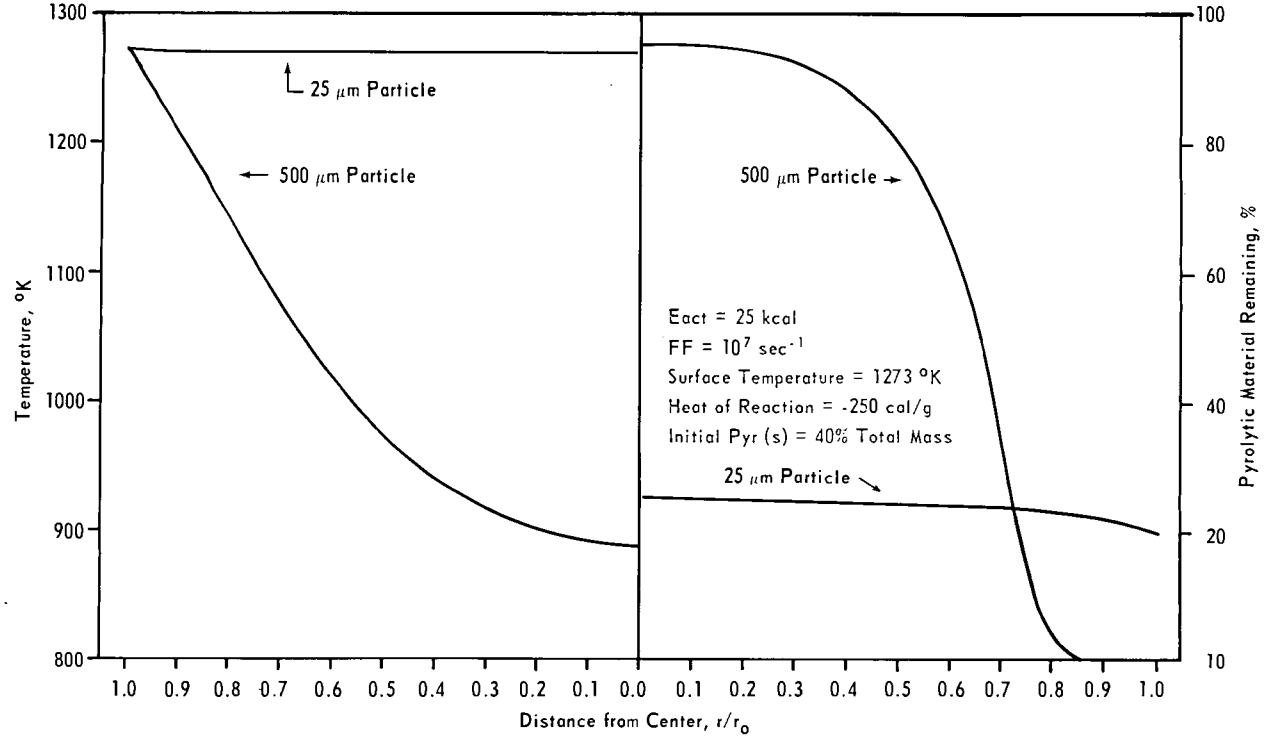

Figure 3. TEMPERATURE AND REMAINING PYROLYTIC MATERIAL PROFILES AT 75% REACTION COMPLETION

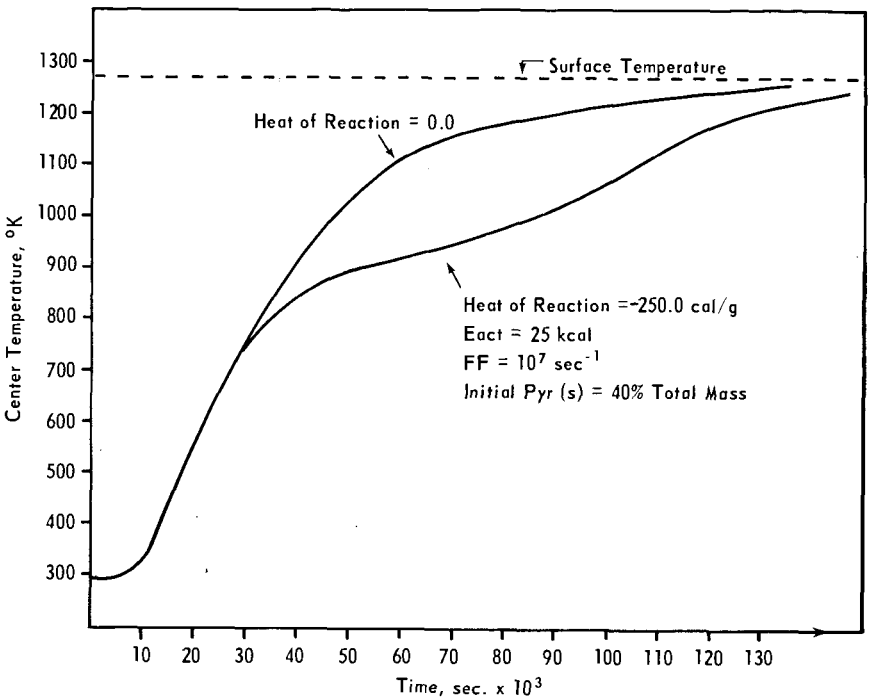

Figure 4. TEMPERATURE RESPONSE OF PARTICLE CENTER (500 μm PARTICLE)